SELECTING HIGH-ORDER MODES IN SOLID STATE LASER RESONATORS

University of Fort Hare
Together in Excellence

A dissertation submitted in fulfilment of the requirements for the degree of

MASTERS OF SCIENCE

By

KELACHUKWU IHEANETU

In the Department of Physics
Faculty of Science and Agriculture at the University of Fort Hare

Supervisor: Prof. A. Forbes

Co-Supervisor: Dr. G. Makaka

June 2014

Declaration

I, Kelachukwu Iheanetu, declare that this dissertation titled, 'Selecting high-order modes in solid state laser resonators' and the experimental work described in this dissertation was carried out at the Council for Scientific and Industrial Research, National Laser Centre, while registered with the University of Fort Hare, Alice under the supervision of Professor Andrew Forbes and co-supervised by Doctor Golden Makaka.

The study present in this work is the author's original work and have not been submitted previously in entirety or in part at any other university for a degree.

Signed: ________________________________

Date: ________________________________

Dedication

To God be the glory for His grace.

Acknowledgements

I wish to thank my supervisors Prof. Andrew Forbes for his inspiration and encouragements, and my co-supervisor Dr. Golden Makaka for his constant counseling and encouragements. I also want to thank the Council for Scientific and Industrial Research and the National Laser Centre for providing the needed funds, research facilities and technical expertise without which it would not have been possible to complete this work. I am very grateful to the GMRDC and my colleagues in UFH for their support and encouragement during the course of this work.

I equally wish to extend my heartfelt gratitude to Sandile Ngcobo, Darryl Naidoo, and Dr. Angela Dudley (in CSIR) for the guidance and lectures during the time of the experiments. I cannot forget all my friends in the Council for Scientific and Industrial Research and National Laser Centre, thanks very much for all your support. My dear brother Godwin Nebo and friends UFH, thank you for your encouragements.

Summary

The first chapter considered the fundamental processes of laser operation: photon absorption, spontaneous and stimulated emissions. These processes are considered when designing a laser gain medium. A four-level laser scheme was also illustrated. Then, the basic components and operating principle of a simple laser system was presented using a diode end-pumped Nd:YAG solid state laser resonator. The second chapter considered laser light as light rays propagating in the resonator and extensively discussed the oscillating field in the laser resonators. It examined the characteristics of the fundamental Gaussian mode and the same theory was applied to higher-order modes.

Chapter three started with an introduction to beam shaping and proceeded to present a review of some intra-cavity beam shaping techniques, the use of; graded phase mirrors, diffractive elements – binary phase elements and spiral phase elements. Also, a brief discussion was given on the concept of conventional holography and digital holography. The phase-only spatial light modulator (SLM) was presented, which by default is used to perform (only) phase modulation of optical fields and how it can be use to perform amplitude modulation also. Finally, a detailed discussion of the digital laser which uses the intra-cavity SLM as a mode selection element was presented, since it was the technique used in the experiment. The elegance of dynamic on-demand mode selection that required only a change of the grey-scale hologram on the SLM was one quality that was exploited in using the digital laser.

The next two chapters presented the experiments and results. The concept of the digital laser was first used in the experiment in chapter four, to assemble a stable diode end-pumped Nd:YAG solid state laser resonator. Basically, the cavity was of hemispherical configuration using an intra-cavity SLM (virtual concave mirror) as a back reflector and a flat mirror output coupler. A virtual concave mirror was achieve on the SLM by using phase modulation to generate the hologram of a lens, which when displayed on the SLM made it to mimic a concave mirror. Then the next phase was using symmetric Laguerre-Gaussian mode function, of zero azimuthal order to generate digital holograms that correspond to amplitude absorbing concentric rings. These holograms, combined with the hologram that

mimics a concave mirror were used on the SLM to perform high-order Laguerre-Gaussian modes selection in the cavity. The fifth chapter presented the results of the mode selection and considered the purity of the beam at the output coupler by comparing measured modal properties with the theoretical prediction. The outcome confirmed that the modes were of high purity and quality which further implied that the cavity was indeed selecting single pure high-order modes. The results also demonstrated that forcing the cavity to oscillate at higher-order modes ($p = 3$) extracted $\approx 74\%$ more power from the gain medium compared to the fundamental mode ($p = 0$), but this extra power is only accessible beyond a critical pump input power of ≈ 38.8 W.

Laser brightness describes the potential of a laser beam to achieve high intensities while still maintaining a large Rayleigh range. It is a property that is dependent on beam power and its quality factor. To achieve high brightness one needs to generate a beam that extracts maximum power from the gain with good beam quality. Building on the experiments demonstrated in this study, one can make the correct choices of output coupler's reflectivity, the laser gain medium's length and doping concentration and the pump mode overlap for a particular mode to further enhance energy extraction from the cavity, and then using well known extra-cavity techniques to improve the output beams quality factor by transforming the high-order mode back to the fundamental mode. This will effectively achieve higher laser brightness.

Contents

List of Tables

List of Figures

List of Abbreviations

LCD: liquid-crystal display

MASER: microwave amplification by simulated emission of radiation

LASER: light amplification by simulated emission of radiation

SLM: spatial light modulator

LCOS-SLM: liquid crystal on silicon spatial light modulator

GPM: graded phase mirrors

DPE: diffractive phase element

SPE: spiral phase element

DVI: digital video interface

OAM: orbital angular momentum

CCD: charged coupled devices

List of Symbols

$\triangle E$: energy difference

h: Planck's constant

v: Bohr's frequency

R: radius of curvature

L: length of cavity

g_i: Geometric parameter

l: azimuthal mode index

p: radial mode index

m: mode index

n: mode index

L_{pl}: Laguerre polynomial of radial mode index p and azimuthal mode index l

ω: angular frequency

c: speed of light

ρ: distance

k: wave-number

z: propagation axis

z_R: Rayleigh range

A: complex-valued amplitude

I: intensity

ϕ: azimuthal angle

dS: surface element

$\triangle q$: complex radius of curvature

$\triangle u$: electric field expressed in complex scalar wave amplitude

w_0: beam waist

P: Power

M^2: the beam propagation factor

$\Delta\varphi$: phase shift

f_g: grating's spatial frequency

V_p: mode volume

l_0: length of the gain medium

δ: round-trip losses

θ_0: angular divergence

B: Brightness

λ: wavelength

H_{mn}: Hermit polynomial for mode indexes m and n

$\hbar$: Plank's constant $h/2\pi$

N: number of 2π phase discontinuities

Chapter 1

Introduction

A laser is a device that has the ability to generate or amplify spatially and temporally coherent radiation at frequencies that runs through the electromagnetic spectrum [1]. The principle of laser generation was derived from MASER working principle. This acronym MASER stands for Microwave Amplification by Simulated Emission of Radiation hence when this principle was extended to the optical frequencies of the electromagnetic spectrum it gave rise to the acronym LASER (Light Amplification by Simulated Emission of Radiation).

The laser operation is controlled by how electromagnetic radiation interacts with matter and this process is called stimulated emission. Laser light is highly coherent, monochromatic and directional unlike other light sources, for example the room lamp which emits radiation in all directions. It is these properties of a laser that makes it easy to achieve high intensity light. The concept of Laser was first demonstrated with a flashlamp-pumped solid-state ruby (Cr^{3+}) material doped sapphire rod as the gain medium [2]. Since this discovery in 1960, numerous other types of materials have been used as gain media including gas, liquid, and solid-state crystals to achieve laser operation. Its unique properties have made it possible for lasers to find applications in the medical, military and communication industries.

1.1 Fundamentals to Lasers

In an atomic system, atoms and ions can exist in discrete energy levels. When these atoms changes from one energy level to another, it is associated with the absorption or emission of a photon [1]. The energy E of the emitted photon is proportional to the difference in energy (E_2–E_1) between the two energy levels and can be described by the Bohr relation $\triangle E = E_2 - E_1 = hv$. Where h is Planck's constant and v is the frequency of the absorbed or emitted photon.

The Maxwell-Boltzmann distribution can be used to describe the population of energy levels in an atomic system at thermal equilibrium which states that lower energy levels have a higher population of atoms than the higher energy levels. If a photon of frequency v interacts with the atomic system, the atom is raised ("pumped") to a higher energy level with the absorption of the photon. Figure 1.1(a) shows atomic transition by photon absorption. The process of optically exciting atoms in an atomic system to make transition from a lower energy-level to a higher energy-level by the absorption of photons is known as optical pumping. Electrical and chemical pumping are other forms of laser pumping techniques but will not be discussed in the current work.

For laser action to occur, a condition of "population inversion" must be created in the optical gain medium. Population inversion is the state where there is higher number of atoms in the higher energy level than that in the lower energy level in the gain medium [1]. This excited atom is unstable at the upper energy level and will radiate by spontaneous or stimulated emission and return to the stable lower energy-level. Figure 1.1(b) illustrates atomic transition by spontaneous emission while Figure 1.1(c) illustrates atomic transition by stimulated emission of radiation. The pumping process can be used as a means of depositing energy in the gain medium (by exciting more atoms to upper energy level) which will be extracted in the form of a laser beam.

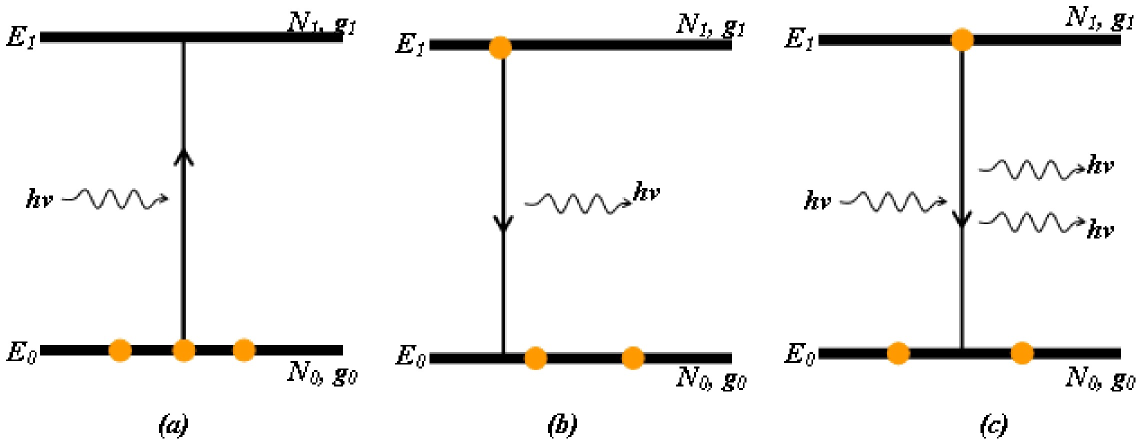

FIGURE 1.1: A schematic diagram to illustrate (a) absorption, (b) spontaneous and (c) stimulated emission.

When population inversion is achieved in the gain medium, with the passing of an incident photon of the right frequency on this gain medium, it will stimulate the excited atoms in the higher energy level to transit to a lower energy level with the emission of an additional photon (Figure 1.1(c)). The emitted photon is of the same frequency, direction and polarization as the incident photon [3]. This forms the bases for the amplification process of laser operation.

1.1.1 Gain Medium

It is very important that the gain medium must have very good optical, mechanical and thermal properties to withstand the harsh operation conditions of the laser. Below are some of the major criteria for selecting a laser active ion host [3].

- ◊ The gain medium must have a homogeneous refractive index to ensure good beam quality. The refractive index must have very small temperature dependence thus reducing thermal lensing effect under severe pumping conditions. It should also have minimal scattering losses to reduce its overall losses.

- ◊ The gain medium should have high mechanical and thermal tolerance to withstand high power operation without being subjected to excessive stresses, and probably fracture due to thermal load.

- ◊ The gain medium must have lattice sites that are able to accept the dopant ions. The local crystal field must be such that it induces the required spectroscopic properties.
- ◊ The gain medium must be such that it can be grown to adequate sizes without losing its good optical and mechanical properties.

Single crystals, glasses and ceramics are three primary solid-state materials which posses the above mentioned qualities. Neodymium (Nd) doped yttrium aluminium garnet ($Y_5AL_5O_{12}$ or YAG) single crystals has gained dominance over all the other host materials.

1.1.2 Active Ions

Rare earth (lanthanide) ions act as very good candidates as active ions in solid-state laser materials because they have numerous sharp emission lines throughout most of the visible and infrared part of the electromagnetic spectrum [3]. The emission lines are still very sharp even in the presence of the Stark effect (local crystal field) due to the shielding of the outer electrons.

The outermost electrons of these ions form a complete rare gas shell, which is the xenon shell with two $5s$ and six $5p$ electrons [3]. Inside the xenon shell is the $4f$ shell that are incompletely filled. The electrons that are present in the $4f$ shell can be raised into the empty levels by light absorption. The sharp absorption and emission lines that are observed in rare earth ions are due to these particular transitions which are shielded by the outer xenon shell [3].

Rare earth ions are used in the solid-state laser gain media in either a divalent or trivalent form. A divalent rare earth ion is formed when the atom loses its outer $6s$ electrons while a trivalent ion is formed if it gives up the $5d$ electron, or if it has none and gives up one of the $4f$ electrons [3].

Neodymium (Nd^{3+}) is the specific rare earth ion that is considered in the this work.

1.1.3 Diode-End-Pumping

The first high power laser was achieved using a flash lamp-pumped solid state system which was later developed into a diode pumped configuration because of its numerous advantages over the flash lamp-pumped systems. Some of these advantages include higher brightness, higher overall efficiency, a more compact design with respect to the cooling geometries and better frequency stability than the flash lamp-pumped systems [4]. The efficiency of flash lamp-pumped and diode pumped-systems are compared in Table 1.1.

Table 1.1: Comparing the efficiency of diode flashlamp pumped and diode pumped systems [5].

Nature of Efficiency	Pump Source	
	Lamp	Diode
Radiation	50%	40%
Projection	35%	95%
Absorption	50%	98%
Quantum	40%	76%
Excitation	3.5%	28.3%

After the first diode pumped solid state laser was demonstrated [6], it was found that GaAs lasers would be ideal to optically pump Nd-doped gain media [4]. The Nd:YAG crystal has become the dominant material used as gain medium because the Nd^{3+} ions have exceptional spectroscopic properties as well as a strong absorption in the emission bands of GaAsP, GaAs and GaAIAs laser diodes. The first diode-pumped Nd:YAG crystal was done in a transverse geometry using a single GaAs diode [7] which revealed that a diode pumped solid state laser can act as a temporary energy storage devices and possess potential to achieve high peak powers. This ability comes from the fact that they have long upper state lifetime giving way for a large amount of input radiation from the source, to be collected by the gain medium.

There are many diode pumping geometries that have been implemented in the past, but the transverse and end-pumped geometries are often the most favourable choices. In the transverse geometry, the optical pump radiates the gain medium at the direction perpendicular to the optic axis of the gain medium while in a end-pumped system (Figure 1.2), the gain medium is irradiated along (parallel to) the optical axis of the gain medium. The end-pumping geometry has higher absorption efficiency of the input radiation because of the co-linearity of the (axis of the) gain medium and that of the pump emitted laser radiation compared to the transverse geometry [4].

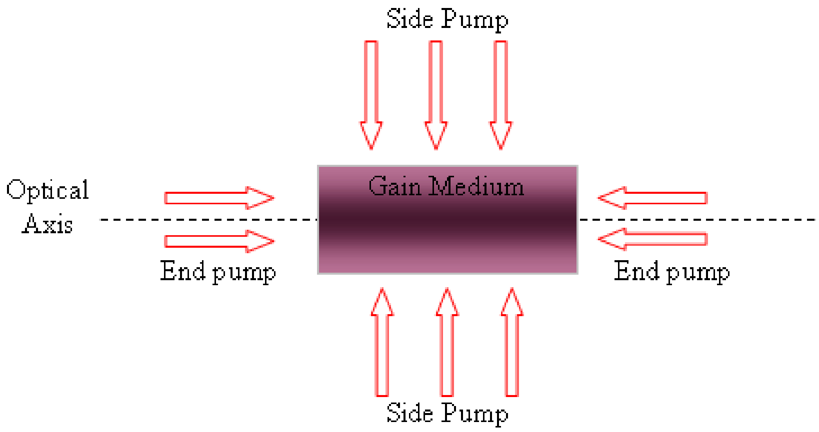

FIGURE 1.2: Schematic to illustrate side and end-pump geometries.

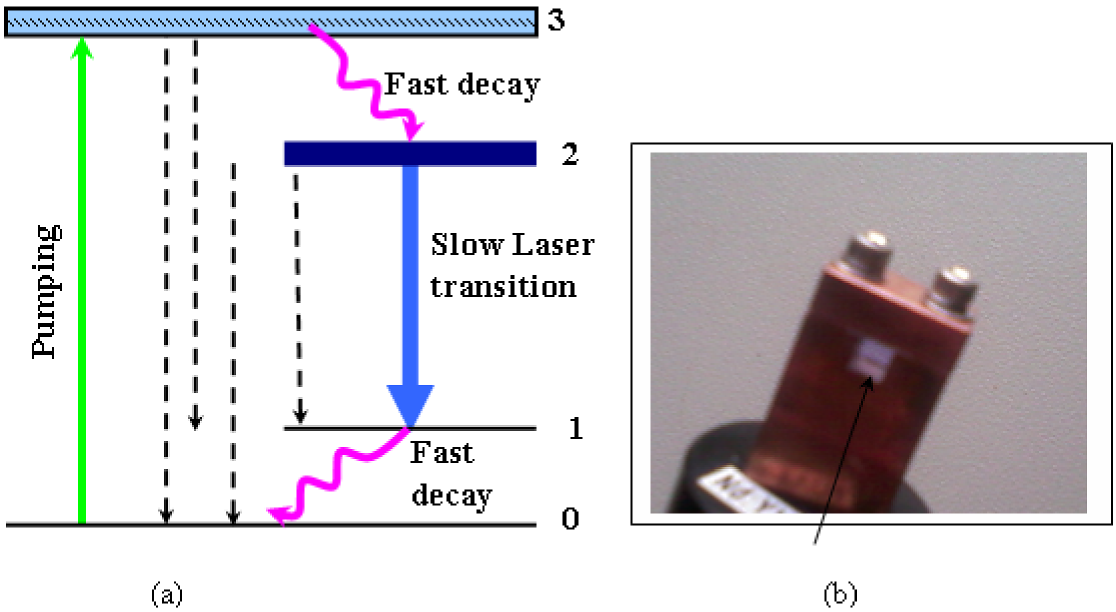

FIGURE 1.3: (a) Simplified schematic diagram of a 4-level laser system, illustratively showing the elements required for laser action. The dash lines show possible spontaneous transitions [3] [4]. (b) Picture of Nd: YAG crystal (the arrow pointing).

For the purpose of illustration, let us consider a laser cavity that uses a laser diode which emits radiation at 808 nm wavelength as the pump source, and a Nd:YAG crystal as the gain medium. Figure 1.3(a) shows the energy levels and atomic transition that exists when pumping a Nd:YAG crystal (that is a 4-level energy laser system). Figure 1.4 shows the absorption spectrum against wavelength for a Nd:YAG crystal, which shows that it has a very high absorption line at 808 nm wavelength, corresponding with the emission wavelength of the pump source so as to ensure optimum absorption.

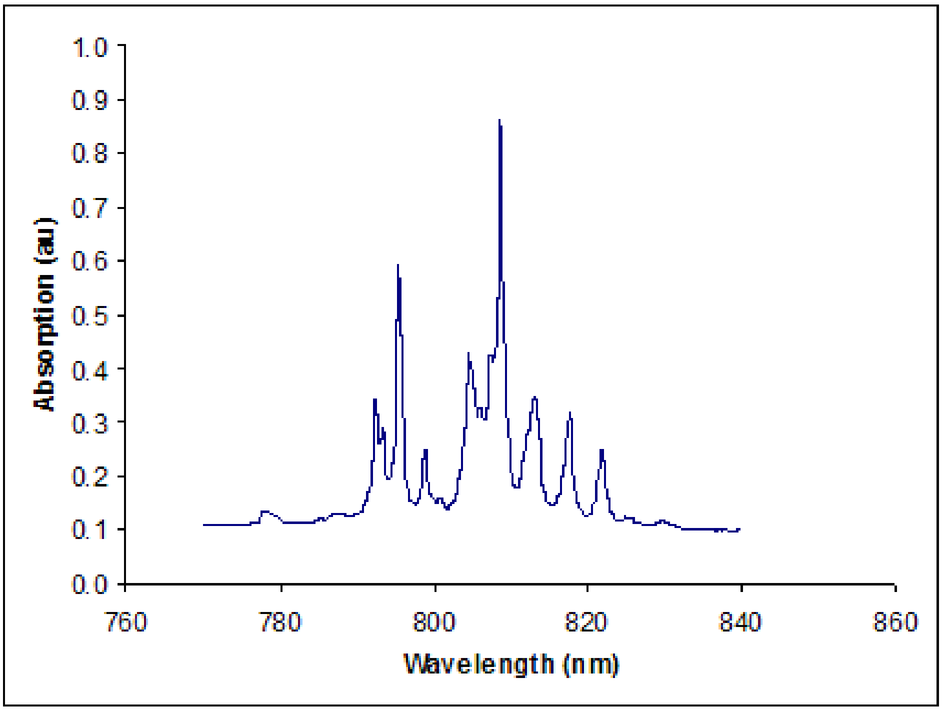

FIGURE 1.4: The absorption spectrum of Nd:YAG crystal [8].

When the laser is used to pump the crystal, atoms at the ground state energy (level 0) absorb photons of energy and transits to the excited state energy level 3 at a very fast rate. Then, because these excited atoms are unstable in this upper energy level, they make fast spontaneous radiationless decay to level 2 releasing the energy difference (between level 3 and 2) as heat (in the crystal). The atom at level 2 further makes a slow spontaneous transition to energy level 1 with the release of the excess energy as a photon (laser) in the infrared wavelength, 1064nm which corresponding to the energy gap ($\Delta E = hv$) between the two levels. The emitted photon (laser), when passing through these energy levels stimulates more atoms in the excited energy level 2 to emit photons and decay to energy level 1 and the second stimulated photons in turn stimulate more atoms to radiate and decay to the ground state as they pass through the crystal. As the chain continues, the laser is thereby amplified.

It is this phenomenon that gave rise to the concept of amplification by stimulated emission. Finally, the de-excited atoms at energy level 1 through a fast radiationless transition, decay to the ground state energy (level 0) with the release of the extra energy as heat in the crystal. So, atoms in the ground state absorb high energy photons and get excited to level 3, then drop some part of that energy through spontaneous transition to level 2 as heat, then through slow decay transit to level 1 with emission of laser light. Subsequently, through fast radiationless decay transit to the ground state (energy), releasing the excess energy as heat. The atomic transitions between levels 3 and 2, and 1 and 0 do not emit any radiation but only occur through vibrational relaxation in the crystal. The quantum efficiency of a laser cavity is the energy of the output photon divided by the input energy required for producing that laser, assuming the rest of the system is perfectly efficient. The quantum efficiency of a Nd:YAG crystal is about 80%.

1.2 Resonators

Laser resonators are generally comprised of two spherical mirrors which are positioned such that diffraction losses in each round trip are controlled. There are two broad classes of resonator cavities, stable and unstable resonators. The radius of curvature of the mirrors and distance between them normally known as the length of the cavity L, determines the stability of the resonator cavity. There are many configurations which has been in use today, but in Figure 1.5 we present some of the common ones, where the shaded region represents the oscillating field [10].

The field inside the laser cavity oscillates until it attains a steady state condition thus emitting a laser beam. As the electric field passes from one mirror to the other in the cavity it experiences diffraction losses due to the aperturing effect of the gain medium and finite size of the mirrors. The assembly that produces the field with the lowest diffraction losses is a stable resonator, and on attaining a steady state condition will emit laser beams. A laser resonator can be designed using some certain boundary conditions; these conditions can be used to determine the stability of the resonator.

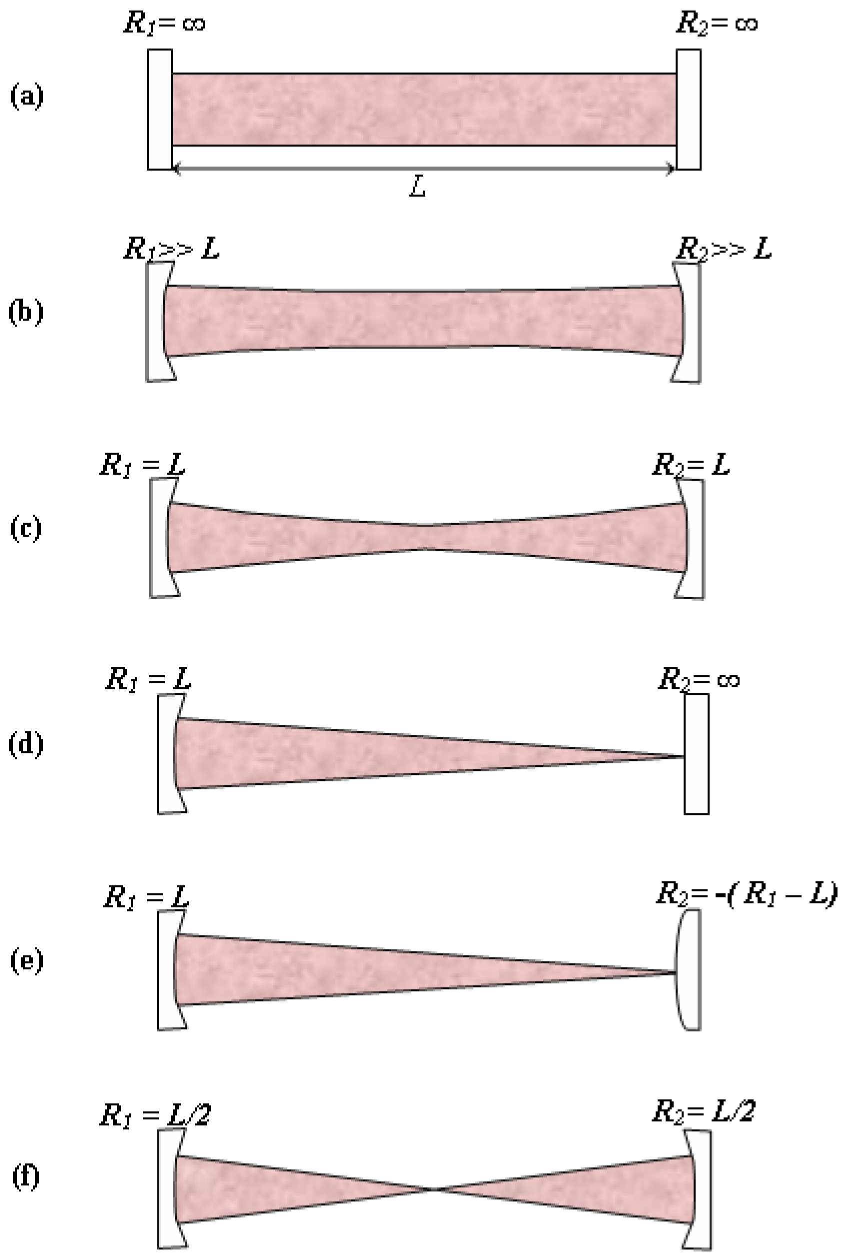

FIGURE 1.5: Various laser cavity configurations where the shaded region represents the optical field patterns. (a) Plane parallel, (b) large-radius mirrors, (c) confocal, (d) hemispherical, (e) concave-convex and (f) concentric [3][9][11].

1.2.1 Resonator Stability

Stability of the resonator is an important factor for determining if light rays will be confined in the cavity that contains two mirrors. Laser resonators are considered to be a periodic optical system and ray-optics can be applied to understand [11] the propagation of light in such a system. Employing the technique of matrix optics and considering only paraxial rays, we can critically analyze and understand how light rays bounce back and forth off the two mirrors. A ray that is confined inside a periodic resonator cavity will bounce back and forth off the mirrors as illustrated in Figure 1.6 completing m round trips. We can determine the rays position and inclination (y_{m+1}, θ_{m+1}) if its position and inclination (y_m, θ_m) are known [9][11].

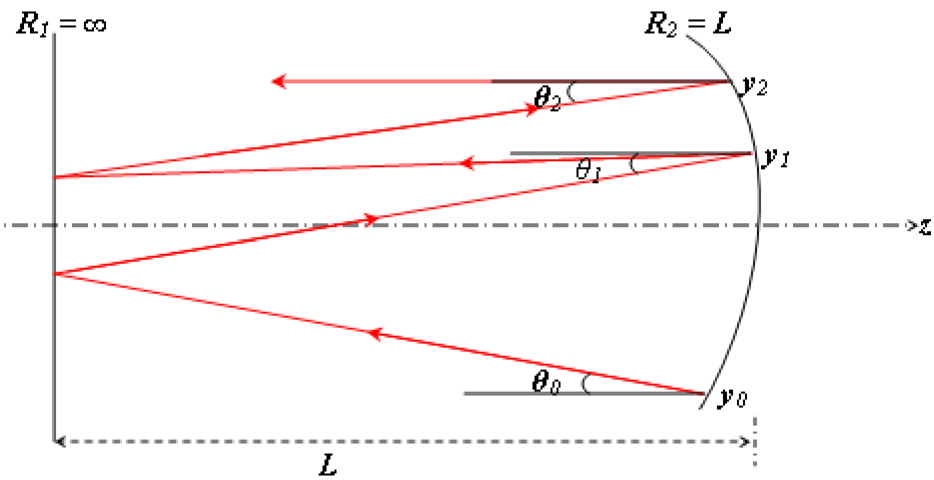

FIGURE 1.6: A schematic diagram showing the inclination and position of a ray as it completes two rounds trip in a hemispherical resonator.

The linear relationship of a ray of light traveling in such a periodic optical system can be expressed in matrix form as [11]

$$\begin{bmatrix} y_{m+1} \\ \theta_{m+1} \end{bmatrix} = \begin{bmatrix} A & B \\ C & D \end{bmatrix} \begin{bmatrix} y_m \\ \theta_m \end{bmatrix} \tag{1.1}$$

The ray-transfer matrix, M (ABCD matrix) for the ray confinement in Figure 1.6 can be expressed as

$$M = \begin{bmatrix} 1 & 0 \\ -\frac{2}{R_2} & 1 \end{bmatrix} \begin{bmatrix} 1 & L \\ 0 & 1 \end{bmatrix} \begin{bmatrix} 1 & 0 \\ 0 & 1 \end{bmatrix} \begin{bmatrix} 1 & L \\ 0 & 1 \end{bmatrix} \tag{1.2}$$

$$M = \begin{bmatrix} 1 & 2L \\ -\frac{2}{R_2} & 1 - \frac{4L}{R_2} \end{bmatrix} \tag{1.3}$$

There are different resonator configurations with respect to the type of mirrors used in the cavity, radius of curvature and the distance of separation, L between them in the cavity. A combination of resonator parameters, radii of curvature R_i, (for the two mirrors) and length of cavity L, can be selected to meet a particular design for any resonator but these parameters determines the stability or instability of that configuration. The geometric parameters (or g-parameters) gives the stability or instability of a resonator configuration and are generally given as [1]

$$g_i = 1 - \frac{L}{R_i} \tag{1.4}$$

where the index i, is 1 for the first mirror and 2 for the second one. The product $g_1 g_2$ must satisfy the condition

$$0 \leq g_1 g_2 \leq 1 \tag{1.5}$$

(where $g_1 = \left(1 - \frac{L}{R_1}\right)$ and $g_2 = \left(1 - \frac{L}{R_2}\right)$) for the resonator to be stable [11] [12] [13]. Equation (1.5) above is the resonator stability equation in general form. In the case of the hemispherical configuration, the radius of curvature of the flat (plane) mirror is infinity, (∞) and that of the concave one is chosen to be equal to L (distance between the two mirrors) so the g-parameter product is equal to 1 and it satisfies the stability criteria.

The plot of stability, the g-parameters show which type of resonator is stable. The graph of g_2 against g_1 shows this in Figure 1.7 below.

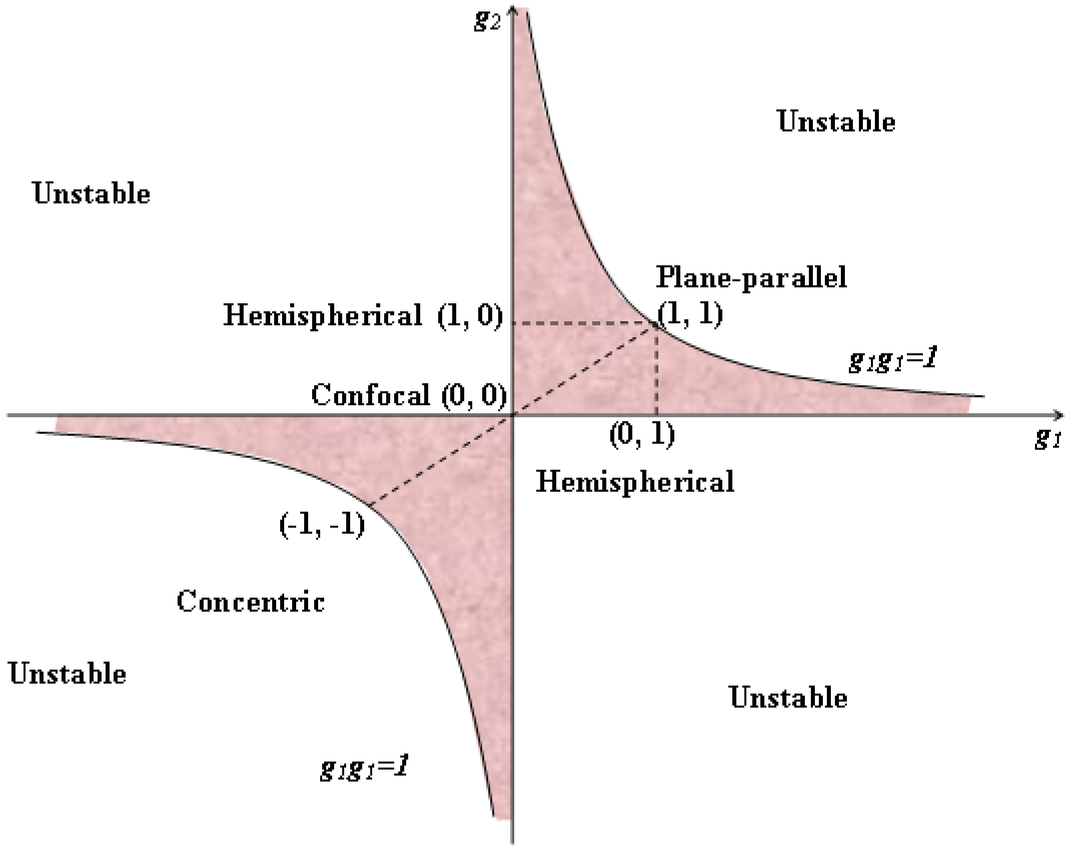

FIGURE 1.7: Plot of stability diagram showing which type of resonator is stable and which is unstable (the shaded regions represent regions of stability)[3][10][12].

The shaded region in Figure 1.7 represents the plot of g_2 against g_1 for stable resonators. That is the region bounded by the coordinate axis and hyperbola $g_2 = \pm\frac{1}{g_1}$ to satisfy equation (1.5) except for the special case of $g_2 = g_1 = 0$ [3]. Points that lies exactly on the axis or on the hyperbola lines are marginally stable. The resonators cavity whose g–parameters obey the relation $g_2 g_1 < 0$ or $g_2 g_1 > 1$ represented by the un-shaded region are unstable and does not satisfy equation (1.5). The transverse distribution of the field oscillating inside the cavity is called a mode and there are various kinds of these modes. The Gaussian mode is the lowest order mode that is generally considered to be the fundamental mode in stable resonators. It is characterized by the transverse spreading of the field in free space and the beam size.

Figure 1.5 illustrates the various designs of stable resonators which are often employed in practical laser cavities, and it will be good to discuss their general properties and their relation with the oscillating field, in particular the Gaussian modes. The plane-parallel (Figure

1.5(a)) or the long radius resonator (Figure 1.5(b)) is regarded as the limiting condition for both mirrors as the radius of curvature approaches infinity, $R_1 \approx R_2 \approx \infty$ which implies that $g_1 \approx g_2 \approx 1$. The size of the Gaussian beam becomes identically large and if the mirrors' radii of curvature tends towards infinity, also the beam size slowly tends towards infinity. In Figure 1.7, the point (1, 1) is the stability boundary for a perfect planar system and Gaussian theory no longer holds beyond this point. Hemispherical configuration (Figure 1.5(d)) has the characteristics that $R_1 = L$ and $R_2 \approx \infty$ with $g_1 = 0$ and $g_2 = 1$. This happens to be the most common practical laser resonator design for medium and low power gas lasers. This produces a very small Gaussian beam size in the plane mirror R_2 and a relatively large size beam on the concave mirror R_1. The fields distribution shape is cone like and if the length of the cavity is slightly increased the size of the Gaussian beam increases significantly on the concave mirror but results in a much smaller beam size on the plane mirror. The confocal resonator configuration (Figure 1.5(c)) is characterized by the radii of curvature of two concave mirrors being equal to the length of the cavity, $R_1 = R_2 = L$ with $g_1 = g_2 = 0$ and is located at the point origin, (0, 0) in Figure 1.7. The name confocal implies that the focal point of the two mirrors coincides with each other at the center of the cavity resonator. The condition for confocality is such that the centre of curvature of the mirrors are located exactly the same on the opposite side of the mirrors and the Gaussian beam spot sizes are identical on the mirrors. In the stability boundary of Figure 1.7 (in the third quadrant on the hyperbola) is situated the concentric resonator (Figure 1.5(f)) configuration which are characterized by $R_1 = R_2 = L/2$ with $g_1 = g_2 =$ -1. The size of the Gaussian beam tends to infinity on the mirrors. It is a perfect configuration and beyond that point Gaussian theory is no longer valid. The concave-convex resonator configuration (illustrated in Figure 1.5(e)) is characterized by $R_1 = L$ and $R_2 = -\,(R_1 - L)$. The g-parameters extend the regions of the stability diagram beyond $g_1 = 0$ or $g_2 = 1$ and have a large transverse field distribution that makes them difficult and impractical in Gaussian mode generation. This system is equivalent to a half symmetric system that is twice as long. The size of the beam on the mirrors can be considerably different; with the minimum beam size located on 1 and transversely spreads to mirror 2. The range that is allowed corresponds to the vertical line in Figure 1.7 between points (1, 1) and (1, 0) [1] [3] [9].

1.2.2 Laser Oscillator

A basic laser oscillator is composed of an optical pump source, two reflective mirrors positioned on the opposite sides of a laser material (the gain medium) in such a way that their planes are perpendicular to the optic axis of the gain medium and their optic axis coincides with that of the gain medium. The mirrors are so positioned to provide optical feedback for the cavity. Figure 1.8 shows a schematic of a basic laser resonator cavity. The pump source is used to excite atoms to the upper energy level (as discussed in section 1.1) hence creating population inversion which helps stimulated emission to occur.

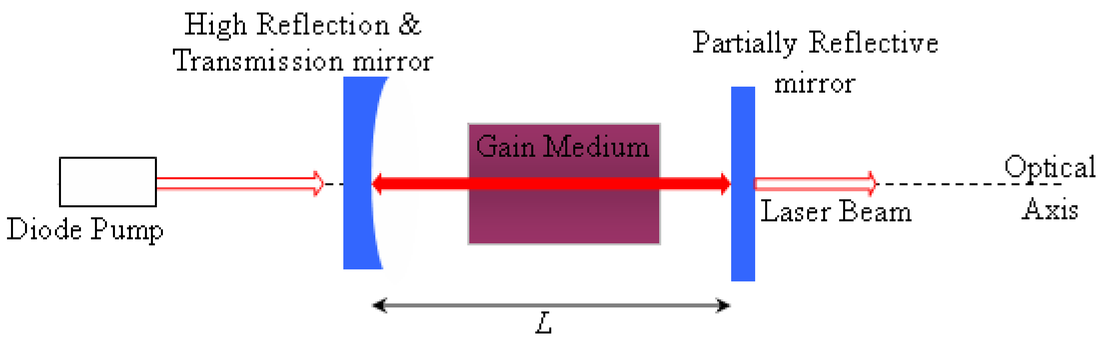

FIGURE 1.8: A schematic of a basic solid-state laser resonator.

If a small number of photons are released by spontaneous emission at the laser frequency along the optical axis, amplification of the photons will occur by means of stimulated emission as they pass through the gain medium. The amplified photons are reflected back into the gain medium by one mirror and get re-amplified as they pass through the gain medium to the other mirror causing more atoms to radiate. The re-amplified photons again undergo further re-amplification as they complete another cycle through the gain medium to the other mirror. The photons are said to complete a cycle when it passes through the length of the cavity twice and if each time it completes a cycle the net gain minus the mirror losses is more than unity, the intensity of the laser increases. One of the mirrors is designed such that it has high transmission at the pump wavelength (input coupler) but highly reflective in the cavity wavelength while the other mirror (output coupler) is partially reflective at the cavity wavelength and has high transmission at the diode pump wavelength. And because the output coupler is partially reflective at the cavity wavelength, it allows a small percentage of the radiation incident on it to transmit through it, to produce the output beam from the cavity.

In the resonator cavity, as the radiation bounces back and forth off the resonator mirrors a standing wave condition is created inside that cavity. The number of these waves whose half-wavelength (nodes) can fit exactly within the cavity is called the cavity longitudinal modes and the transverse field distribution which reproduces itself after one round trip is called its transverse modes. The fundamental of these transverse modes are Gaussian in nature and the field can be approximated using a Gaussian function. Apart from the fundamental Gaussian modes, the resonator can have high-order modes with more complex intensity distributions.

1.3 Proposed Research

1.3.1 Introduction

Laser beams propagating in Laguerre-Gaussian (LG) modes has gained a lot of interest from the community due to their characteristic phase singularity at the center, orbital angular momentum, and multiple connected topology [14][15][16][17]. Laguerre-Gaussian beam, LG_{pl} describe a set of propagation modes and further describes the radial electric field as being proportional to the product of a Gaussian and an associated Laguerre polynomial L_{pl}. If the value of l is greater than zero, the electric field will have an azimuthal phase change of $l\theta$, which results in a phase singularity in the field and a null in the intensity at the center of the beam [67]. These beams have found applications in optical tweezers for macroscopic particles, where they transfer their orbital angular momentum to rotate macroscopic particles causing them to rotate in the direction of helicity of the beams [15]. LG beams are used to write optical waveguides in atomic vapours, the vortex nature is exploited in the study of optical applications. LG modes can be generated in a laser cavity [9][16][18][19] or by subsequently converting a Hermite-Gaussian beam to LG beam [14], or the use of a diode lasers source and applying extra-cavity conversion of Gaussian beams to LG modes. Some of the extra-cavity methods include spiral phase plates [17], computer generated holograms [20] and diffractive optics [21].

1.3.2 Problem Statement

The generation of donut shaped laser beams has been of great interest to the community in recent times. Many intra-cavity beam shaping techniques have been employed to produce donut beams. Some of these techniques include (but not limited to) amplitude aperture and the use of diffractive optical elements. Generally, most intra-cavity beam shaping methods achieve mode selection by introducing low losses to the desired mode and very high losses to every other mode thereby allowing only the desired mode to oscillate in the cavity.

The use of amplitude absorbing (concentric) rings in combination with an aperture to select LG modes in the cavity is a well known technique [22] [23] but the challenges with these methods are that they require re-alignment of the optical setup and the fabrication of a new optical component each time a new LG mode is required. In our approach we demonstrated intra-cavity LG mode selection using the spatial light modulator (SLM) as the mode selecting element [24], which requires only a different grey-scale image to be displayed on the SLM when a new mode is to be selected and no re-alignment of the optical setup is required.

1.3.3 Aim

The aim of this project is to generate intra-cavity high-order Laguerre-Gaussian modes in a solid state laser resonator.

1.3.4 Objectives

To achieve the above mentioned aim, the following objectives were outlined:

1. To build a diode pumped solid state laser resonator cavity.

2. To selectively generate high-order Laguerre-Gaussian modes inside a laser resonator cavity.

3. To test the purity of these generated Laguerre-Gaussian modes.

4. To determine and confirm the quality of the generated laser beam.

1.3.5 Literature Review

Shaping of the output beam of a laser resonator cavity is almost as old as the discovery of laser itself. Beam shaping can be done outside the cavity (extra-cavity) or inside the resonator cavity (intra-cavity). The default intensity distribution of a stable resonator is mostly Gaussian. And the extra-cavity conversion from Gaussian beam to LG propagating modes has been done using spiral phase plates [20], computer generated holograms [21] and diffractive optics [23]. These methods can be used to convert a Gaussian beam into LG_{pl} mode, as well as convert between any two LG_{pl} modes [25][17].

In general, most intra-cavity mode selection methods involve the introduction of the mode selection element inside the resonator cavity in order to introduce low losses for the desired mode and very high losses for all other modes. The application of the technique of amplitude aperture and diffractive optical elements for example, graded phase mirrors, binary and spiral phase plates have been used many times for mode selection in resonator cavities [26]. The insertion of a circular amplitude aperture into the resonator is one of the simplest mode selection methods to obtain the fundamental Gaussian mode. The selection of many single low-order LG modes inside the resonator cavity can be achieved by a combination of wires with an aperture of adjustable size [19]. Also, pump beam shaping can be used to control the cross-section intensity distribution profile of the mode that can oscillate in a diode pumped solid state laser resonator cavity [27]. And it has also been shown that intra-cavity lenses with spherical aberration can be used to perform LG mode selection [19] [28]-[32].

The fundamental Gaussian mode of a stable laser resonator although of good quality is usually of low power. So, to generate high power lasers some [33]-[35] have considered increasing the power of the optical pump source to extract maximum power from the gain medium at low-order modes. But this approach looses out in that it is not utilizing the power that is available at high-order modes from their mode volume hence it is not considered efficient. While other approaches [36][37] have considered selecting high-order modes to maximize power extraction from the laser resonator cavity (although of low quality), then consider extra-cavity improvement of the beam quality factor of the modes.

In this project, the approach that is counter intuitive is considered to increase the laser power using intra-cavity selection of high-order LG modes. We propose exciting high-order LG modes that are not known to have good beam quality. Our research study is that since such modes have a larger mode volume [23], more power will be extracted from the laser resonator cavity. Moreover, if we can ensure that we excite pure high-order LG modes, the output laser from the resonator cavity will both be of high power and of good quality. Our aim is to select such modes using intra-cavity phase and amplitude techniques, and to consider the mode purity and laser efficiency.

In our method, one of the resonator cavity coupling mirrors was a spatial light modulator (SLM) on which was encoded different amplitude absorbing masks (rings) that corresponded to the desired LG modes that were selected [24]. The method of using intra-cavity absorbing rings for beam shaping has been employed before to generate high-order LG modes by many others [22][23]. The later requires re-alignment and fabrication of new optical components each time a new LG mode is desired. But this research investigation required encoding the amplitude absorbing rings on the SLM so that for any new desired LG mode what was required was the change of the phase mask on the SLM and the desired mode was selected in the cavity. There was no need for re-alignment of the optical setup. Also, mode purity and cavity efficiency was determined.

1.3.6 Methodology

1. First, with a Hamamatsu (LCOS-SLM X110468E) SLM, 1% doped Nd:YAG crystal rod (30 mm length by 2 mm radius) as gain medium, a 75 W high power Jenoptik (JOLD 75 CPXF 2P W) laser diode pump (at 808 nm wavelength) and a partially reflective (60% reflectivity at 1064 nm) flat mirror output coupler were assembled in an end-pumped hemispherical cavity configuration. The digital hologram (grey-scale

image) of a lens was programmed on the SLM, with focal length $f = R$, so that the SLM mimics the curvature of a mirror with radius of curvature R. The laser diode was used to end-pump the Nd:YAG crystal with the SLM (concave mirror) and flat mirror setup in a L-shaped cavity design and the stability of the cavity was tested. The beam quality factor of the output Gaussian laser mode was measured (using Photon Inc Modescan 1780 camera).

2. Second step was on the resonator setup, using symmetric LG mode function of zero azimuthal order ($l = 0$) LG_{p0}, to generate digital holograms that corresponds to amplitude absorbing rings (masks) for the LG_{p0} modes (using the second order intensity moment, $I(r,z) = |E_{p0}(r,z)|^2$) for p equal to 0, 1, 2 and 3. And for each of these LG_{p0} modes, the corresponding digital hologram was combined with that which mimics the curvature of a lens. Then, the combined digital hologram was programmed on the SLM. When the laser diode optical pump source was switched on, the amplitude absorbing masks allowed only the desired single order (p) mode to oscillate in the resonator cavity to produce LG_{p0} modes.

3. To confirm the purity of each p mode the near- and far-fields laser beam width was measured, and $w_{p0} = w_0\sqrt{2p+1}$ was used to calculate the near-field size (where w_{p0} is the high-order mode width and w_0 is the Gaussian field beam width). The experimental data was compared with the theoretically calculated data.

4. To ascertain the quality of the output laser, measurement of the M^2 beam quality factor of the modes was done with M^2 camera (Photon Inc Modescan 1780). The measured beam quality factor of each mode was also compared with the theoretically calculated one for the corresponding high-order mode to show that they are of good quality.

5. And finally the power of the output laser was measured and the graph of the optical slope-efficiency of the resonator cavity was plotted and path to achieve a high power laser was demonstrated.

This new approach may be used to realize future high brightness lasers, which would certainly be of relevance to applications where a high power must be delivered in a reasonable size at a distant target.

1.4 Dissertation Outline

This section gives the structure of the study.

Chapter one presented an introduction to Lasers, optical resonator cavity, and the proposed research work. The aim and objective were outlined and the method used in achieving them was also briefly introduced.

Chapter two presents some of the modes that can oscillate in a stable resonator cavity. The default Gaussian mode of a stable resonator was discussed with its properties and the field parameters were presented. High-order modes of a stable resonator in rectangular and cylindrical coordinate were also presented.

Chapter three presents a synthesis of literature on the different intra-cavity beam shaping techniques. A detailed discussion on the use of the spatial light modulator (SLM) and the concept of the digital laser were given since that is the techniques that were employed in the experiment to perform intra-cavity beam shaping.

Chapter four presents the methodology used in our experiment to setup a diode pumped solid state laser resonator and how we used digital hologram on the intra-cavity SLM to perform LG mode selection.

Chapter five presents the results and analysis. This is where the findings of the research are presented.

Chapter six presents conclusion and future work. The conclusions that were drawn from the findings, limitations of the research and future work are also presented.

1.5 Summary

In this chapter the fundamentals of Lasers, the proposed research work and structure of this dissertation were presented.

As an introduction the basic principle, components and operation of a laser was presented. Photons' interaction with matter; photon absorption, spontaneous and stimulated emissions of radiation were elaborated upon. A four-level laser scheme was described. The basic components of a laser resonator cavity were also presented, which includes: an optical pump source, two mirrors and a laser gain medium. The material properties for a good laser gain medium were outlined and the stability condition of the resonator cavity was also explained. The end- and side-pumped geometries were discussed with some advantages of end-pumped over the latter. The operating principle of a simple diode pumped solid state laser resonator that uses a Nd:YAG crystal as gain medium was also explained.

This chapter also presented an introduction to the proposed research work, the problem statement and aim. The objectives were outlined and a brief introduction of the methodology that was employed to achieve the listed objectives using an intra-cavity SLM as a mode selecting element were also given. Finally the structure of the dissertation was presented.

Chapter 2

Resonator Cavity's Transverse mode

2.1 The Gaussian Beam

In a resonator cavity as the radiation propagates forward and backward at a steady state condition, longitudinal and transverse modes develop in the cavity which is separated in frequency in their standing waves. This separation is linked with the different modes in the resonator. The longitudinal modes are as a result of the reflectivity peaks of the resonator that are within the spectral width of its gain medium. These modes correspond to a set of equally spaced discrete frequencies $\omega_q(\omega_q = 2q\pi(c/2L))$, that represents the resonant frequencies at which there are exactly q half-wavelengths along the resonator axis between the two mirrors at steady-state oscillation case [1]. Where q is the index label for each resonant frequency axial mode and denotes a longitudinal mode and L is the length of the cavity.

The Transverse mode refers to the field distribution in a plane perpendicular to the axis of propagation (optical axis) of the resonator. Similar to the longitudinal modes the transverse modes also correspond to a set of discrete frequencies $\omega_q(\omega_q = (q\pi + (n + m + 1)\cos^{-1}(g_1 g_2))(c/L))$ [1]. But the frequency spacing between modes are not just dependent on the length of the cavity, L only but also on the curvature of the mirrors. The resonant frequencies of these modes can be expressed not only in Cartesian coordinate but also in cylindrical coordinate by replacing the $(n+m+1)$ term with $(2p+l+1)$ [3]. Where the indices m, n, p and l represent a particular transverse mode.

2.1.1 The Gaussian Electric Field

In a laser resonator, the radiation will spread as it bounces between the mirrors and suffer distortion in its transverse amplitude and phase profile due to diffraction effects caused by the aperturing of the mirrors and gain medium. This radiation will oscillate roughly in the form of a uniform quasi-plane-wave [1] and this wave is approximated as a paraxial wave situated about the axis of propagation. This gives room for the spherical wavefront of the radiation to be approximated using parabolic approximation [38]. There are two principle approaches that have been applied in understanding the propagation of the paraxial waves; the first is the differential approach through the paraxial wave equation and the second is an integral approach which employs Huygens' Principle expressed in the Fresnel approximation. The latter has been adequately used to describe the properties of optical resonators [39]. The Paraxial wave of the electric field can be described as a scalar wave quantity given by:

$$\widetilde{E}(x,y,z,t) = \widetilde{E}(x,y,z)\exp(i\omega t), \tag{2.1}$$

where ω is the angular frequency, x, y and z are the Cartesian coordinate, while $\widetilde{E}$ is the phasor amplitude of any vector component of an electric field. A solution for the fields amplitude at some z position for a given initial field distribution $\widetilde{E}(x_0, y_0, z_0)$ in the propagation plane can be obtained using the Fresnel-Kirchoff integral. The general solution that corresponds to a spherical wave diverging from a source point is given as [1]:

$$\widetilde{E}(r, r_0) = \frac{1}{\rho(r, r_0)}\exp(-ik\rho(r, r_0)), \tag{2.2}$$

where $\widetilde{E}(r, r_0)$ is a field at point r due to a source at position r_0 and $\rho(r, r_0)$ is the distance from the source point s_0 to the plane s along the propagation axis z (Figure 2.1) given as

$$\rho(r, r_0) = [(x - x_0)^2 + (y - y_0)^2 + (z - z_0)^2]^{-1/2}. \tag{2.3}$$

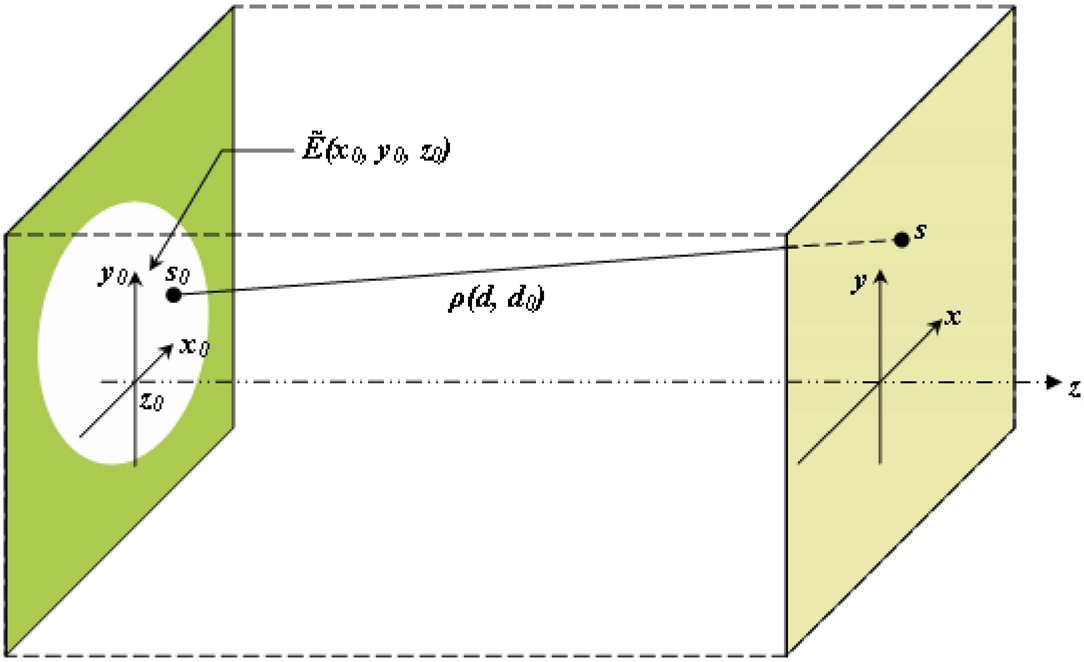

FIGURE 2.1: Illustration of the relationship between some initial electric field at point d_0 and integrated field d using Fresnel-Kirchoff integral.

For an electric field at some transverse position x, y along the axis of propagation of this spherical wave (Figure 2.1), the Fresnel approximation to diffraction indicates that the distance $\rho(r, r_0)$ may be expanded in a power series. We can neglect all terms higher than the quadratic term in this expression as the Fresnel approximation assumes that the contribution of the high-order terms to the complex component is relatively small compared to the quadratic term. We can thus approximate a spherical wave by a quadratic phase variation as observed on a transverse plane at a distance $z - z_0$ from the source point.

The Huygens' integral suggests that physically, for any incident field $\widetilde{E}(x_0, y_0, z_0)$ over a closed surface S, the field at each point on the surface is regarded as the source for a uniform spherical wave which radiates from that point and is termed a Huygens' wavelet (Figure 2.2). The total field at a new position (s, z) within or beyond the closed surface can be calculated as sum of the Huygens' wavelets coming from all points on the closed surface. A spherical wave approximation is now connected with the Huygens' integral. Generally, the wavelets can be treated as spherical waves with the form of equation (2.1) and it leads to the Huygens' integral equation of the form [1] given by

$$E(s,z) = \frac{i}{\lambda} \iint_S \widetilde{E}_0(s_0, z_0) \frac{\exp[-ik\rho(r, r_0)]}{\rho(r, r_0)} \cos\theta(r, r_0) dS, \tag{2.4}$$

where $\widetilde{E}_0(s_0, z_0) = \widetilde{E}(x_0, y_0, z_0), i/\lambda$ is a normalization factor and $\cos\theta(r, r_0)$ is the obliquity factor which is the angle between a line joining the two points by the distance $\rho(r, r_0)$ and the normal to the surface element dS (Figure 2.3). If the angle θ is limited to small values, the factor becomes approximately equal to 1.

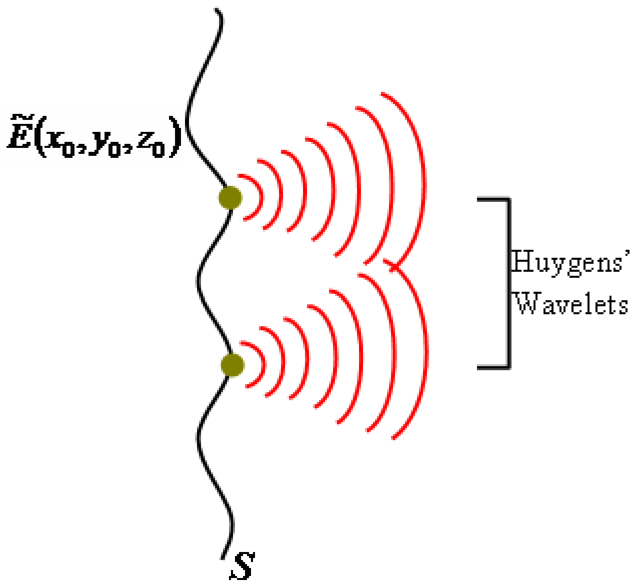

FIGURE 2.2: A Simple illustration expressing Huygens' Principle [1].

Using an initial field and substituting the spherical wave approximation into the same component in equation (2.4), an output field $\widetilde{E}(x, y, z)$ at a distance $z = z_0 + L$, can be obtained from the Huygens' integral in the Fresnel approximation as [1]:

$$\widetilde{E}(x,y,z) = \frac{i\exp(-ik(z-z_0))}{\lambda(z-z_0)} \iint \widetilde{E}_0(x_0, y_0, z_0) \exp\Big(-ik\frac{(x-x_0)^2 + (y-y_0)^2}{(z-z_0)^2}\Big) dx_0 dy_0, \tag{2.5}$$

where $\widetilde{E}_0(x_0, y_0, z_0)$ is the initial electric field distribution at a point (x_0, y_0, z_0) in space, (x, y, z) is some new point in space, x and y represent the transverse variation from x_0 and y_0 respectively, and $z = z_0 + L$, where L is the longitudinal distance. In equation (2.4) the obliquity factor is approximately equal to 1 as the denominator, $2(z{-}z_0)$ is large and the change in the transverse coverage of the wave is small for the propagation over the distance L.

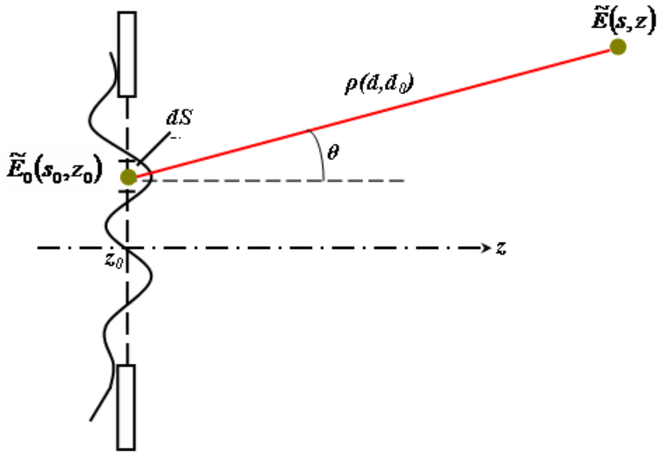

FIGURE 2.3: Illustration showing geometrical realization for the evaluation of Huygens' integral in the Fresnel approximation [1].

The Huygens' integral in the Fresnel approximation can be used as the basis of determining specific laser modes which oscillate in the laser resonators. The eigensolutions to equation (2.5) represent these electric field distribution. It is very good to get an analytical form of a Gaussian wave and then show that it is indeed an eigenfunction of equation (2.5)

The electric field in equation (2.4) produced as a result of the application of Fresnel approximation in the paraxial approximation can be written in the form of a complex scalar wave amplitude given as [1]:

$$\widetilde{u}(x, y, z) = \frac{1}{R^{'}(z)} \exp\left[-ik\frac{(x{-}x_0)^2 + (y{-}y_0)^2}{2R^{'}(z)}\right], \tag{2.6}$$

where the radius of curvature of this wave at the z plane is $R^{'}(z) = z{-}z_0$. The expression for the radius of curvature in the general form is given as $R^{'}(z) = R_0 + z{-}z_0$, where R_0 is the radius of the initial field. The spherical wave's amplitude extends to infinity in the transverse direction as opposed to falling off from the axis. So this spherical wave is therefore not useful physically and we consider the possibility of complex values for the point coordinates. To simplify the procedure we set the values of x_0 and y_0 to be equal to zero and consider z_0 as complex parameter by substituting it for an arbitrary complex parameter $\widetilde{q}_0$. One can then express the radius of curvature as $R^{'}(z) = \widetilde{q}(z) = \widetilde{q}_0 + z{-}z_0$, where $R_0 = 0$ with the introduction of a new parameter, the complex radius of curvature, $\widetilde{q}(z)$. $\widetilde{q}(z)$ has real and imaginary parts given as $\left(\frac{1}{\widetilde{q}(z)} \equiv \frac{1}{q_r(z)} - \frac{i}{q_i(z)}\right)$. Applying this expression in equation (2.6) we have [1]:

$$\widetilde{u}(x, y, z) = \frac{1}{\widetilde{q}(z)} \exp\left[-ik\frac{x^2 + y^2}{2q_r(z)} - k\frac{x^2 + y^2}{2q_i(z)}\right], \tag{2.7}$$

Considering equation (2.7) for this complex source beam, the exponential term has an imaginary and real quadratic transverse variation. The imaginary variation corresponds to a quadratic phase front considered to be a spherical wave with a real radius of curvature and the real variation gives a Gaussian amplitude where the transverse fall off from the axis is determined from the imaginary part of $\frac{1}{\widetilde{q}(z)}$. Incorporating this result in equation (2.7) we have a complex scalar wave amplitude given as

$$\widetilde{u}(x, y, z) = \frac{1}{\widetilde{q}(z)} \exp\left[-ik\frac{x^2 + y^2}{2R(z)} - \frac{x^2 + y^2}{2w^2(z)}\right], \tag{2.8}$$

where $R(z)$ is the real radius of curvature and $w(z)$ is the Gaussian beam size. These terms at any plane z can be derived from the complex radius of curvature as

$$\frac{1}{\widetilde{q}(z)} = \frac{1}{R(z)} - i\frac{\lambda}{\pi w^2(z)}. \tag{2.9}$$

For a Gaussian beam, the electric field is commonly expressed as [1]

$$\widetilde{E}(r, z) = E_0 \frac{w_0}{w(z)} \exp\left[\frac{-r^2}{w^2(z)}\right] \exp\left[-ikz - ik\frac{r^2}{2R(z)} + i\phi(z)\right], \tag{2.10}$$

where E_0 is a constant, w_0 is the beam waist and $r = (x^2 + y^2)^{1/2}$ is the radial beam coordinate. The phase of this field is comprised of a plane wave kz, and a phase retardation component $\phi(z) = \arctan(\lambda z / n w_0^{-1/2})$ called the Guoy phase shift.

2.1.2 The Gaussian Beam Width and Curvature

The complex radius of curvature, $\widetilde{q}(z)$ of some field at a position along the propagation axis which is at distance z relative to an initial position of curvature $\widetilde{q}_0(z)$ is given as:

$$\widetilde{q}(z) = \widetilde{q}_0(z) + z. \tag{2.11}$$

Equation (2.11) may be rewritten differently as $\big(1/\widetilde{q}(z) = 1/(\widetilde{q}_0(z) + z)\big)$ to be consistent with equation (2.9). If we assume that the initial complex curvature $\widetilde{q}_0(z)$ has an infinite real curvature at a position where z is equal to zero ($z = 0$), to simplify equation (2.9) we have $1/\widetilde{q}(z) = -i\lambda/\pi w_0^2$. Substituting this expression and equation (2.9) into equation (2.11) we get the expressions for the real radius of curvature $R(z)$ and the Gaussian beam width $w(z)$ [1]

$$R(z) = z\left[1 + \left(\frac{\pi w_0^2}{\lambda z}\right)^2\right] = z\left[1 + \left(\frac{z_R}{z}\right)^2\right] \tag{2.12}$$

and

$$w^2(z) = w_0^2\left[1 + \left(\frac{\lambda z}{\pi w_0^2}\right)^2\right] = w_0^2\left[1 + \left(\frac{z}{z_R}\right)^2\right], \tag{2.13}$$

where $z_R\big(= \pi w_0^2/\lambda\big)$ is called the Rayleigh range. It is the distance from the beam waist w_0 to a spot where the width is larger by a factor of $\sqrt{2}$ ($\sqrt{2}w_0$) (Figure 2.4).

2.1.3 Divergence

The divergence of a laser beam results from the fact that the beam width, $w(z)$ increases as the beam propagates. If the propagation distance is much larger than the Rayleigh range, $z \gg z_R$, the beam width increases linearly with propagation distance and $w(z)$ can be written as [1]

$$w(z) \approx \frac{\lambda}{\pi w_0} z. \tag{2.14}$$

The far field angular divergence, θ_0 is given by

$$\theta_0 \approx \frac{\lambda}{\pi w_0}. \tag{2.15}$$

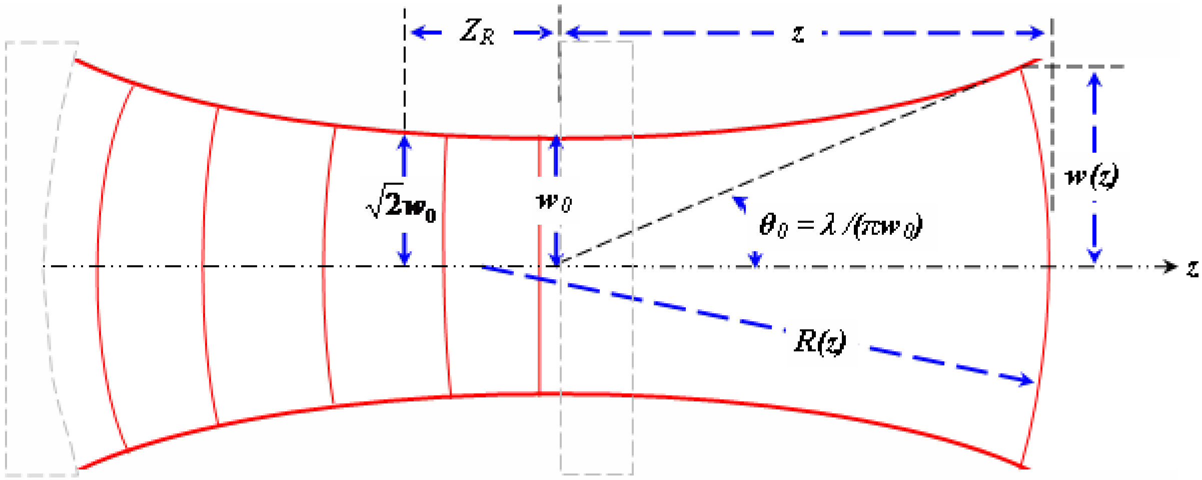

FIGURE 2.4: Divergence of a Gaussian beam in free-space due to diffraction [7].

2.1.4 Intensity

The optical intensity, I of a laser beam can be defined as the optical power per unit area, which is transmitted through an imagined surface perpendicular to the axis of propagation [41]. Generally speaking, the Gaussian beam has its peak intensity at the waist position, where the over-all peak intensity occurs at the mid point of the beam ($r = 0$ and $z = 0$).

The expression for the optical intensity of any laser beam is given as $I(r, z) \propto |E(r, z)|^2$. Its units are $\mathrm{Wm^{-2}}$ or $\mathrm{Wcm^{-2}}$. A Gaussian beam has its intensity given as [1]

$$I(r, z) = I_0 \left[\frac{w_0}{w(z)}\right]^2 \exp\left[-\frac{2r^2}{w^2(z)}\right], \tag{2.16}$$

where I_0 is the peak intensity, w_0 is the radius of the beam waist, r is the radius of the beam at a propagation distance z. Figure 2.5 is the intensity distribution profile of a Gaussian beam showing the intensity plotted against size and inset is a two dimensional density plot.

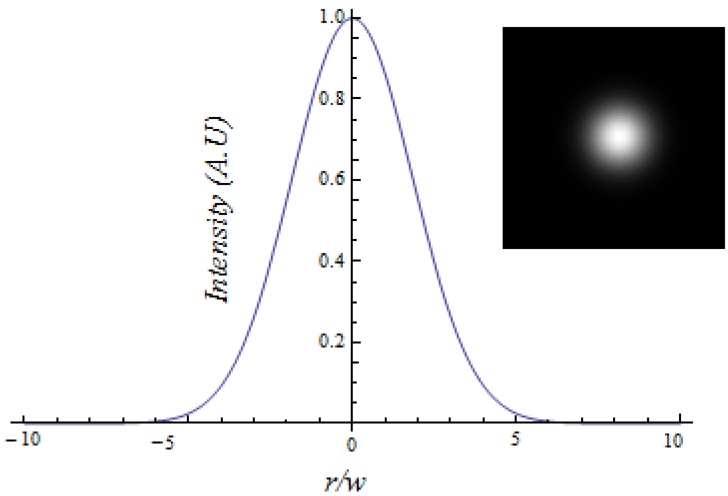

FIGURE 2.5: The graph of Gaussian beam intensity profile where inset is a transverse image of the beam.

2.1.5 Beam power

The power of an optical beam is the integral of the optical intensity over some finite transverse plane given as [1]

$$P = \int_0^\infty I(r) 2\pi r dr. \tag{2.17}$$

A Gaussian's beam power is given by half the product of the peak intensity and beam area which is independent of propagation distance z. The power enclosed in a circle of $r_0 = w(z)$

about the optic axis in the transverse plane is about 86% of the total power of the beam. The total power of a Gaussian beam is given by

$$P = \frac{1}{2} I_0 \Big(\pi w_0^2\Big). \tag{2.18}$$

2.1.6 The M^2 Beam Propagation Factor

The beam propagation factor or the M^2 factor or beam quality factor is a measure of a real beam's deviation from the "ideal" Gaussian mode, both in amplitude and in phase [6] [7] [42]. The M^2 factor is a standard developed by ISO [43] to be used to test the quality of a laser beam. This actually tells us by how much the far-field angular spread compares to a Gaussian mode and helps one to determine the near-field size from the far-field size and vice-versa. It is also defined as the beam parameter product divided by λ/π, the beam parameter product for a diffraction-limited Gaussian beam at the same wavelength. A definition of beam width which is pertinent in the development of M^2 factor, is the variance of the intensity or field of a beam. Every real laser beam's propagation is known [41] to follow a simple rule for the change in beam size with propagation distance if the beam size is defined as the second moment of the intensity [39][44]. Expressed differently, the beam propagation factor tells how the real beams parameter product compare to that of a diffraction limited Gaussian beam at the same wavelength, given as

$$M^2 = \frac{\theta w_0 \pi}{\lambda}, \tag{2.19}$$

where w_0 is the beam waist.

2.1.7 Laser Brightness

The brightness, B of a laser beam is defined by the power density per solid angle of the radiation from a light source [5] [40]. It is particularly important because it gives the idea of how much a laser beam can achieve high intensities while still maintaining a large Rayleigh range for small focus angles [9]. A source with constant brightness is said to be isotropic [10] and brightness is given as [44]

$$B = P\left(\frac{\pi}{\lambda M^2}\right)^2 \tag{2.20}$$

where P is either the average or the peak power at the output, λ is the wavelength and M^2 is the beam quality factor. Hence, excellent beam quality and high output power is required for high brightness.

2.1.8 The Gaussian Beams in Laser Resonators

As earlier stated, the fundamental mode of a stable resonator is considered to be the Gaussian mode and particularly that which comprise of two curved mirrors. Light beam that bounces back and fourth between the resonator cavity mirrors experiences periodic focusing action. Modeling of laser resonators allows for the curvature of the cavity mirrors to be expanded as a set of periodic focusing system of lenses and if diffraction can be ignored the Gaussian mode can be confined between the mirrors in the cavity. This will be so if the dimensions of the mirrors are very large as compared to the beam width on the two mirrors. If the radii of curvature of the mirrors match that of the wavefront of the (incident) Gaussian mode on each of them, the beam will be reflected back exactly on itself with an exact reversed wavefront curvature and direction.

In determining high-order modes formation and propagation within the resonator, the Gaussian beam is fundamental and that is why the Gaussian beam width on each mirror is a very important factor. Let us consider a resonator of length L with a curved mirror (M_1) and flat mirror (M_2) of radii of curvatures R_1 and R_2 corresponding to the back reflector and the output coupler respectively (Figure 2.6). The length of the cavity L is equal to the distance d_1 of the Gaussian beam waist from the width w_1 on mirror M_1, while the distance d_2 of beams waist from mirror M_2 is zero since the beams waist occurs exactly on the flat mirror. Including some of the unknown quantities in Figure 2.6 is the beam waist w_0 and inherently the Rayleigh rage $z_R = \pi w_0^2/\lambda$. As the beam propagates inside the cavity between the two mirrors its curvature changes, and an important condition for a stable state Gaussian oscillation is that the Gaussian beam must match the curvature of the mirror that it is incident on. After taking into account the length of the resonator, we have these equations [1]:

$$R(d_1 = L) = L + z_R^2 = -R_1, \tag{2.21}$$

$$R(d_2 = 0) = \infty = +R_2, \tag{2.22}$$

$$L = -d_1. \tag{2.23}$$

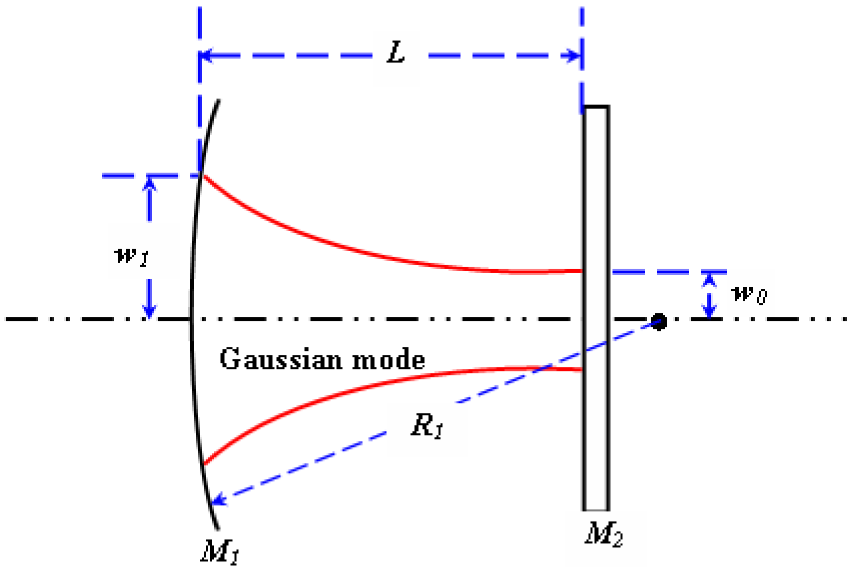

FIGURE 2.6: Mode parameters of a resonator which sustains Gaussian beam oscillation.

The flat mirror M_2 is considered to have a positive radius of curvature, and mirror M_1 a negative radius of curvature relative to the beam waist, hence d_1 is considered to be a negative distance. As previously mentioned, the geometric parameters of a resonator are $g_1 = 1 – L/R_1$ and $g_2 = 1 – L/R_2$ for the mirrors M_1 and M_2 respectively. Using these g-parameters and the equations (2.21) to (2.23), the Rayleigh range of the Gaussian beam contained between the mirrors are given by [45]:

$$z_R^2 = \frac{g_1}{1-g_1} L^2 \tag{2.24}$$

and the position of the mirrors relative to the beam waist position is given as

$$z_1 = L \qquad \text{and} \qquad z_2 = 0. \tag{2.25}$$

Using equations (2.24) and (2.25), we then have the beam waist width to be given as:

$$w_0^2 = \frac{L\lambda}{\pi}\sqrt{\frac{g_1}{1-g_1}}. \tag{2.26}$$

From this result in combination with equations (2.13) and (2.25) the beam width on the two mirrors are given as

$$w_1^2 = \frac{L\lambda}{\pi}\sqrt{\frac{1}{1-g_1}} \qquad \text{and} \qquad w_2^2 = w_0^2 = \frac{L\lambda}{\pi}\sqrt{\frac{g_1}{1-g_1}}. \tag{2.27}$$

The widths of the beam on the mirrors and propagation within a stable laser (hemispherical) resonator cavity may be determined by the use of these equations. The Gaussian mode is frequently the first oscillation mode above laser threshold, however higher input power allows modes of other frequencies to also oscillate and coexist with the Gaussian mode in the cavity. These high-order modes are also eigensolutions of equation (2.5) and can be expressed in rectangular and circular symmetry that correspond to Hermite-Gaussian and Laguerre-Gaussian modes respectively.

At high input power when multiple modes are oscillating simultaneously in the cavity, the Gaussian mode cannot be distinguished from all the other modes and the common technique of selecting only a Gaussian mode is to introduce an intra-cavity aperture along the propagation axis. The size of the aperture is selected such as to introduce high losses to all the high-order modes but low (or no) losses to the Gaussian spot size depending on the position of the aperture inside the cavity.

2.2 High-order cavity modes

The Gaussian mode is considered to be the fundamental mode of a stable resonator particularly those consisting of two curved mirrors. Again, when modeling laser resonators the curvatures of these mirrors allows them to be expanded as a stable periodic focusing system of lenses. Steady-state solutions to the Huygens' integral in the Fresnel approximation are represented by eigensolutions of this equation. When this integral is solved analytically it yields an infinite number of eigensolutions and the shape and size of the mirrors determines which eigensolution will represent oscillating mode or set of oscillating modes [9]. The geometry of the mirrors sets the boundary condition in the eigensolutions especially if the mirrors are rectangular or circular. Eigensolutions that have either rectangular or circular symmetry will then be the oscillation mode selected in the laser resonator cavity and these symmetries correspond to Hermite-Gaussian and Laguerre-Gaussian modes respectively.

2.2.1 Hermite-Gaussian mode

There are many solutions to the Huygens integral in the Fresnel approximation in rectangular symmetry that resembles Hermite-Gaussian cross section. This family of solutions may be separated from one another in their vertical and horizontal directions. In the same way as in the Gaussian beams case, a trial solution to equation (2.5) is proposed and we can determine a propagation dependent electric field eigensolution for the family of rectangular symmetry as [13]:

$$\begin{aligned} E_{mn}(x,y,z) &= \frac{E_0}{\sqrt{1+(z/z_R)^2}} \exp\left[-\left(x^2+y^2\right)\left(\frac{1}{w_0^2(z)}+\frac{ik}{2R(z)}\right)\right]\times \\ & H_m H_n\left[\frac{2xy}{w_0^2(z)}\right]\exp\left[-i(m+n+1)\arctan\left(\frac{z}{z_R}\right)\right], \end{aligned} \tag{2.28}$$

where E_0 is a constant, z_R is the Gaussian Rayleigh range, $w_0(z)$ is the Gaussian beam width at a propagation distance z and H_m and H_n are Hermite polynomials. The indices m and n are the transverse electric field distribution mode index in the horizontal and vertical direction respectively, denoted by TEM_{mn}. When $m = n = 0$, $E_{00}(x, y, z)$ yields a Gaussian field distribution. The intensity of these eigenmodes is given as $I(x, y, z) \propto |E(x, y, z)|^2$ and Figure 2.7 is the transverse intensity profiles for different rectangular symmetric modes. The Hermite-Gaussian mode intensity is used to infer the beam width using the second order intensity moments which yields analytically [40]:

$$w_{m,n}(z) = w_0\sqrt{2(m+n)+1}\sqrt{1+\left(\frac{z}{z_R}\right)^2}, \tag{2.29}$$

where w_0 is the Gaussian waist width and m and n are the mode indices. The Hermit-Gaussian waist width and far field divergence are given as $w_{m,n} = w_0\sqrt{2(m+n)+1}$ and $\theta_{m,n} = \theta_0\sqrt{2(m+n)+1}$ respectively. And also, the beam propagation factor for the Hermit-Gaussian modes is given as [44]:

$$M^2_{m,n} = 2(m+n)+1. \tag{2.30}$$

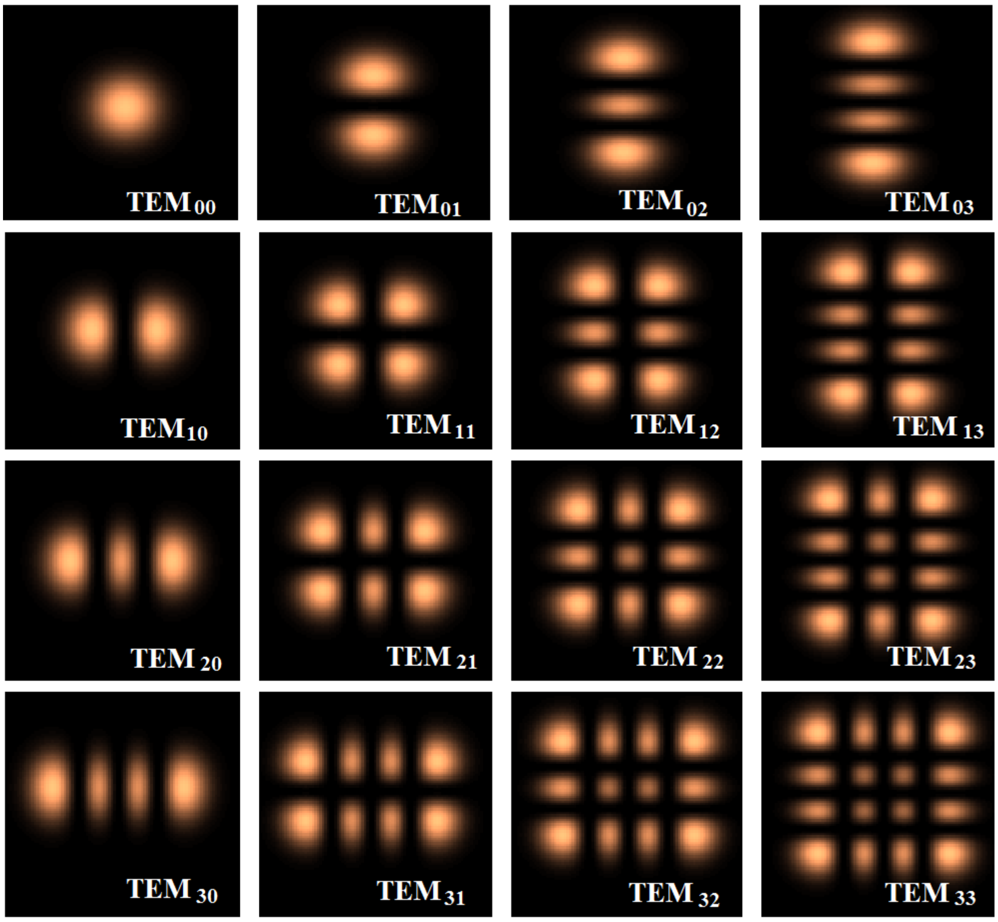

FIGURE 2.7: Mathematically generated transverse intensity distribution profile of Hermit-Gaussian TEM_{mn} modes.

2.2.2 Laguerre-Gaussian modes

The trial solution to the Huygens integral in the Fresnel approximation can also be derived in circular symmetry which corresponds to the Laguerre-Gaussian cross section as in the Hermite-Gaussian case. This family of solutions can be represented as LG_{pl}, where p is the radial order and azimuthal order is, l. The electric field distributions of the eigensolutions to equation (2.5) is given as [44]:

$$
\begin{aligned}
E_{pl}(r,\phi,z) \qquad &= \frac{E_0}{\sqrt{1+(z/z_R)^2}}\exp\left[-r^2\left(\frac{1}{w_0^2(z)}+\frac{ik}{2R(z)}\right)\right]L_{pl}\left[\frac{2r^2}{w_0^2(z)}\right]\times \\
&\exp(il\phi)\left[\frac{\sqrt{2}r^2}{w_0(z)}\right]^{|l|}\exp\left[-i(2p+|l|+l)\arctan\left(\frac{z}{z_R}\right)\right], \qquad (2.31)
\end{aligned}
$$

where r and ϕ are the radial and azimuthal coordinates respectively, E_0 is a constant, the Gaussian beam width at some propagation position z is $w_0(z)$, l is the azimuthal mode index, p is the radial mode index and L_{pl} is the generalized Laguerre polynomial. The intensity is also given by $I(r,\phi,z) = |E_{pl}(r,\phi,z)|^2$. Figure 2.8 is the circular symmetric transverse intensity distribution profile of different LG modes. LG_{00} is the lowest order Laguerre-Gaussian mode which is a pure Gaussian mode. Using the second order intensity moments, the analytical solution to the beam width is given as [41]:

$$
w_{pl}(z) = w_0\sqrt{2p+|l|+1}\sqrt{1+\left(\frac{z}{z_R}\right)^2}. \qquad (2.32)
$$

The expression for the Laguerre-Gaussian waist width and far-field divergence are $w_{pl} = w_0\sqrt{2p+|l|+1}$ and $\theta_{pl} = \theta_0\sqrt{2p+|l|+1}$ respectively. The beam propagation factor is given as:

$$
M_{pl}^2 = 2p+|l|+1. \qquad (2.33)
$$

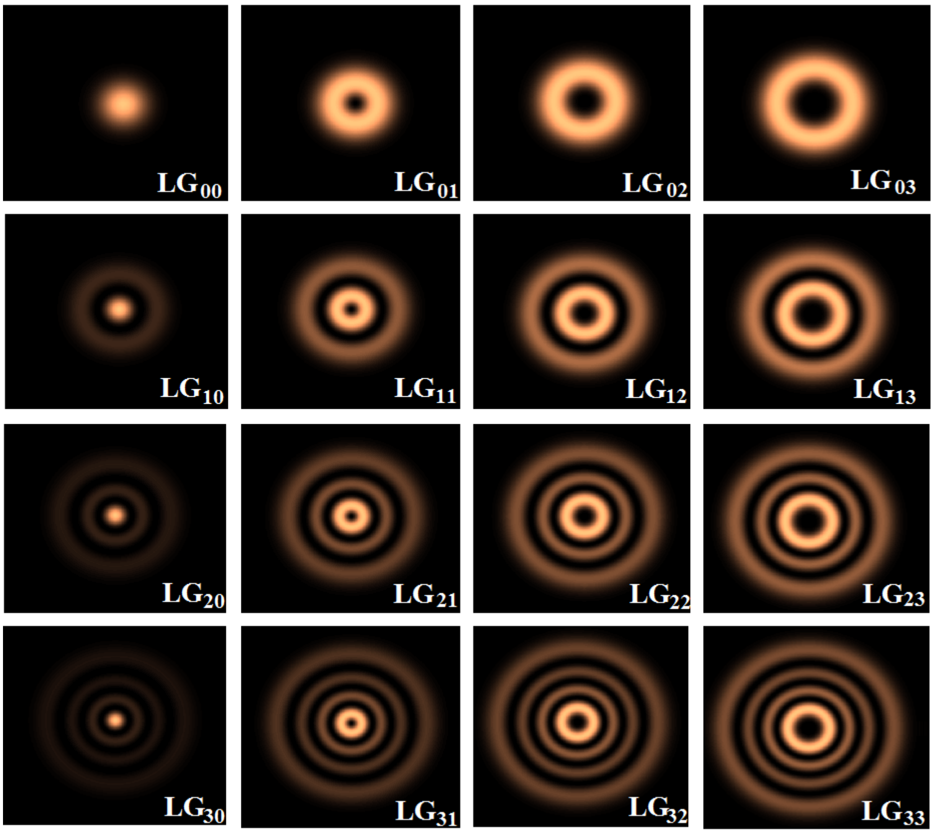

FIGURE 2.8: Mathematically generated transverse intensity distribution profile of LG_{pl} modes.

When circulating in optical resonators, modes of the same order experience same resonance conditions, due to $\exp(i(2p + |l| + 1) \arctan(z/z_R))$ phase term, so that the cavity has a degenerate family of modes. LG_{pl} modes have a characteristic ringed shape because of the L_{pl} term, while the azimuthal phase index $\exp(il\phi)$ is responsible for the orbital angular momentum of $l\hbar$ per photon [4].

2.2.2.1 Orbital Angular Momentum

It is a well known fact that orbital angular momentum (OAM) may be associated with the spatial distribution of light. Laser beams that possess OAM have helical phase front [14] and hence have azimuthally-varying Poynting vector. The electric field or mode of such beam has an azimuthal angular dependence of $\exp(il\phi)$ and carries OAM of $l\hbar$ per photon, where ($\hbar$ is Plank's constant h divided by 2π) l is the azimuthal mode index [4] and tells the number of azimuthal phase rotations of the field in one full cycle from 0 to 2π. As this beam is propagating, the phase is undefined at the center and is known as a point of phase singularity, that results in zero intensity at the center (see Figure 2.9(c)). Laguerre-Gaussian beams are good examples of beams that carry OAM.

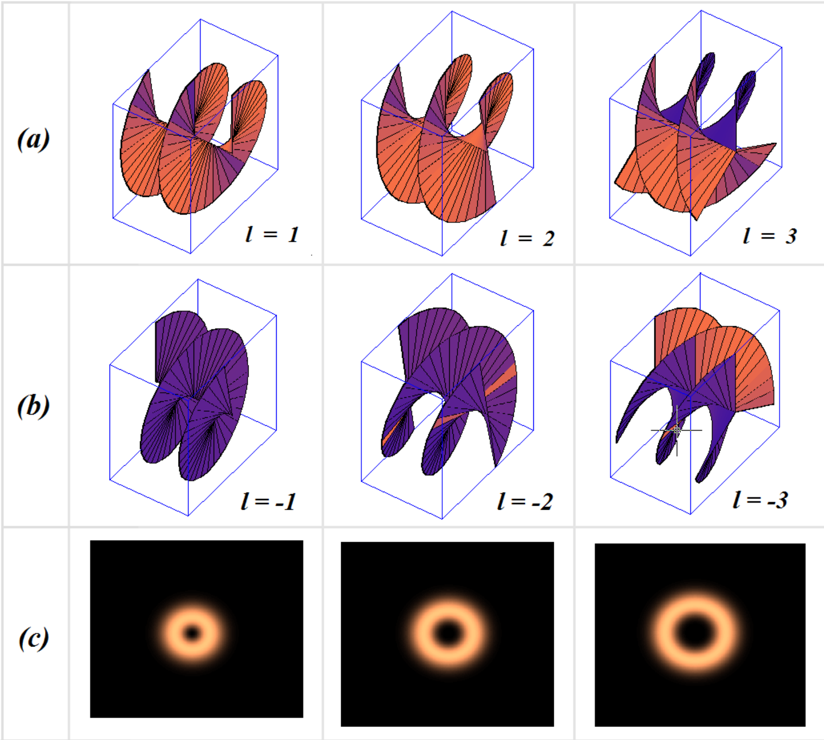

FIGURE 2.9: Row *(a)* are 3-dimensional plot of helical phasefronts of beams carrying OAM charge of $l > 0$ (l = 1, 2, 3) while *(b)* are for $l < 0$ (l = -1, -2, -3) and *(c)* are the theoretically calculated corresponding intensity distribution profile of beams with zero intensity at the center. The diameter of the null center increases as the value of l increases.

The phase of a vortex beam rotates as it propagates in corkscrew-like manner along the direction of propagation. $LG_{p\pm l}$ mode possesses intensity profile that is radially symmetric and when l is not equal to 0 it has a zero intensity at the center (Figure 2.9 row (c)). The phase structure of the beam wind as a function of angle ϕ and in the plane perpendicular to the direction of propagation, the phase smoothly advances with ϕ. When $l > 0$ (LG_{p+l}) (Figure 2.9 row (a)) the direction of winding is anti-clockwise but clockwise (Figure 2.9 row (b)) for $l < 0$ (LG_{p-l}).

The p in $LG_{p\pm l}$ mode tells how many rings of nulls intensity will be contained in the cross-section intensity distribution profile of the beam (Figure 2.8) for $p > 0$ and no rings for p

$= 0$. So the transverse intensity distribution profile of the beam for the same value of l but opposite in sign has exactly the same transverse profile.

2.3 Summary

In this chapter an analysis of the transverse field distributions of the optical field that oscillates in laser resonators at steady-state condition was presented. The eigensolutions to the Huygens' integral using the Fresnel approximation gives the field distributions known as the normal modes. The Gaussian mode is considered to be the fundamental eigensolution of a laser resonator cavity and an analysis that is characterized by its transverse intensity distribution, physical size, the field's curvature and divergence were also done. We have studied high-order eigensolutions to the Huygens' integral using the Fresnel approximation in the rectangular and circular symmetry where these solutions fit into the family of Hermite-Gaussian and Laguerre-Gaussian functions respectively. The propagation of these high-order modes in the resonator are developed from the Gaussian mode. Finally, we explained that the Laguerre-Gaussian (LG_{pl}) modes are good examples of laser beams that carry orbital angular momentum. The wavefront of beams that carry orbital angular momentum rotate as it advances along the propagation axis, however when the azimuthal order is not equal to zero, it has a null intensity at the center which increases as the absolute value of the azimuthal order increases.

The next chapter will be presenting different techniques of generating these Laguerre-Gaussian modes.

Chapter 3

Intra-Cavity Laser beam Shaping

3.1 Introduction

The transverse intensity distribution of the field emerging from the laser resonator cavity is one of the very important properties of a laser. The transverse profile of this emerging field determines its divergence and focusability. In general, because of diffraction, the field distribution is generally non-uniform, but is a combination of discrete transverse patterns. And each pattern is a property of a specific mode or combination of modes that is propagating between the resonator cavity mirrors. This transverse field distribution is maintained inside the resonator along the propagation path and finally emerges from the output coupler.

Laser cavity modes can be selected, controlled and modified by the use of specially designed intra-cavity elements so as to get a certain desired output laser beam. This output beam can be modified further and reshaped outside the resonator. Intra-cavity elements can be used to shape the field distribution of a particular mode, such that even as the field distribution changes along the propagation path inside the cavity, it will return to its original distribution after a round-trip. Most intra-cavity elements achieve mode selection by the introduction of low losses to a specific desired mode, but high losses to all other modes.

In this chapter, the various mode selection and shaping techniques in a stable resonator cavity are considered.

In laser resonators, each specific transverse field distribution (the transverse modes) which reproduces itself after each round-trip is said to be self-consistent. The solution to a round-trip wave propagating inside the resonator of a self-consistent field could be determined. The round-trip wave field propagation equations were solved in rectangular or circular symmetry to yield the Hermite-Gaussian or Laguerre-Gaussian modes respectively [1] [12]. In the cylindrical coordinates Laguerre-Gaussian, LG_{pl} modes are characterized by the p radial nodes and l angular nodes. For the purpose of this dissertation, we will limit our discussion on Laguerre-Gaussian modes.

Intra-cavity elements can be used in laser resonators to shape a particular transverse mode pattern and to discriminate and select a specific single order mode out of the many modes that oscillate in the resonator. Many of the mode-shaping methods modify the transverse field distribution of the lowest order mode into the desired field distribution. And since, the shaped mode is no longer a free space mode which does not change as it propagates, the desired transverse mode is obtained at a specific location in the resonator, for instance the output coupler while at other locations it may have a different transverse field distribution.

In subsequent sections we will be considering different mode shaping and selection techniques, depending on the type of intra-cavity elements used, which may be specially designed mirrors, diffractive elements, phase elements etc, used to control the output laser.

3.2 Graded phase mirrors

The graded phase mirrors (GPM) are specially designed mirror which have a non-spherical phase profile. This type of mirror was used in a resonator [46] [47] to obtain a shaped non-Gaussian fundamental mode at the output coupler. The schematic diagram of a resonator with a GPM is shown in Figure 3.1. The cavity mirrors are a flat mirror output coupler and a GPM back reflector mirror whose phase profile is different from that of a spherical mirror of radius $R = L$ by a phase shift of $\Delta\varphi$.

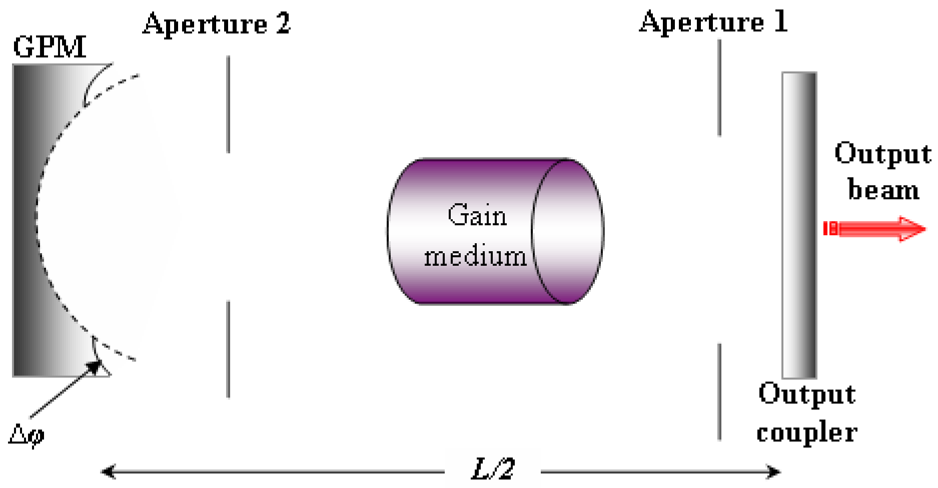

FIGURE 3.1: Schematic diagram of a resonator configuration with a graded phase mirror. $\Delta\varphi$ is the phase difference between the GPM profile and the spherical mirror (dashed line) of radius $R = L$ [47].

One can control the field distribution of the mode by controlling the phase shift. To determine the phase profile of the GPM, one starts with a desired fields intensity distribution at the output coupler (at this point the phase distribution should be uniform). Then this field propagates a distance that is equal to the length of the cavity $L/2$, and the resulting phase distribution is determined using the Kirchhoff-Fresnel diffraction integral. The phase profile of the GPM is then set as the conjugate of this phase, namely a passive phase conjugate mirror for the desired mode [48]. The graded phase mirrors introduce significantly high losses to the high-order modes but low losses to the fundamental mode. This way one can choose (design) the GPM back reflector that will produce the desired mode at the output coupler thereby performing intra-cavity beam shaping.

The GPM has been used to setup custom CO_2 laser resonators [49] [50] that selected super-Gaussian modes of order 4 and 6 as compared to the default Gaussian mode.

3.3 Diffractive elements

Diffractive optical elements can be used to transform one optical wavefront into another. Replacing the back reflector (mirror) of a laser resonator cavity is another option that can be employed to perform shaping [49]. The design of this mirror (back reflector) is similar to that of the passive phase conjugate GPMs, but is nearly flat (having many phase shifts - grating) and with maximum phase variation of 2π, so that the phase profile has several 2π steps. The light that is reflected from this mirror is a sum of the interfering wave components that is emanating from each slit in the phase grating. The optical path length in space through which diffracted light from the grating may pass defer, and so will the phases of the light waves at that point. If the path difference between the light from adjacent slits is equal to $\frac{1}{2}$ the wavelength, the waves will be out of phase and will have destructive interference resulting to a minimum in intensity [49]. Also, when the path difference is equal to a wavelength, the phases will constructively interfere to produce a maximum in intensity. This concept can be used to design a mirror that will introduce low loses to the desired mode and very high loses to all other modes. The diffractive mirror has been used to generate a square 20th-order-super-Gaussian mode [48] [51]. Figure 3.2 is the schematic illustration of a typical resonator configuration that uses diffractive elements. It uses a flat mirror as the output coupler, a diffractive mirror as a back mirror and an intra-cavity phase grating is placed at about the middle of the resonator cavity.

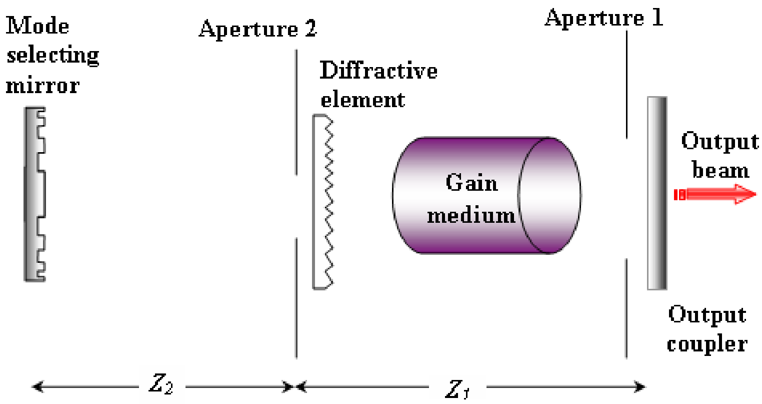

FIGURE 3.2: Schematic of a resonator with a diffractive back mirror, a flat output coupler, and an intra-cavity element[51].

Two apertures are inserted into the cavity and their diameters are chosen such that negligible losses is introduced to the fundamental modes. The intra-cavity diffractive optical element is a sinusoidal phase grating of the form $\exp[im\sin(2\pi f_g x)]$ [48], where f_g is the spatial frequency of the grating and m represents the modulation index.

The intra-cavity generation of high-order LG_{p0} modes with selected radial order p $(= 0 - 5)$ has been demonstrated [23]. They employed the technique of amplitude masks composed of absorbing rings to be inserted inside the cavity. The radii of these rings were selected to coincide with the nulls of intensity of the desired LG_{p0} modes.

3.4 Binary phase elements

The intensity distribution profile of an incident beam can be changed by binary phase elements, just the same way as the diffractive mirrors. The sizes of the features in phase elements are significantly larger than that of the diffractive elements, hence reducing the difficulty in fabrication [48]. In this section we will be discussing how to perform mode-selection with binary phase elements that consist of only two phase levels.

To selectively attenuate certain regions of a modes intensity distribution to discriminate it from other modes by the use of intra-cavity absorbing elements such as wire grids are the simplest method of mode selection. Since such elements introduce losses by absorption they heat up in the process and are therefore considered to be relatively inefficient. One can obtain a much better efficiency by using a non-absorbing phase elements that introduces losses by diffraction and interference. So, let us look at how binary phase elements can be exploited to introduce low losses to some specific modes and discriminate other modes while selecting one that will exit the resonator cavity.

The absorbing wires were replaced with phase-shifting masks [52] in order to select high-order transverse modes. The phase-shifting masks were designed in such a way that they introduce a nearly π phase shift along the narrow lines of the wires, while zero phase shift was introduced to all the other areas. These phase masks introduces a relatively low losses to the desired mode but very high losses to the other modes. A more general and different binary phase elements have been developed [53] which is useful for selecting only a desired high-order transverse mode. The binary discontinuous phase elements (DPEs) were designed to match the phase distribution and selectively reverse the phase of the desired mode. DPEs have a specific phase distribution with sharp phase changes, hence they introduce minimal losses to the desired transverse mode but very high losses to the other modes. Figure 3.3

is an illustration of a resonator cavity that uses a DPE which is placed near the output coupler.

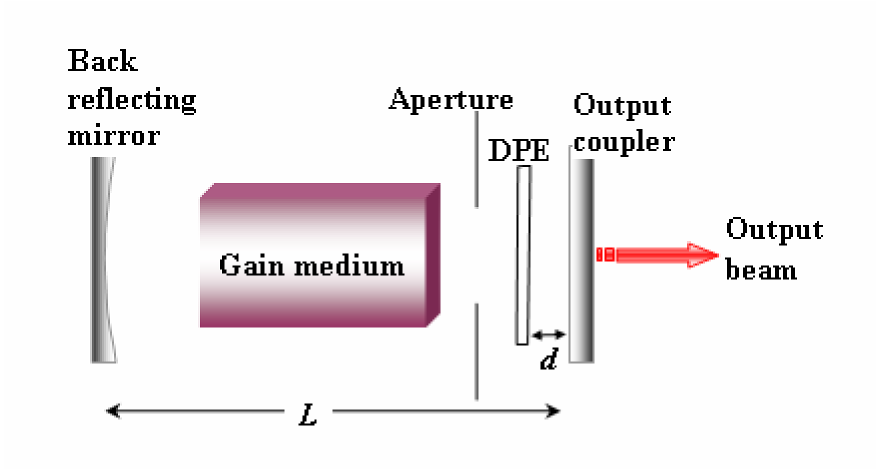

FIGURE 3.3: Schematic of a laser resonator cavity with a DPE placed near the output coupler.

The DPE is normally inserted near one of the cavity mirrors, preferably near the output coupler. It is designed in such a way that the discontinuous phase changes of either 0 or π occurs at the interface between adjacent parts of the desired mode distribution where the intensity is very low. In Figure 3.4 are illustrations of some representative DPEs that can be used to select (a) TEM_{01}, (b) TEM_{02} and (c) LG_{20}. A typical instance is Figure 3.4(c) ($l = 1$), a DPE that is designed to select the azimuthal mode index l that introduces an angular phase dependent shift of the form [48]

$$\varphi(r,\theta) = \begin{cases} 0 & 3\pi/2 + 2\pi m > l\theta > \pi/2 + 2\pi m, \\ \pi & 5\pi/2 + 2\pi m > l\theta > 3\pi/2 + 2\pi m. \end{cases} \quad m \text{ integer} \tag{3.1}$$

It is important to note that for every positive value of l, the DPE has a point of singularity at the origin, which corresponds to the zero intensity in the origin of a LG_{pl} modes with $l \neq 0$. Some representative DPEs are shown in Figure 3.4.

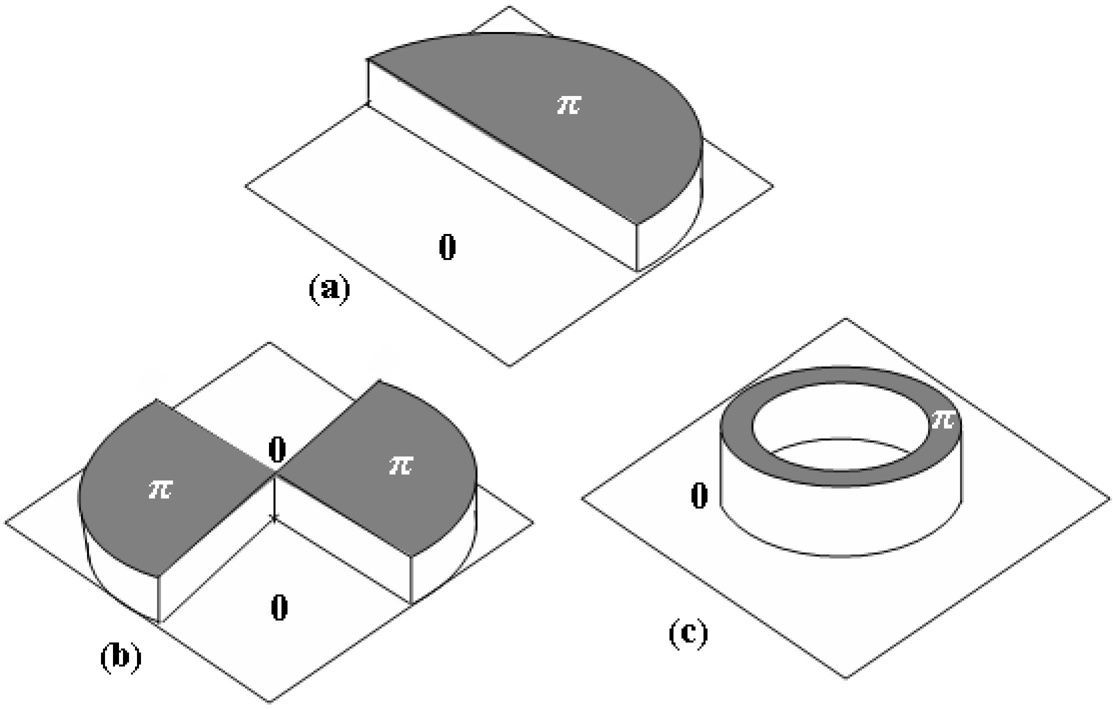

FIGURE 3.4: Representative DPEs that can be used to select TEM_{01},(b) TEM_{02},(c) LG_{20} [48].

When a beam has passed through the DPE, adjacent spots and adjacent rings of the desired modes field distribution, that are ordinarily opposite in phase (π phase shift) will now possess the same phase [48]. Then, the output coupler reflects back this modified field distribution so that as it passes the second time through the DPE, all the modifications cancels out and reverts back to their original values [48]. In the cavity shown in Figure 3.3, if the distance d between the cavity mirror and the DPE is very short compared to the length of the cavity L ($d \ll L$), then the intensity distribution of the desired mode does not change as it passes through the DPE (twice completing a round-trip). As implied earlier, the phase change introduced by the first pass through the DPE is cancelled by the return-trip. Moreover, at the location where the intensity is very strong, all other modes whose intensity distribution is different suffer a sharp phase change. Given the fact that $d \gg \lambda$, leads to a strong divergence, where phase change introduced by the first pass through the DPE is no more cancelled by the phase change introduced by the return-trip. The result is that all other modes are suppressed except the desired mode. Higher harmonics of the desired mode may not be affected by the DPE, but this can be handled by the use of a simple aperture.

3.5 Spiral phase elements

The spiral phase element (SPE) or plate sometimes referred to as vortex lens, is an optical transparent material which has a gradual increasing spiralling thickness. When a beam is incident on the SPE, it imposes a vortex structure on the beam by linearly varying the optical path length, thereby inducing a phase shift in the beam. SPEs introduce a phase shift of $\exp(iN\theta)$, (where θ is the azimuthal angle) to the beam passing through them. Figure 3.5 (a), (b) and (c) shows some representative examples of SPEs with N equal to 1, 2, and 3 respectively, where N is the number 2π phase discontinuities.

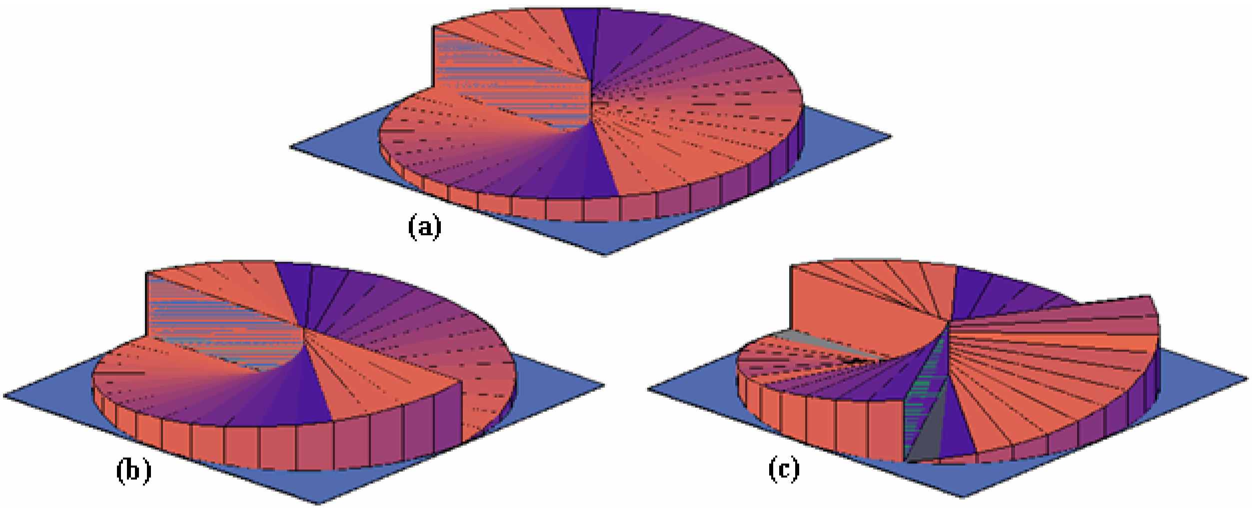

FIGURE 3.5: Spiral phase elements (SPEs) with (a) $N = 1$, (b) $N = 2$, and (c) $N = 3$. The height of discontinuities represent 2π phase shifts.

The height of the discontinuities needed to achieve a 2π phase shift per passage (4π phase shift in the reflected beam) is wavelength (λ) for a reflective element and $\lambda/(n\text{–}1)$ for a transmitive element [17], where n is the refractive index. It can be seen from Figure 3.5 that there is a phase singularity at the origin of the SPEs.

The concept of SPEs has been applied inside laser resonator cavity to discriminate and select high-order helical Laguerre-Gaussian modes. SPEs can be placed inside a laser resonator cavity to discriminate and select high-order helical LG modes. Using this method, based on azimuthal mode discrimination, the SPEs are lossless for the desired mode but introduce high losses to all other modes. The SPEs, essentially changes the phase of the beam's wavefront passing through them, in accordance with $\exp(+iN\theta)$ or $\exp(-iN\theta)$ [17]. A schematic diagram of two laser resonator setups with SPEs are shown in Figure 3.6. Figure 3.6(a) is a laser resonator cavity having two SPEs adjacent to the cavity mirrors. Reflective SPEs can also be used in the place of cavity mirrors. The angular modes index of the mode passing through the first SPE twice is changed by $-2N$, that is, the mode with angular index l is changed to l–$2N$ and the second SPE changes it back again to l. These SPEs will change modes with an angular index of $l = +N$ to those with $l = -N$. The result of this is that because modes of opposite l have the same transverse intensity distribution, only these mode will maintain the same distribution before and after passing through the SPEs. Although, the radial distribution of all the other mode will have the same form of a combination of LG modes, each will posses a different angular modes index l, so they will be wider, and will suffer higher losses for modes having $l \neq N$.

Figure 3.6(b) is a cavity configuration with one SPE replaced by an element which reverses the angular phase (example is a cylindrical lens focused on the resonator mirror). In this configuration, each time a mode passes through the SPE its angular index is changed by $-N$, and the cylindrical lens simply reverses the sign of the angular index. Again, only the LG modes whose value of angular mode index, l equal to N ($l = N$), have their radial distribution maintained after each round-tip and all other modes have the radial distribution wider causing them to suffer significantly higher losses.

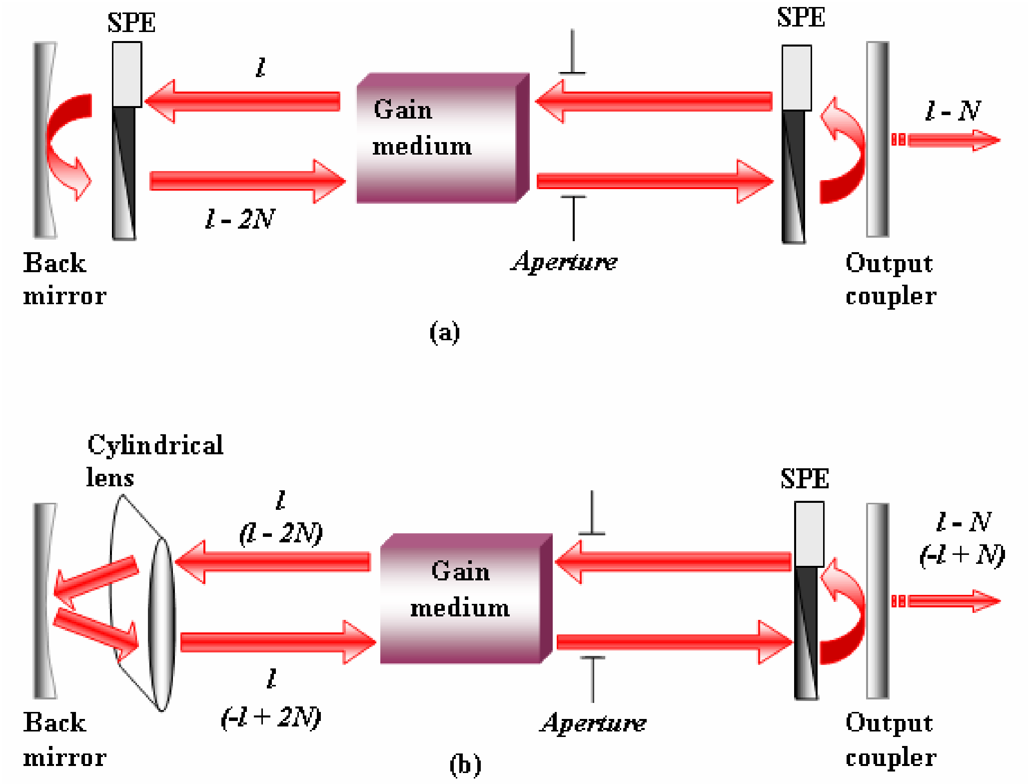

FIGURE 3.6: Laser resonator configurations with SPEs: (a) a configuration with two SPEs, each of which is placed adjacent to the cavity mirrors; (b) a configuration with a single SPE, placed adjacent to the output coupler, and with a cylindrical lens (which reverses the angular phase) focused on the back mirror. The angular indices are indicated along the round-tip (second trip is in parentheses).

3.6 Digital holography

Conventional holography entails creating a hologram by illuminating an object with a laser beam (Figure 3.7(a)) [54]. The interference pattern that is obtained between this object beam and the reference beam is recorded onto a photographic film and is called a hologram [60]. If this process is reversed and illuminating the hologram (or interference pattern) with the initial reference beam at the same angle of incidence (as was used when the hologram was produced), the object beam is reconstructed (Figure 3.7(b)).

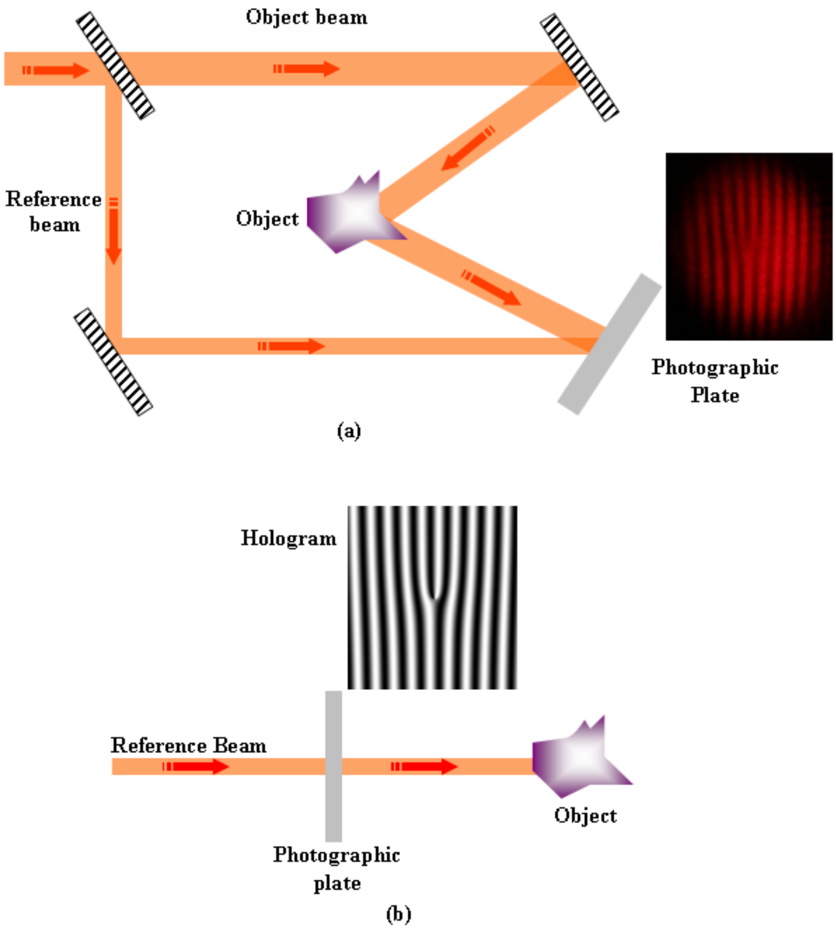

Figure 3.7: Schematic diagram to illustrate the principle of (a) a hologram construction and (b) using the hologram to construct the desired beam [55].

When it comes to the case of digital holography there is no need for an existing physical object beam. If one can find a way to mathematically formulate the interference pattern between the reference beam and the object beam which one wants to reconstruct, this interference pattern can be computed and is normally called a computer-generated hologram. This computer-generated hologram can later be printed onto a photographic film and used as in the earlier techniques. After the invention of liquid crystal display devices, these computer-generated holograms can be implemented digitally, allowing for the elimination of the printing of physical holograms. Instead a hologram that is mathematically calculated is used to directly address a liquid-crystal display (LCD) (Figure 3.8), which allows a single LCD to be re-used to display different holograms with no need of re-aligning the optical setup when a hologram is changed. A good example of this type of device is the spatial light modulator (SLM). The next section gives a little more detailed explanation on the SLM.

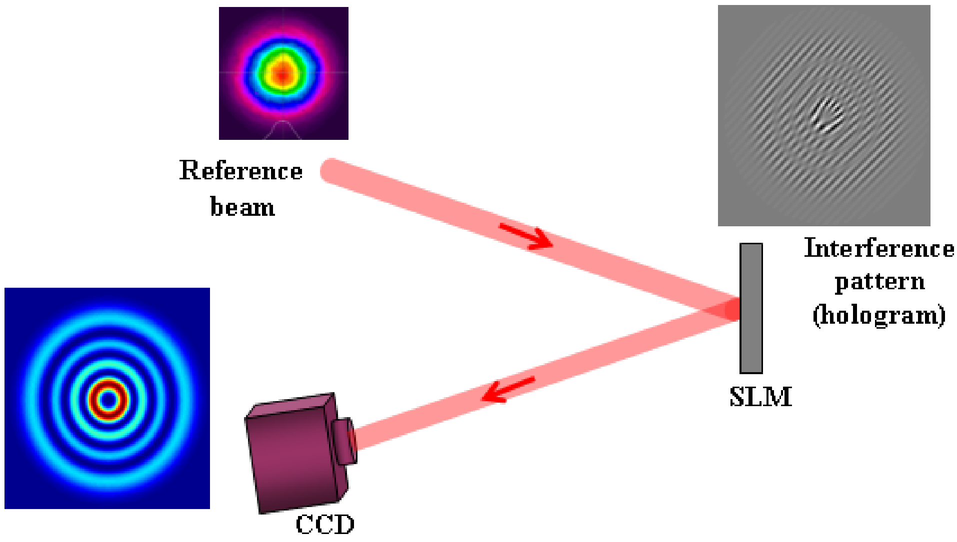

FIGURE 3.8: Schematic diagram illustrating the action of beam shaping using the SLM (top right is the interference pattern displayed on LCD of the SLM while bottom left is the shape of the resultant beam measured with the CCD).

3.6.1 The Spatial light modulator (SLM)

A spatial light modulator is a device whose liquid-crystal display (LCD) was designed for the construction of digital holograms. Just as the name implies it can be used to modulate the phase (and in some cases amplitude) of an incident beam. The SLM that was employed in this work is the Hamamatsu Liquid Crystal on Silicon-Spatial Light Modulator (LCOS-SLM) X110468E and it is a phase-only device which implies that it can be used to alter only the phase structure of the reference beam. It can also be used to perform amplitude modulation, which we shall see in subsequent sections.

Figure 3.9 shows the picture of this SLM. The SLM comprises of a LCOS chip (and housing), controller and a Digital Video Interface (DVI not shown). The liquid crystal (LC) is programmed through a circuit board via the controller which is connected to a computer using the DVI interface. Mathematically, a grey-scale image (interference) pattern between this reference beam and an incident beam that we wish to modulate is computed and programmed onto the SLM, where it is possible to modulate the phase of the reference beam as illustrated in Figure 3.8. The phase of the reference beam is changed in proportion to the shade of grey present in each pixel in the computer generated digital image (hologram).

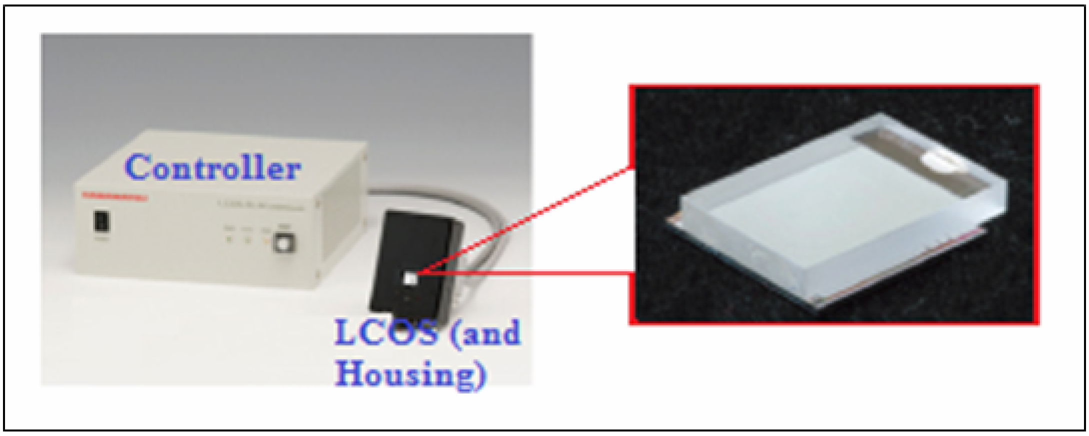

FIGURE 3.9: Picture of a Hamamatus LCOS-SLM showing the controller, LCOS (with housing) [56].

The liquid crystal display (LCD) has an effective area of 16mm by 12mm and spatial resolution of 25 light points (pixels) per millimetre (lp/mm). The display works by the mechanism of electrically controlled birefringence. Figure 3.10 shows an illustration of the components of this LCD. The LCOS chip is made up of a parallel-aligned nematic liquid crystal layer to change the phase of light, transparent electrode in front and a C-MOS circuit. The LC molecules that make up the pixels are aligned parallel to the electrodes when no electric field is on the electrodes (Figure 3.10) but in the presence of an electric field, the molecules are forced to bend in the direction of the applied electric field.

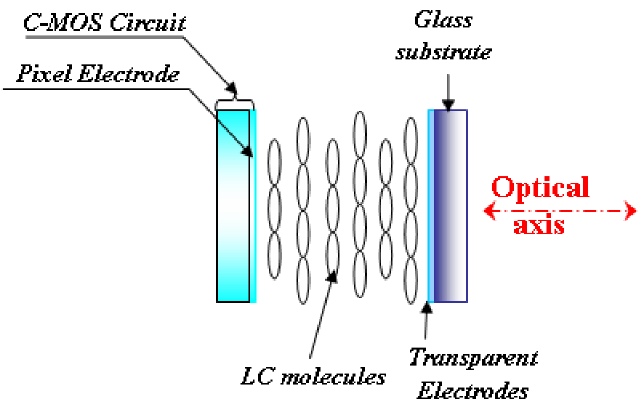

FIGURE 3.10: Illustration of a pixel of LCMOS chip

A hologram is practically a grey-scaled image. These grey-scale holograms are represented with 256 grey-levels and the voltages applied across each pixel are adjusted appropriately relative to the shade of grey present at corresponding pixel in the hologram. This is illustrated in Figure 3.11, where black indicates no phase modulation, which implies that no voltage is to be applied to the corresponding electrodes. Increasing the grey-level (that is phase modulation) implies increasing the voltage applied across the pixels. If no voltage is applied across the pixel, the molecules are aligned parallel to the electrode but when the voltage is increased the molecules tilts further away from their initial orientation [55].

The beam that is illuminating the liquid crystal (LC) molecules needs to be linearly polarized, and parallel to the axis of the LC molecules which is vertically polarized. When the molecules tilt in the direction of the applied electric field, the refractive index seen by the incident beam changes, hence the phase also change as given by [55]

$$\delta = \frac{2\pi}{\lambda} dn, \tag{3.2}$$

where δ is the phase-shift experience by the beam of wavelength λ, d is the optical path length in the LC pixel and n is the refractive index of the LC pixel, which is proportional to the applied voltage across the electrodes. Figure 3.11 is a schematic diagram illustrating how the grey-scale value present in the hologram is translated into electric field applied across an array of LC molecules which results in the molecules tilting in the direction of applied electric field. Thereby changing the refractive index of the LC pixel, hence the phase of the incident beams.

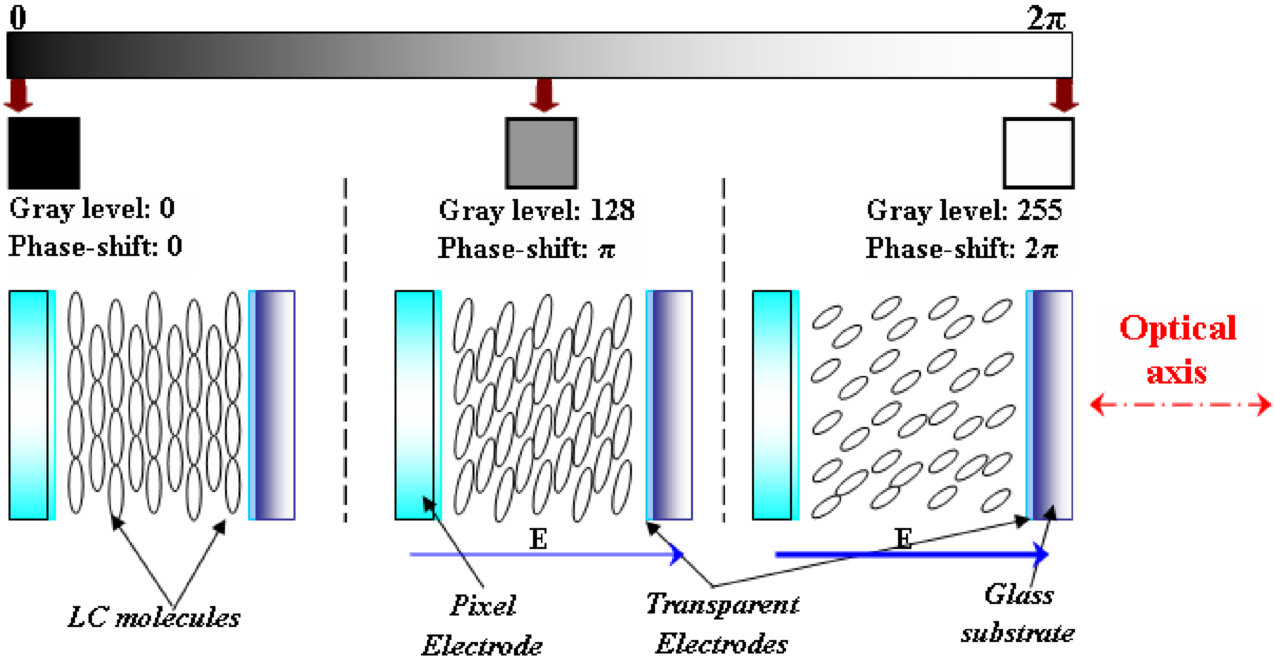

FIGURE 3.11: A schematic diagram illustrating how the grey-scale value present in the hologram is translated into electric field applied across an array of LC molecules.

From equation (3.2) it is clear that phase modulation is dependent on the wavelength of the incident beam. Hence, for the grey-level of 128 representing π phase shift, the voltage required to produce this phase shift for different wavelength of the incident beam will differ. This is the reason why it is necessary to calibrate the SLM to adapt its electro-optical response when moving from one laser source to another. The purpose of calibrating the SLM is to ensure that for the working wavelength, a phase shift from 0 to 2π is achieved within the 256 grey-levels. So that a phase shift assigned to the grey-levels does produce the appropriate voltages applied to the electrodes of the pixel to achieve correct phase modulation [55] (A detailed procedure for calibrating the SLM can be obtained in [55]).

The spatial light modulator has some efficiency drawbacks. The major drawback is that the entire incident beam is not diffracted to produce the desired object beam. This is as a result of one, the structure of the LCD and two, the diffraction efficiency of the SLM.

The LCD is made up of a two-dimensional array of pixels, with some spacing between the pixels that makes the LCD to function as a two-dimensional grating, thereby resulting in light being diffracted into multiple diffraction orders. When the beam illuminating the LCD fall on a non-pixel space between pixels the beam will not be reflected and is lost. This is known as the "fill factor", which means that some portion of the area of the LCD is not covered by pixels while others are [55]. This contributes to the SLMs efficient problems.

The other issue with the SLM is that it is unable to diffract the entire incident beam into the required object beam. It has diffraction efficiency of about 95%. This means that a 95% of the incident beam is diffracted while about 5% is un-diffracted. Hence, the beam reflected off the LCD of the SLM consist of a superposition of the diffracted object beam and the un-diffracted reference beam, which results in a reduction in quality of the required mode. This issue can be overcome by placing a grating on top of the computer-generated hologram so as to split the diffracted object beam into the first order and the un-diffracted reference beam into the zero order.

3.6.2 Amplitude and phase modulation with the phase-only SLM

The SLM is a phase-only device which implies that it can be used to perform phase control of light by default but if someone wants to encode an aperture, one would need a SLM that has the ability to control both phase and amplitude of the incident beam. Figure 3.12 is an illustration of (a) a physical circular aperture, (b) a complex amplitude modulation that can be used on the phase-only SLM to produce an amplitude mask, and (c) is a zoomed-in image of the checkerboard pattern used to create the amplitude mask. If one wants to encode a hologram of an aperture like the one in Figure 3.12 (a) such that light would transmit only within the circular aperture and not else where, you will need a SLM that allows phase and amplitude modulation. We can still achieve phase and amplitude modulation using a phase-only SLM by addressing the areas where we do not want light to transmit with a checkerboard pattern. Figure 3.12 (b) is a hologram that can be used to accomplish a physical aperture if encoded on a phase-only SLM. This hologram would only allow light within the circle to transmit and not in the dark area.

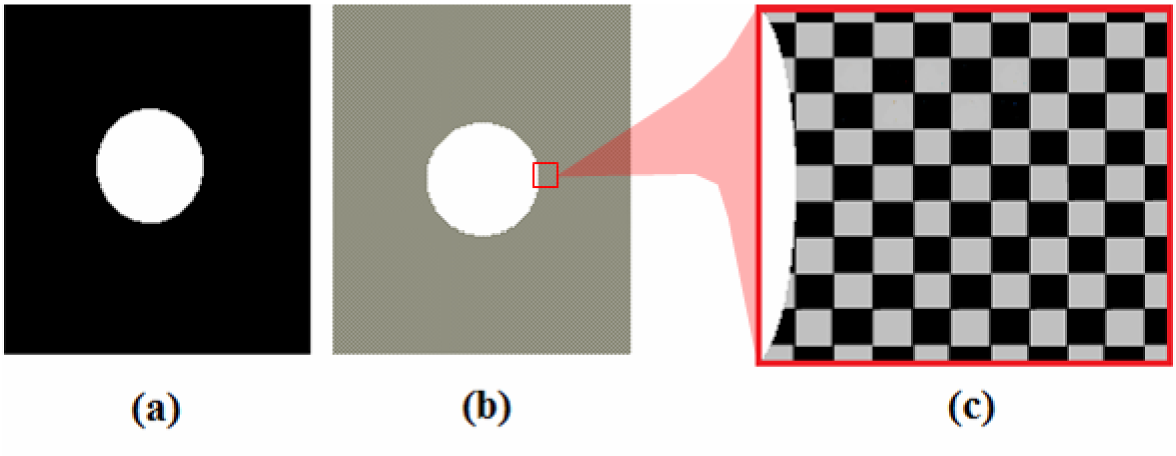

FIGURE 3.12: Illustration of (a) physical circular aperture; (b) complex amplitude modulation which can be used on a phase-only SLM to produce an amplitude mask; (c) a zoomed-in image of the checkerboard pattern used to create the amplitude mask.

Now to see how this pattern that consists of alternating sets of pixels which have phase values that are out of phase by π, can be used to achieve an amplitude mask, lets consider Figure 3.13. Figure 3.13(a) is the schematic representation of two phase-only values on the complex plane. The weighting of each of the phase values, 0 and π are equal in the checkerboard pattern, which in the complex plane approach translates to each vector (A_A and A_B) having the same amplitude, but pointing in opposite directions along the x-axis [56]. This leads to a resultant vector, A_C that has no amplitude (implying no DC component) and is positioned at the origin of the complex plane. Since, A_C has no amplitude, it implies that the average of the field at the checkerboard hologram is zero.

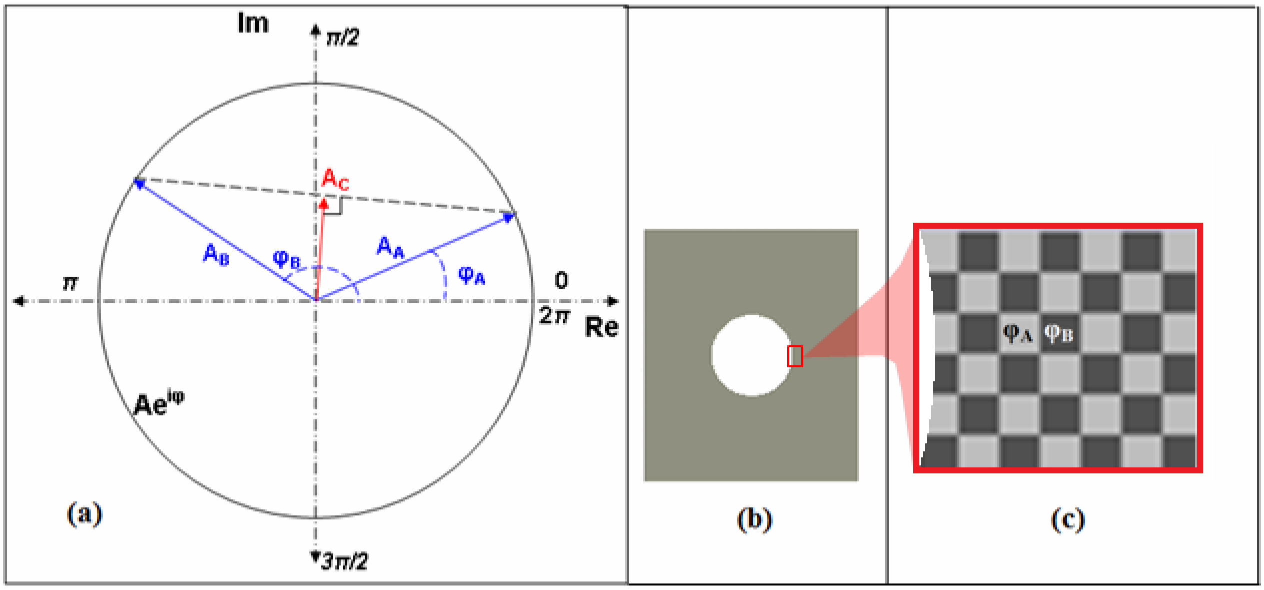

FIGURE 3.13: (a) Schematic complex plane representation of the angles φ_A and φ_B for the vectors A_A and A_B, represent two adjacent phase values in the hologram. A_C is the resultant amplitude. (b) Is the digital hologram while (c) is a zoom in checkerboard pattern with two phase values φ_A and φ_B.

The result is zero intensity along the propagation axis in the Fourier plane, with the light shifted away from the origin due to the high spatial frequency of the checkerboard. But when the SLM is addressed with a single grey-level the resultant vector in the complex plane, A_C has amplitude lying along the positive x-axis, meaning that the average amplitude at this phase-mask is non-zero, thereby producing on-axis intensity in the Fourier plane [56].

3.6.3 The digital Laser

All these other methods discussed above for mode selection require custom optics, for example, a diffractive mirror or phase plate designed to select a specific mode and when a new mode is required a new mode selecting element will need to be designed. There will also be need to realign the optical setup. There has been attempts in the past to use deformable mirrors [57] [58] to perform dynamic intra-cavity mode selection but such elements are limited in the phase profile that they can accommodate [57] [59]. So, it has not found much application in mode selection. Before 2013 no technique has been demonstrated to perform dynamic intra-cavity on-demand mode selection.

These limitations of intra-cavity on-demand laser mode shaping have been overcome through the use of intra-cavity digital hologram, implemented on a phase-only reflective spatial light modulator (SLM) [24]. This SLM was used to form a rewritable holographic mirror in place of one of the cavity mirrors. This allowed a high resolution on-demand mode selection, with a wide range of phase values. The "digital laser" may be used to implement phase-only, amplitude-only or both intra-cavity mode selection, by simply changing the digital hologram (grey-scale picture) written to this device [24]. A great deal of detail is given to the "digital laser" here because that is the concept we used in our experiment.

Figure 3.14 the schematic diagram of the setup of the digital laser. The digital laser is a conventional folded resonator cavity configuration which uses a Nd:YAG crystal as the gain medium (Figure 3.14). It is a hemispherical cavity that uses the phase-only reflective SLM as the back reflector mirror. On this SLM is created a digitally addressed holographic mirror. The SLM that is suitable to be used for this purpose is required to have high resolution, high efficiency, and high reflectivity at the desired vertical polarization, a small phase-amplitude cross-talk, and reasonable damage threshold and a large phase shift at the laser wavelength [24].

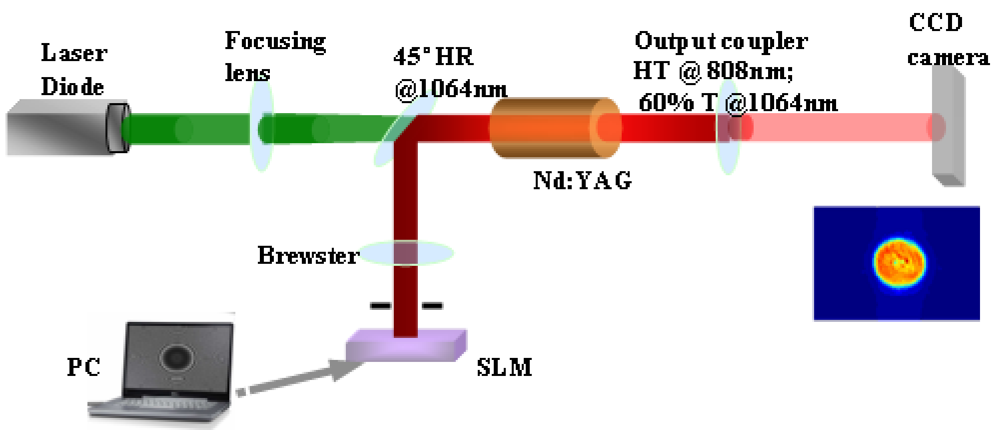

FIGURE 3.14: Schematic of the digital laser [24].

3.6.3.1 The concept of the digital laser

A standard (conventional) hemispherical resonator cavity is made up of a concave mirror with radius of curvature R, and a flat mirror (radius of curvature is ∞) as shown in Figure 3.15. The stability condition satisfies equation (1.5). For the digital laser, the concave mirror was replaced with the SLM on which was programmed a digital hologram that mimics a conventional concave mirror with radius of curvature, R chosen to ensure that the resonator formed a stable plano-concave cavity (Figure 3.15) [24].

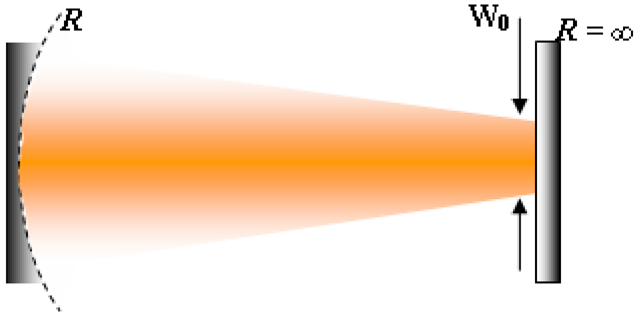

FIGURE 3.15: Schematic of a simple hemispherical cavity [24].

The required hologram of a lens to be programmed on the SLM is chosen such that the focal length f, is equal to the radius of curvature R, so that the hologram mimics the curvature of the mirror. The waist size of the Gaussian mode that oscillates in such a cavity at the flat mirror is given by [13] [24]

$$w_0^2 = \frac{\lambda}{\pi}\Big(L(R{-}L)\Big)^{\frac{1}{2}}, \tag{3.3}$$

where the laser cavity wavelength is λ and the length of the cavity is L.

Their are some power losses with the SLM because of some of the efficiency problems outlined earlier, so two major conditions must be met simultaneously for the digital laser to work. One is that the resonator cavity gain must be sufficiently high to overcome the losses, but the intensity of the oscillating radiation inside the cavity must not exceed the damage threshold of the SLM [20]. These conditions where met by simply using a high power pump source and an L-shaped cavity design to avoid irradiating the SLM with the pump source.

The Hermite-Gaussian, Laguerre-Gaussian, Flat-top and airy beams where selected in the cavity. Using complex amplitude modulation to generate digital holograms that were used to perform amplitude modulation on the phase-only SLM [56] [24].

3.7 Summary

This chapter started with a general introduction to beam shaping and discussed the basic concept employed in most intra-cavity laser beam shaping methods. In general, most intra-cavity beam shaping techniques, involve the use of intra-cavity elements which introduce low losses to the desired mode but high losses to all other modes. A review of different intra-cavity beam shaping techniques; graded phase mirrors, diffractive elements - binary phase elements and spiral phase elements (SPE) were presented. The SPE is an optical transparent material with gradual increasing spiral thickness. It achieves beam shaping by linearly varying the optical path length of the light beam that is incident on it, thereby introducing a phase shift in the beam. Also, a brief discussion on the concept of conventional holography and digital holography in beam shaping was presented. The concept of conventional holography involves the recording of an interference pattern (hologram) between an object beam and a reference beam onto a photographic film, and later using this hologram with the initial reference beam to reconstruct the object beam. But the concept of digital holography on the other hand, involves mathematically formulating the interference pattern (digital hologram) between the reference beam and object beam that can be recorded onto a photographic film. And later, with the use of this computer generated hologram (CGH) and a reference beam the desired object beam can be constructed. The spatial light modulator (SLM) eliminates the need for printing the hologram but the hologram can be used to directly address its liquid crystal display (LCD) and the LCD can be reused to display different holograms. When a reference beam is used to illuminate the LCD on an SLM displaying a CGH, it will produce the desired object beam in accordance with the CGH.

A CGH is basically a grey-scale image that is generated such that when displayed on the SLM can vary the voltage applied across each pixel of the SLMs LCD, in accordance with the grey-level on the corresponding pixel. The phase-only SLM can be used to perform phase control of light by default but it can also be used to achieve both phase and amplitude modulation of light. The checkerboard technique can be used on the SLM to produce amplitude masks on the phase-only SLM. The checkerboard is a pattern that consists of alternating sets of pixels which have phase values that are out of phase by π. The SLM has been used extensively to perform extra-cavity beam shaping using both phase and amplitude techniques. The digital laser used this same concept of beam shaping using the SLM but inside the resonator cavity. This was achieved by first, using phase modulation to program the curvature of a concave mirror on the intra-cavity SLM, and further using the checkerboard approach to generate amplitude masks that were used on the (intra-cavity) SLM to change the intensity distribution profile of the circulating beam in the cavity. This way, the digital laser was used to produce the desired transverse beam shape at the output coupler. In the digital laser, selecting a different mode just requires changing the grey-scale hologram and on-demand mode selection is an elegant that is quality provided by the digital laser.

Chapter 4

Methodology

The previous chapter reviewed many methods of intra-cavity beam shaping but the idea of the digital laser was the method employed in the experiment using the intra-cavity SLM to perform mode selection. The fact that any mirror with any radius of curvature of choice can be programmed on the intra-cavity SLM and that dynamic (on-the-fly) beam shaping can be achieved with the digital laser is one merit that was exploited in using the concept of the digital laser in the experiment. The experiment was done in two stages, one was the assembling of a stable resonator cavity using an intra-cavity SLM and the second was selecting different high-order modes in the cavity by encoding different amplitude masks on this SLM.

4.1 The concept

The concept of the digital laser involves using the method of phase modulation to generate digital holograms which when displayed on the LCD of the SLM allows it to mimic a concave mirror of focal length f. A flat mirror was used as the output coupler and the SLM (virtual concave mirror) as a back reflector, to setup the hemispherical cavity configuration. Figure 3.15 shows an illustration of this cavity. The Nd:YAG crystal and a laser diode pump were used to assemble the diode end-pumped solid state laser resonator cavity with a Nd:YAG crystal as the gain medium. Setting up a stable resonator cavity with the Nd:YAG crystal was the first stage of the experiment and then, considering a symmetrical generalized Laguerre-Gaussian mode of zero azimuthal order and p radial order denoted as LG_{p0} at the waist. Using equation (2.31) and setting $l = 0$ and $z = 0$ we have

$$E_{p0}(r) = E_0 \left[\frac{2r^2}{w_0^2}\right] L_p \exp\left[\frac{-r^2}{w_0^2}\right], \tag{4.1}$$

where L_p is the Laguerre-Gaussian polynomial and all the other symbols have there normal meaning. To simplify equation 4.1, we introduce a reduced transverse coordinate $X = \dfrac{2r^2}{w_0^2}$. Table 4.1 shows Laguerre-Gaussian polynomial $L_p(X)$ for $p = 0$ to $p = 3$. Recall that LG_{p0} mode denotes a beam made up of a central lobe surrounded by p concentric rings of light and null concentric rings of intensities (see Figure 2.8). The spot size of the w_0 has physical interpretation only for the fundamental mode LG_{00}, which has a Gaussian intensity distribution profile. The intensity distribution profile of high-order LG modes are characterized by a pattern that spreads widely from the axis as the p order increases [60][23].

TABLE 4.1: Laguerre Polynomials

p	$L_p(X)$
0	1
1	$1 - X$
2	$X^2/2 - 2X + 1$
3	$-X^3/6 + 3X^2/2 - 3X + 1$

The transverse spread associated with each p mode can be described by equation (2.32) but setting $l = 0$ and considering the mode at the waist where $z = 0$ we have

$$w_{p0} = w_0\sqrt{2p+1}, \tag{4.2}$$

and using equation (2.33) we have the beam quality factor to be

$$M_{p0}^2 = 2p + 1. \tag{4.3}$$

Figure 2.8 shows that the LG_{p0} mode has a characteristic on-axis intensity which is independent of the p modal order. This contradicts the usual scale law which states that the spreading of a beam results in a reduction in on-axis intensity [23]. Subsequently, we focused our attention on forcing the fundamental mode LG_{00} of our stable resonator to become LG_{p0} in shape. Equation (4.1) was used to implement phase and amplitude modulation as described in chapter 3 to generate the amplitude absorbing masks (holograms) that approximates the zeros of the Laguerre polynomial. Table 4.2 shows the zeros of the Laguerre polynomials.

Table 4.2: Roots of Laguerre Polynomials

p	Values of Raio r_i/w for the zeros of Intensity of LG_{p0} modes		
1	0.707106		
2	0.541195	1.306562	
3	0.455946	1.071046	1.773407

It is important to note the difference between the family of symmetric Laguerre-Gaussian modes, LG_{p0} and the symmetric eigenmodes, TEM_{p0}, of the cavity. In general, when the resonator cavity has apertures and amplitude masks the fundamental mode of the cavity is not the lowest order mode Laguerre-Gaussian basis. The fundamental mode (TEM_{00}) of the cavity is the mode that has the lowest losses and it appears at the laser cavity oscillation threshold [61][23]. This TEM_{00} can be reshaped to become TEM_{p0} with $p > 0$ depending on the absorbing mask hologram used on the SLM.

4.2 Experimental Setup

As stated earlier, the experiment was done in two steps, the first was to assemble a stable resonator cavity and the second was to perform intra-cavity selection of single, LG_{p0} mode using the concept of the digital laser.

4.2.1 Experiment 1 - Setting up the resonator cavity

Figure 4.1 is the picture of the experimental setup while Figure 4.2 shows a schematic representation of the experimental setup.

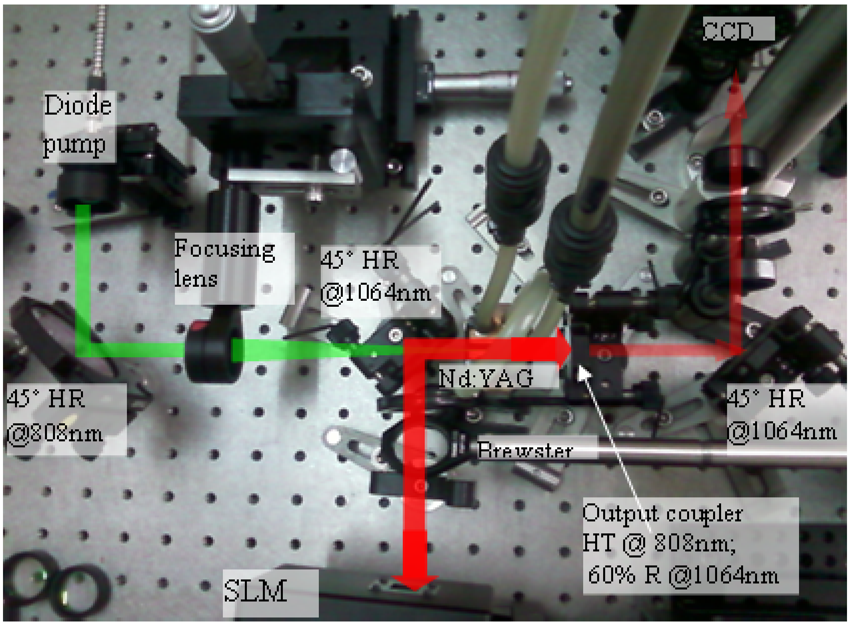

FIGURE 4.1: Picture of the experimental setup.

In order to setup a stable laser resonator cavity, a 75 W high power Jenoptik (JOLD 75 CPXF 2P W) laser diode pump (at 808 nm wavelength) was used to optically end pump a cylindrical Nd:YAG (30 mm length by 2 mm radius) crystal rod. The optical pump was collimated using a 125 mm focal length concave lens and delivered through a plain mirror coated for high transmission at the diode pump wavelength (808 nm) and high reflection at the cavity wavelength (of 1064 nm). The Hamamatsu (LCOS-SLM X110468E) SLM which mimics a concave mirror was assembled with a flat mirror output coupler in an L-shaped hemispherical resonator cavity configuration. The LCD (and housing) of the SLM was mounted on a X-Y mechanical stage. The reason for the L-shape is to ensure that the high power diode pump does not damage the SLM because of direct illumination. The Brewster window is an important component of this resonator cavity which forces the resonator to oscillate in the desired vertical polarization. The output coupler has 60% reflectivity at 1064 nm. The SLM (concave mirror) had a 91% reflectivity in the vertical polarization but 93% reflectivity in the horizontal polarization which was not desired. So, the intra-cavity Brewster window was used to ensure that the cavity oscillated only in the vertical polarization and an aperture was used to select the first diffraction order beam from the SLM. After calibrating [55] the SLM in this vertical polarization an efficiency of about 86% was measured in the first diffraction order while the zeroth order measured about 1%, and the SLMs efficiency had a standard deviation of approximately 0.4% across all grey levels, which implies a minimal amplitude effect during phase modulation.

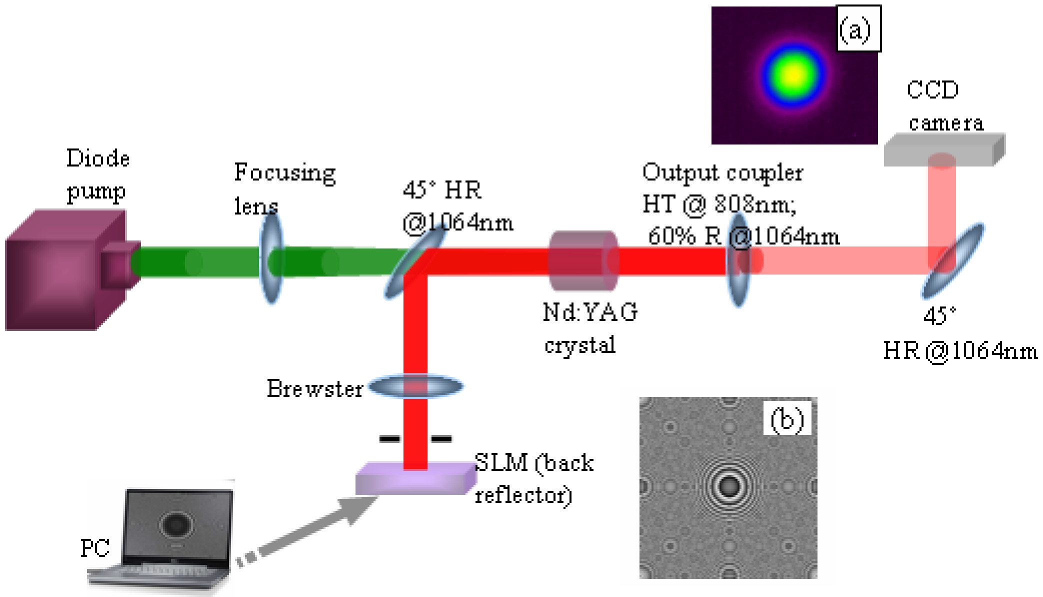

FIGURE 4.2: Schematic diagram of the experimental setup. (a) Transverse image of the output beam (b) Digital hologram of the phase-only radius of curvature displayed on the SLM.

The Nd:YAG crystal was doped with a 1% neodymium concentration and was coated with an antireflection coating to reduce the pump reflection at 808 nm wavelength. The crystal rod was suspended inside a 19°C water-cooled copper block so that the crystal does not over heat and get burnt. The hemispherical cavity (of length 160 mm) was made up of an 86% high (vertical) reflectivity digital concave mirror SLM, with 200 mm radius of curvature and a 60% reflectivity flat mirror at 1064 nm wavelength.

Using the method of phase modulation as described in chapter 3, a hologram (grey-scale image) of a lens was generated with focal length, $f = R = 200$ mm. Displaying this digital hologram (Figure 4.2 inset (b)) that mimics a concave mirror on the SLM and the laser diode pump source switched on at steady state conditions, the resonator cavity produced the expected laser from the output coupler. Images of the cavity's output beams transverse intensity profile was taken at the flat mirror (near-field) (Figure 4.2 inset (a)), and at the far-field with a CCD camera (Photo Inc. USBeamPro). The output beam from the flat mirror was telescoped into Photon Inc ModeScan meter using two 125 mm focal length lenses for the beams M^2 quality factor measurement. This output beam was 1:1 image onto a Spiricon CCD (Spiricon, LBA-USB) camera for intensity measurements also.

Special properties of the SLM was discussed in chapter 3. However two other conditions must be satisfied for the cavity to function these include, one that the optical gain from the cavity must be sufficiently high to overcome the losses and secondly, the intensity of the circulating beam inside the cavity must not exceed the damage threshold (25 W/cm^2) of the SLM [24]. These two conditions were addressed by the use of the high power diode pump and the L-shaped cavity configuration to avoid direct illumination of the SLM by the high power pump source.

4.2.2 Experiment 2 - Selecting High order modes

After the experimental setup, we moved on to perform intra-cavity selection of high-order LG modes. Extra-cavity LG mode generation has been exploited using complex amplitude modulation to implement amplitude modulation on the phase-only SLM [62]. This implies that the SLM can be used to create custom amplitude masks - fine wires (loss-rings) [13] that have been employed by others to perform LG intra-cavity mode selection. The digital hologram for the generation of the LG$_{p0}$ modes is composed of a high-loss absorbing annular aperture together with a phase-only radius of curvature. Using the symmetric Laguerre-Gaussian mode function of zero azimuthal order ($l = 0$), LG$_{p0}$, to generate digital holograms that corresponds to amplitude absorbing rings (see illustration in Figure 4.3(c)) for the LG$_{p0}$ modes (using the second order intensity moment, $I(r, z) = |E_{p0}|^2$ for p equal to 0, 1, 2 and 3). And for each of these LG$_{p0}$ modes, their digital holograms were combined with a phase-only radius of curvature and the final combined hologram is used to perform mode selection for the corresponding p - mode in the cavity.

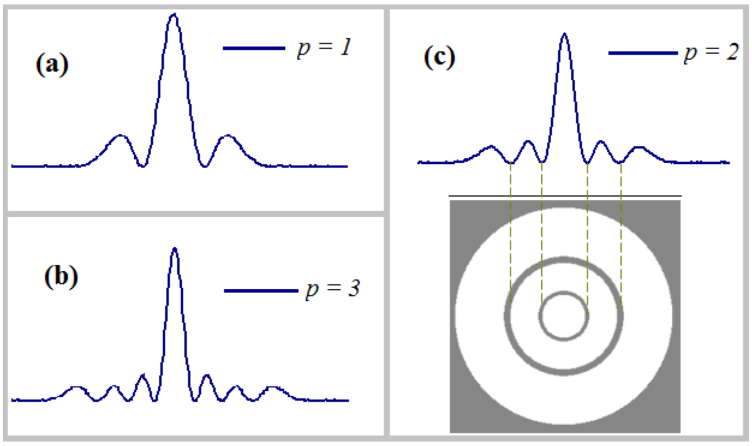

FIGURE 4.3: Mathematical simulated LG eigen modes, showing intensity cross-sections for $p = 1$ to 3, when the correct digital holographic amplitude masks are used on the intra-cavity SLM. (c) An example of such a mask for $p = 2$ is shown, with high-loss (absorbing) rings coinciding with the intensity nulls of the $p = 2$ Laguerre-Gaussian mode.

Figure 4.4 shows an illustration of how the hologram of amplitude absorbing rings was combined with the hologram of a phase-only radius of curvature to produce the resultant hologram for $p = 2$.

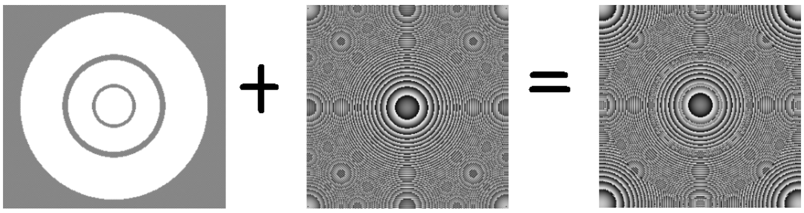

FIGURE 4.4: Illustration of the combination of holographic amplitude mask (left for $p = 2$) and a digital hologram with phase-only radius of curvature (center) and the right most is the resultant digital hologram.

The combined digital hologram (Figure 4.4) is loaded and displayed on the SLM (for each p mode) and with the diode pump switched on. The phase-only radius of curvature hologram effectively allows the SLM to mimic a concave mirror while that for the amplitude mask does mode selection. Figure 4.3 presents mathematically simulated LG eigen modes, showing the intensity cross-section for $p = 1$ - 3, when the correct digital holographic amplitude masks are used on the intra-cavity SLM. Figure 4.3(c) shows how such a mask for $p = 2$ with its high absorbing (loss) rings coincide with the nulls of intensity for this mode.

The transverse intensity distribution images of the output beam from the cavity was taken for each p-order mode at the near- and far-fields using a Spiricon CCD (Spiricon, LBA-USB) camera. The M^2 beam quality factor was measured using Photon Inc ModeScan meter and the power of the output beam was also measured for each p-order mode.

4.3 Summary

This chapter presented how the concept of the digital laser was employed in the experiment. The first phase was the setting-up of a stable diode end-pumped Nd:YAG solid state laser resonator cavity. The cavity uses an intra-cavity Hamamatsu SLM (that mimics a concave mirror) as a back reflector with a flat mirror output coupler to setup an L-shaped hemi-spherical resonator cavity configuration. Then using symmetric Laguerre-Gaussian (LG_{p0}) mode function of zero azimuthal order to generate digital holograms (grey-scale images) that correspond to amplitude absorbing rings for the LG_{p0} modes. Each of these holograms combined with the hologram that allows the SLM to mimic a concave mirror were used on the SLM to perform mode selection in the cavity. The transverse images of the output beam from the laser resonator cavity was taken with a CCD camera, the power and M^2 quality factor of the output beam was also measured for each mode.

Chapter 5

Results

5.1 Introduction

The results of the stable resonator cavity using a virtual mirror implemented on the SLM with no mode selecting elements are presented first, followed by the results of implementing amplitude absorbing masks on the SLM for LG_{p0} modes selection.

5.2 Results of laser resonator cavity

Figure 5.1 shows the CCD measured intensity distribution profile of the output beam from the stable resonator cavity at the near- and far-fields, with the corresponding normalized intensity plot along the x- and y-axis. From 5.1 it can be seen that the transverse intensity distribution profile of the output laser beam from the flat mirror (output coupler) has a good Gaussian profile and implies that the cavity was indeed a stable hemispherical resonator cavity. The experimental intensity distributions obtained at the near- and far-fields show nearly Gaussian cross-sections in both the x- and the y-directions which are in good agreement with the theoretically generated one (see Figure 5.1). The second column of Figure 5.1 presents a fit of the theoretically calculated Gaussian intensity plot with the cross-section intensity distribution plot of the output beam for both cases, which are in good agreement. This confirms that the intra-cavity SLM indeed correctly mimics a concave mirror. The beam size at the flat mirror was measured and found to be $\approx 380\ \mu$m which compares very well with the theoretically (equation (5.1)) calculated size of $\approx 368\ \mu$m.

$$W_0 = \sqrt{\frac{R\lambda}{\pi}}\left(\frac{d}{R-d}\right)^{\frac{1}{4}}, \tag{5.1}$$

where R is the radius of curvature of the curved mirror, λ is the operational wavelength of the cavity (1064 nm), W_0 is the size of the Gaussian beam at the waist and d is the length of the cavity.

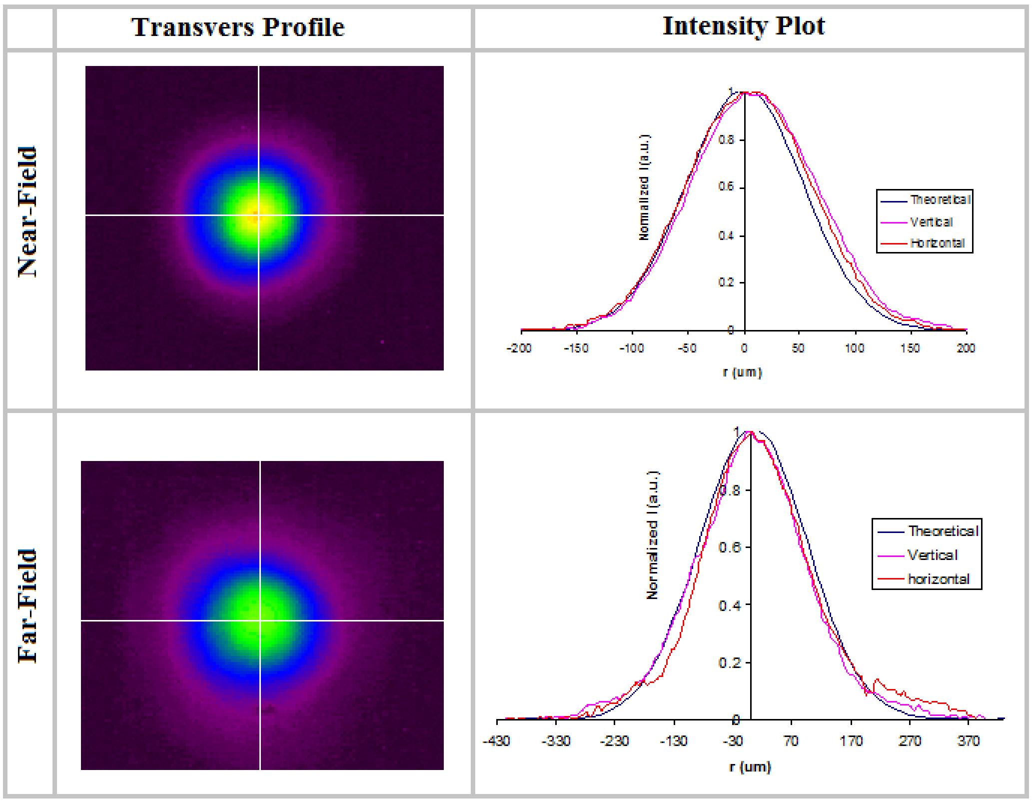

FIGURE 5.1: Transverse intensity distribution profile and normalized intensity plot of the output beam at the near-field and far-field.

The near-field and far-field intensity distribution profile are basically the same but differ with some scale factor (with reference to Figure 5.1). A little asymmetry can be noticed in the beam which can be attributed to fine misalignment in the optical setup. The M^2 beam quality factor was measured directly using the PHOTON Inc Modescan 1780 camera (software). The measured M^2 quality factor was found to be 1.09 which is approximately equal to the theoretically predicted value of 1 for the fundamental Gaussian mode of a stable resonator cavity and this shows that the beam is of good quality. Hence, we have confidently assembled a stable resonator cavity using an intra-cavity SLM as a back reflector.

5.3 Laser Cavity's Mode Selection Results

5.3.1 Mode Purity

Figure 5.2, presents the holograms, CCD measured transverse images of the beam at the near- and far-fields and the theoretically generated intensity prolfile of the modes. In Figure 5.2 are the results of mode selection by the cavity, and in the first column shows the holograms used for each corresponding p mode. The second and third columns are the near- and far-fields transverse intensity distribution profile respectively, taken with a CCD camera. Since LG_{p0} mode are solutions to the Helmholtz equation, it is expected that their near-field and far-field transverse intensity distribution profile will be identical but for a scale factor as can be seen from Figure 5.2. This is a clear indication that they are indeed the desired single $p = 0 - 3$ order modes and showing that only the desired corresponding single order mode is oscillating in the cavity.

From Figure 5.2 it is clear that the modes losses symmetry as the order increases, most likely because of aberrations and thermal lensing inside the resonator cavity. It is very clear that the cavity is selecting the desired single order modes, with the modal properties in good agreement with theoretical prediction. This suggests that the little imperfection noticed in the intensity distribution profile of the modes does not significantly affect the modal properties.

The plot of the experimentally measured intensity distribution profile of the output beam for each mode are shown in Figure 5.3 at the near-field and Figure 5.4 at the far-field. These graphs are in good agreement with the theoretically generated intensity distribution profile for each p mode. The fact that they both have the same profile at the near and far fields entails that it maintains the same (intensity) profile along the propagation axis. This in turn implies that, there existed only a single mode operation in the cavity and no high-order

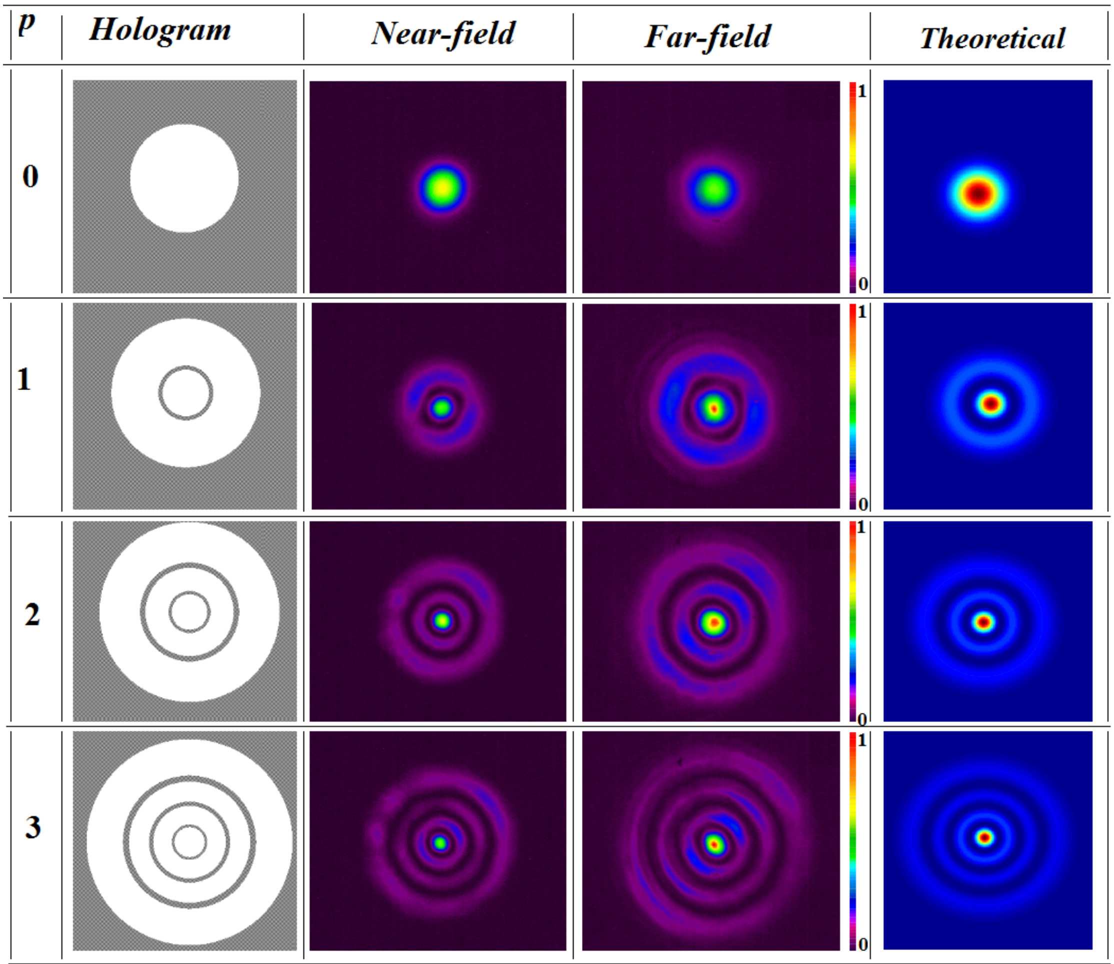

Figure 5.2: Hologram (first column) used on SLM for each mode, (Color online) the output beams cross-section intensity distribution profile at the near-field (second column) and far-field (third column) and the theoretically generated cross-section intensity distribution at the near-field (forth column) for each p, for $p = 0 - 3$ (top to bottom rows).

harmonics of each target mode were oscillating the cavity. This again confirms the purity of each p mode.

The second column of Figure 5.3 is the cross-section intensity plots along the x- and y-axis for each p mode at the near-field, which is in perfect agreement with the plot of theoretically prediction LG eigen modes. The nulls of intensity of the theoretically calculated intensity distribution profile are in agreement with the measured ones. This again confirms that the

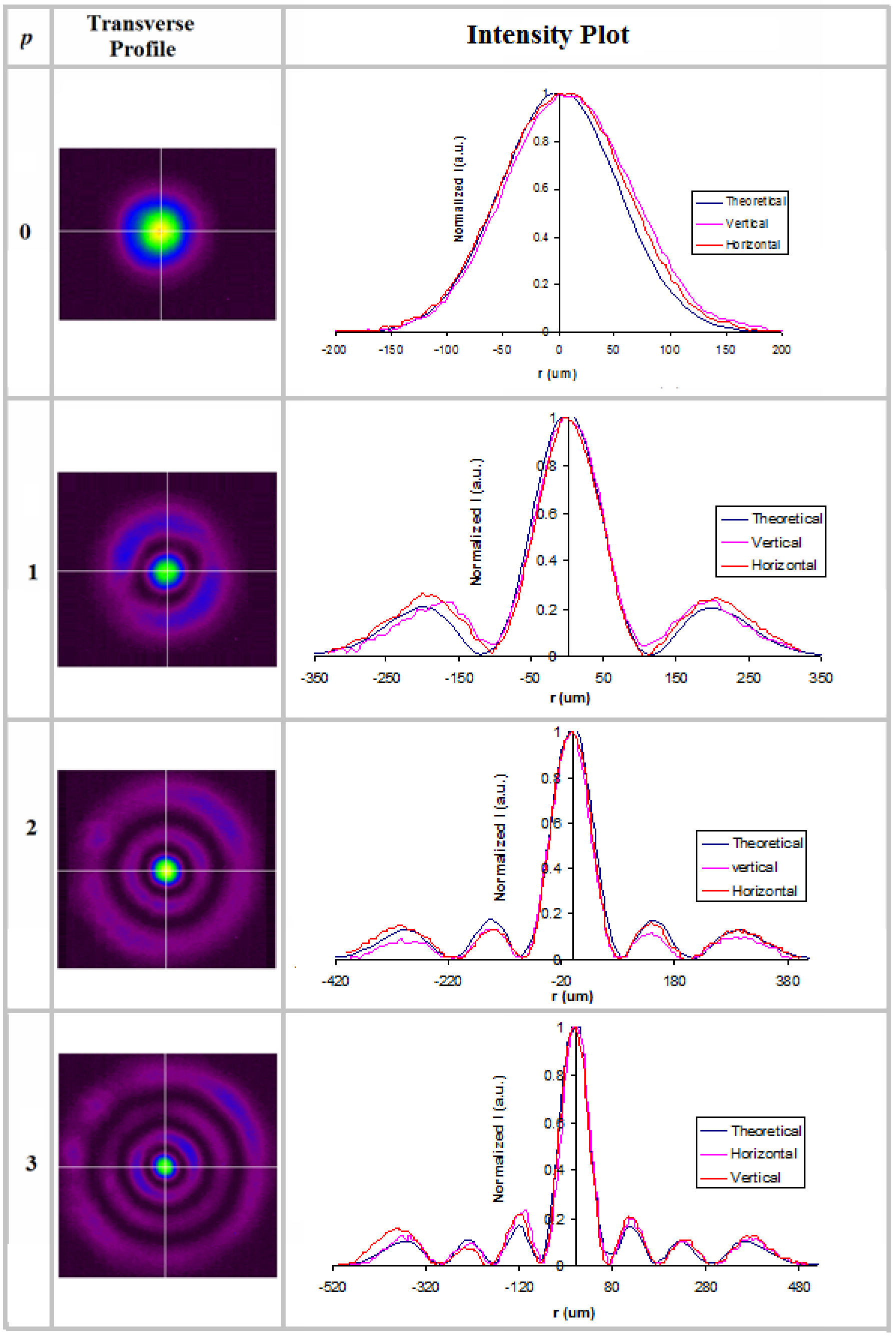

FIGURE 5.3: The first column is the CCD measured near-field transverse intensity distribution profile for each p-order mode. The second column is the normalized cross-section intensity plot along the x- and y-axis for each p mode.

resonator cavity is selecting pure single high-order modes and no high-order harmonics of the desired mode was oscillating in the cavity. Figure 5.4 presents the CCD measured transverse images of the beams and the normalized cross-section intensity plot along the x- and y-axis at the far-field.

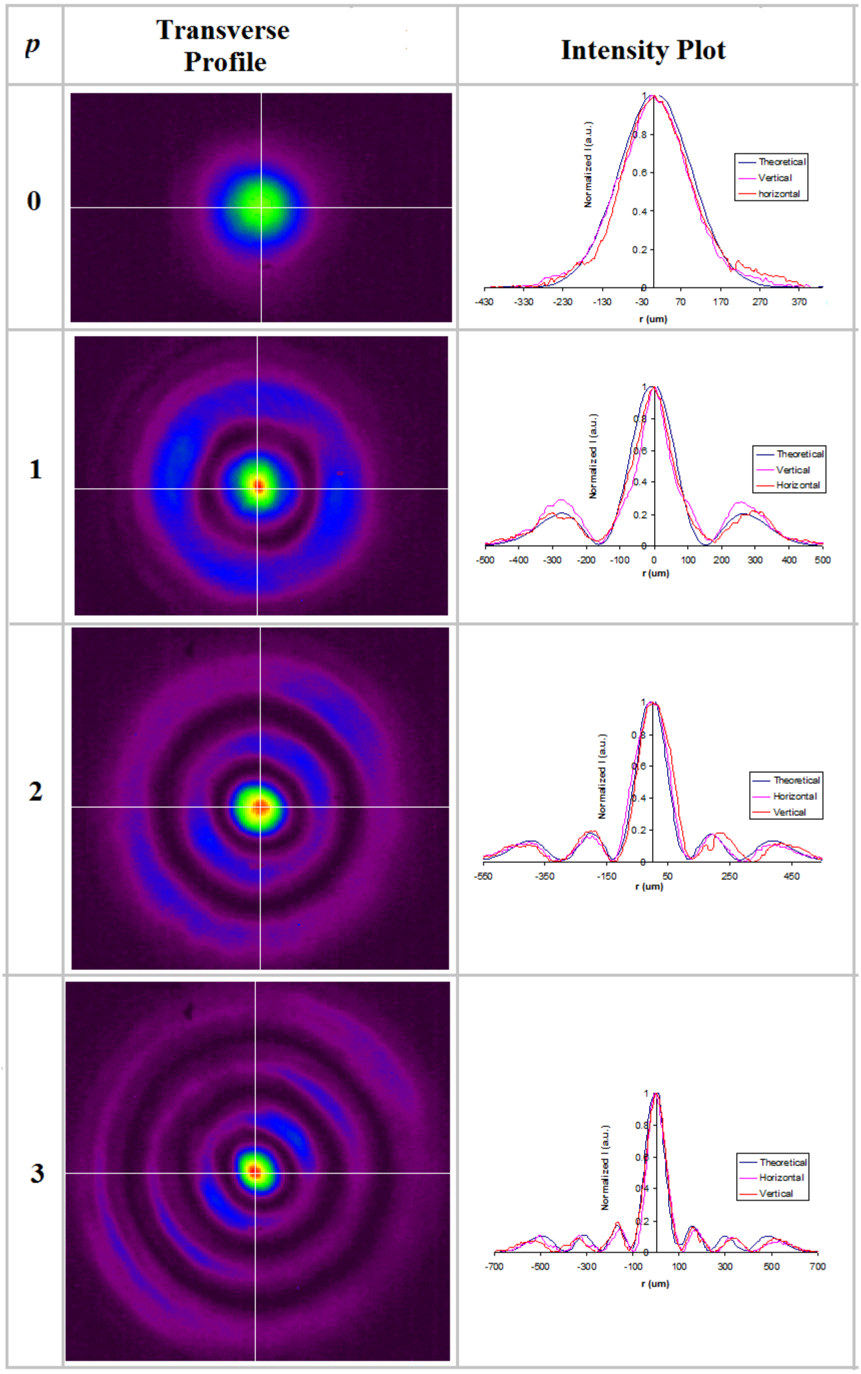

FIGURE 5.4: The first column is the CCD measured far-field transverse intensity distribution profile for each p-order mode. The second column presents the normalized cross-section intensity plot along the horizontal and vertical axis respectively for each p mode.

In the cavity we considered single modes and since the resonator is stable, the mode sizes at the output coupler and the M^2 beam quality factor of the theoretically calculated values can be compared with experimentally measured ones. Figure 5.5 presents the graph of the

M^2 beam quality factor and the graph of the beam sizes. Equation (4.3) and (4.2) were used to calculate theoretically the M^2 beam quality factor and the mode sizes respectively. From Figure 5.5(a), it is clear that the measured value of the M^2 beam quality factor and Figure 5.5(b), the measured beam width for each p-order mode are in good agreement with the theoretical prediction which implies that each mode is indeed of good purity and quality.

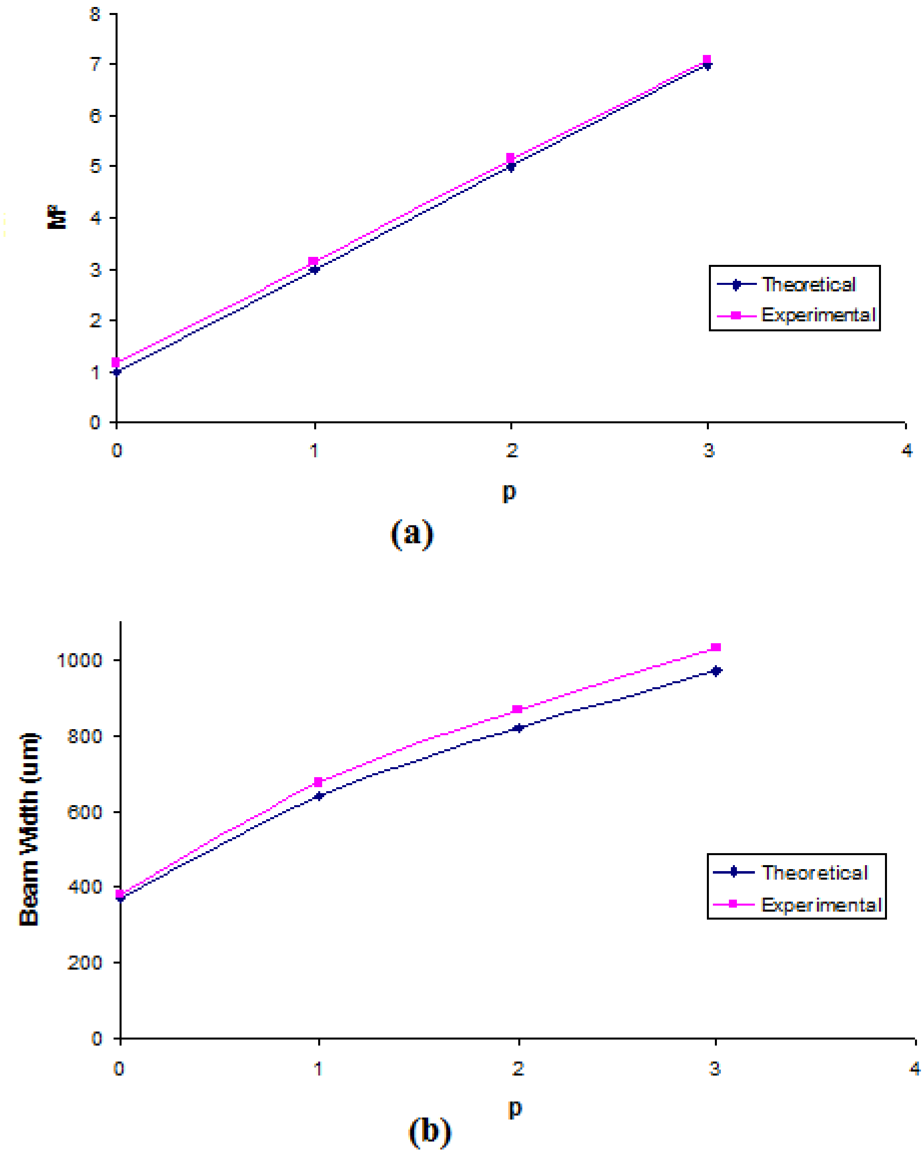

FIGURE 5.5: The plot of the (a) M^2 beam propagation factor against mode order, and (b) beam width against the mode order. In the two cases the theoretical prediction was determined from equation (4.3) and (4.2) respectively

These results show clearly that the cavity was only selecting the desired single high-order modes, with the modal properties in good agreement with theoretical prediction and that their was no high-order harmonics of the desired modes oscillating in the cavity. This suggests that the little imperfection noticed in the intensity distribution profile of the modes does not significantly affect the modal properties.

5.3.2 Mode Volume and Energy Extraction

The power contained in the output laser from a resonator cavity is directly proportional to the mode volume, V_p of a mode given by equation (5.2) [22].

$$\begin{aligned} V_p &= \int_0^{l_0} \pi W^2(z) dz \\ &= (2p+1)\pi w_0^2 l_0 \left(1 + \frac{l_0^2}{3z_R^2}\right) \\ &= M^2 V_0 \left(1 + \frac{l_0^2}{3z_R^2}\right), \end{aligned} \tag{5.2}$$

where the length of the gain medium is l_0, the Rayleigh range is z_R and the mode volume of the Gaussian mode $p = 0$ is V_0. In the limits where the crystal length is much smaller than the Rayleigh range of the beam, $l_0 \ll z_R$, equation (5.2) reduces to $V_p \approx M^2 V_0$. It is very clear that the mode volume is directly proportional to the M^2 beam quality factor. In our case it was calculated that $V_3 \approx 7.14583 V_0$ (using equation (5.2)), which implies that roughly 715% more volume of the crystal is being used by the oscillating beam to produce laser beams by stimulated emission in the cavity at p = 3 more than at p = 0.

Figure 5.6(b) shows the graph of the threshold pump power against the modal order and (a) the slope efficiency of the generated modes. There are power losses in the cavity as the radiation bounces back and forth in the cavity. The output power is also inversely proportional to the round-trip losses, which suggest that the output power can be written as [23]:

$$\frac{P_p}{P_0} = (2p+1)\frac{\delta_0}{\delta_p}, \tag{5.3}$$

where the subscripts p and 0 refer to the modal orders and the round trip losses are denoted by δ.

Analysing equation (5.3) reveals that if the losses increase at a slow rate, it is possible to have a larger amount of power extraction from a high-order mode volume than a lower-order. This is the idea behind selecting high-order modes in the cavity. If we assume that the ratio of the losses, δ_0/δ_p is approximately the ratio of the threshold values (Figure 5.6(b)) then, the ratio P_3/P_0 gives a value of approximately 1.7 (considering $p = 0$ and $p = 3$ modes).

From Figure 5.6 there exists a critical point where the extraction of power from the resonator cavity becomes more beneficial at high-order modes compared to the lowest-order modes, not withstanding that the power losses increase with mode order so also does the mode volume and hence the gain from the cavity. For the donut LG_{p0} modes, there is a point where the extra gain from the cavity far exceed the extra losses as one goes to high-order modes. Figure 5.7 shows the graph of the slope efficiencies for $p = 0$ and $p = 3$. Lets use the case of $p = 0$ and $p = 3$ for an illustration (Figure 5.7). When the value of the pump power is just greater than about 38.8 W, more power is extracted from the cavity for $p = 3$ mode than at $p = 0$ mode, not withstanding the higher power losses at $p = 3$. This manifests when we consider the slope efficiencies. The percentage difference between the slope efficiencies of the cavity at $p = 3$ and $p = 0$ is approximately 74% (Figure 5.6(a)).

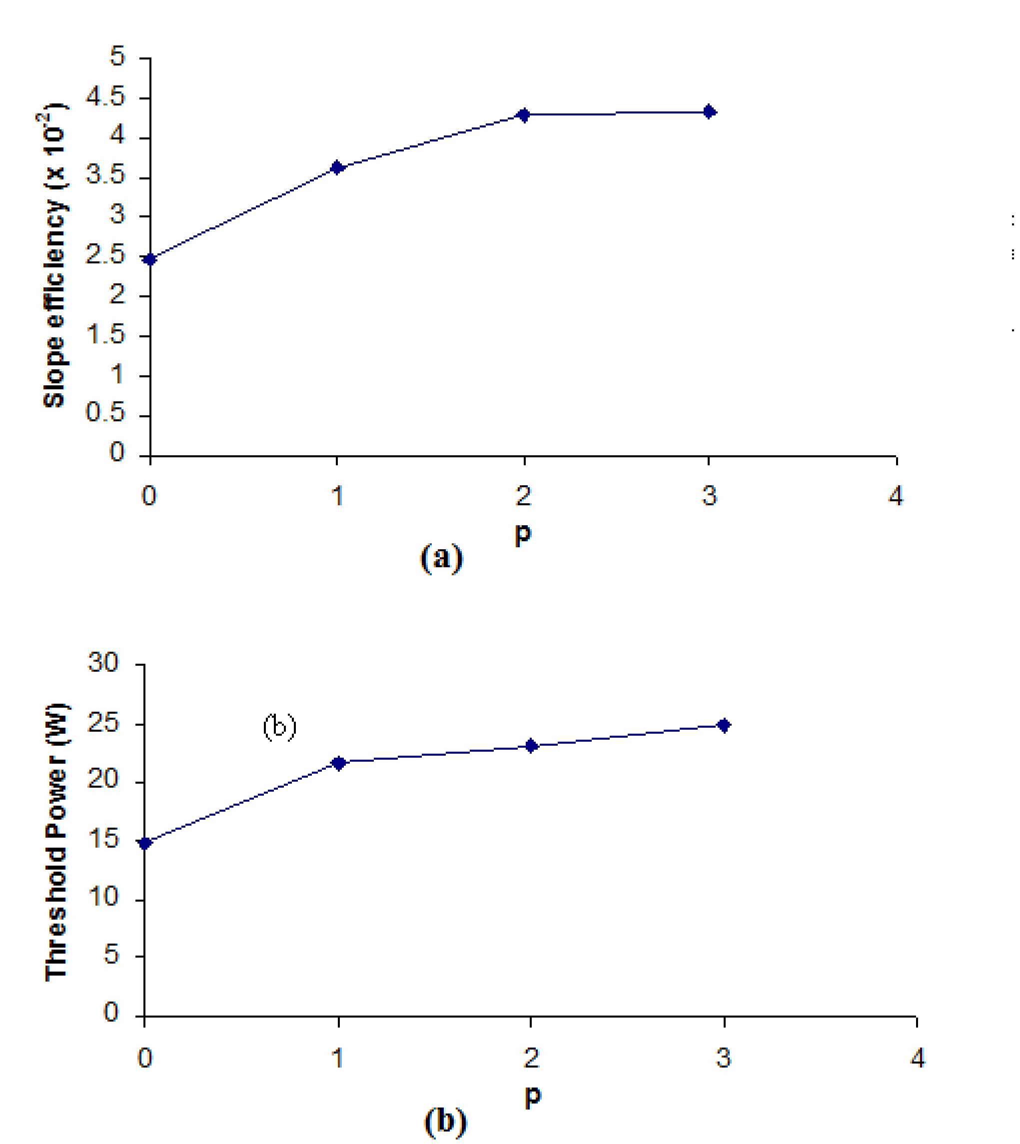

FIGURE 5.6: The graph of the (a) slope efficiency and (b) threshold power against mode order (p). These two graphs can be said to be approximately directly proportional.

This higher efficiency at $p = 3$ becomes dominant when pumping the crystal at a pump power greater than 38.8 W and for every 1 W increase in the input pump power, results in a lot of power extraction from the resonator cavity. What this entails is that for every 1 W increase in pump power above this threshold results is about 74% more power extraction from the cavity compared to the lowest order mode ($p = 0$).

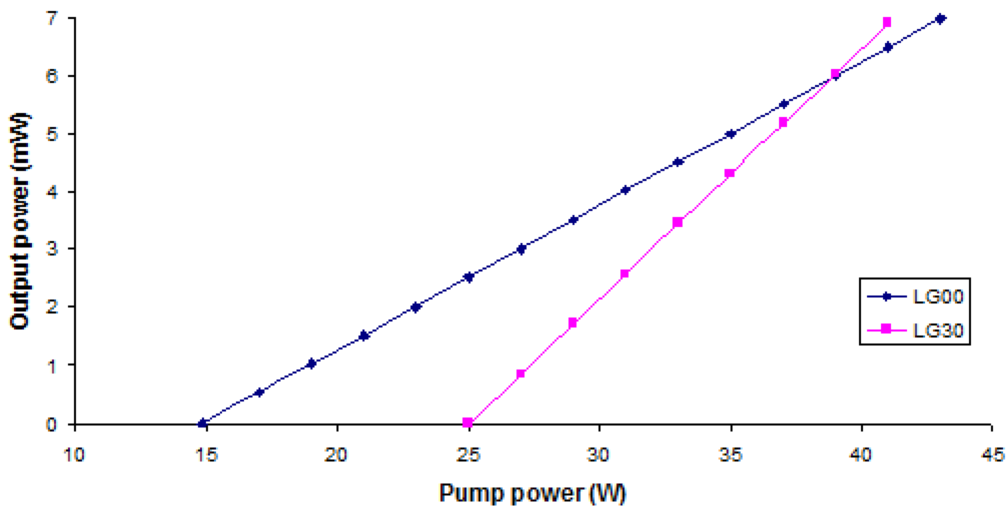

FIGURE 5.7: A plot of the output power vs pump power for $p = 0$ and $p = 3$.

Figure 5.7 shows that at certain critical pump power that the high-order mode extracts more power owing to the significant increase in mode volume.

The large increase in the amount of power extracted from the cavity can be explained when we compare the size of the radiation circulating in the cavity for a Gaussian beam and a high-order mode at $p = 3$. If we assume that the ratio of the width of the modes at the flat-mirror (the nulls of intensity inclusive) is the ratio of the volume of the circulating radiation illuminating the crystal for each mode, then about 600% more volume of the crystal is being used for stimulated emission (by the circulating radiation) at $p = 3$ more than at $p = 0$. Hence, we have a much higher increase in output power from the cavity at $p = 3$.

This gives a quantitative illustration as to how the extra power that was extracted from the cavity (gain medium) was generated. The higher volume at high-order modes provides more enhancement for photon-matter interaction thereby increasing the power of the output laser from the cavity. Therefore, comparing the width of the circulating beam for each mode gives a good estimate by ratio (or percentage) of the area of the oscillating radiation that was causing stimulated emission in the gain medium to generate the output laser.

5.4 Summary

The results of the diode end-pumped Nd:YAG solid state laser resonator (that uses an intra-cavity SLM as a back reflector), shows that the cavity was indeed a stable configuration and that the SLM was correctly mimicking a concave mirror. We have shown that one can selectively excite high-order radial Laguerre-Gaussian modes inside a solid state laser resonator that uses an intra-cavity SLM as a mode selecting element. The mode selection was achieved by using digital holograms which consists of high absorbing concentric rings on the intra-cavity SLM. The modes were shown to be of very high purity. Finally, we verified that the power extraction from the gain medium at a high-order mode (p = 3) beyond a critical pump power of 38.8 W (for the cavity) far exceeds that at the lowest order mode (p = 0) by a value of ≈ 74%. The results suggest a route to high brightness lasers by intra-cavity selection of high-order modes above this critical optical input power and subsequently improve the M^2 beam quality factor.

Chapter 6

Summary of results, conclusion and future study

6.1 Summary of results

The transverse intensity profile of the output beam of a laser resonator is one of the most interesting properties of the output beam because of its numerous applications. Donut shaped beams in particular have been of great interest to the community because of their characteristic phase singularity at the center and many intra-cavity techniques have been used to generate them. The use of intra-cavity absorbing concentric rings for Laguerre-Gaussian mode selection is an old technique but our experiment employed an intra-cavity spatial light modulator (SLM) as the mode selecting element. On this SLM was programmed amplitude absorbing rings (digital holograms) which correspond to LG_{p0} modes zeros of intensities for the desired mode.

In the cavity we targeted selecting single high-order modes, so comparing the modal properties: size and M^2 quality factor for each mode with the theoretical prediction showed the purity and quality of each mode. These comparisons revealed that the modes were of high purity and quality. A final confirmation of the purity of each mode was done, by fitting the theoretically generated transverse intensity plot with the experimentally measured ones, at near- and far-fields. The results were in good agreement which implied that the output laser maintained the same profile as it propagates along the propagation axis, hence no high-order harmonics of each corresponding mode was oscillating in the cavity.

Also, comparing the slope efficiencies of the output laser reveled $\approx 74\%$ higher efficiency at $p = 3$ compared to the Gaussian mode ($p = 0$) but this extra power is only realized above a certain critical pump input power of ≈ 38.8 W.

6.2 Conclusion

In conclusion, we have in this study assembled a stable diode end-pumped Nd:YAG solid state laser resonator cavity which uses an intra-cavity SLM as a back reflector. The cavity has a hemispherical configuration with a flat mirror output coupler and on the SLM was encoded the curvature of a concave mirror. The measured output laser from the cavity was of good purity and quality which in turn implies that it was of stable configuration.

In our approach, we generated concentric amplitude absorbing rings that corresponds to Laguerre-polynomial zeros using digital holograms. These holograms when encoded on to the SLM effectively forced the cavity to oscillate in the corresponding high-order LG_{p0} mode ($p = 0 - 3$). The modal properties of each generated modes were tested to ascertain their purity and quality, and the outcome confirmed that they are of very high purity and quality, hence the cavity was indeed selecting single pure high-order modes.

Thus, forcing the cavity to oscillate at a high-order LG_{p0} mode (at $p = 3$) above a pump input power of ≈ 38.8 W, extracted $\approx 74\%$ more power from the crystal compared to the default Gaussian mode ($p = 0$). This extra power can be translated to higher brightness if extra-cavity improvement of the M^2 beam quality factor is done on the output laser by converting from the high-order mode back to the Gaussian mode. This finally demonstrates a route to high-brightness lasers.

6.3 Future Study

The experiment compromised optimization with respect to the design of the laser cavity, since the same cavity conditions were used for all the modes studied. Hence, the cavity conditions reported here were not optimized for extraction of power, but for mode purity. A careful choice (design) of the output coupler's reflectivity, the optical gain medium's length and doping concentration, and the pump-mode overlap would significantly increase the power extraction efficiency from the cavity for a given mode. Therefore, the power extraction efficiency of such an end-pump configuration (designed with all these considerations in mind) could be made much higher, and could be used to achieve a high-brightness laser. In this research demonstration we focused our attention to the relative modal improvement that follows equation (5.3) that can be compared with the default Gaussian mode, i.e., it is the ratio of the losses and the relative slope efficiencies that is important not the actual values of the output power themselves. In this regard, the slope efficiency was improved by a factor of 74% for the $p = 3$ mode relative to the fundamental Gaussian mode ($p = 0$). It is important to mention that the quoted pump power represents the pump power that was measured from the source and not the actual optical pump power absorbed by the laser crystal. About 60% of the quoted value is the actual pump power absorbed by the laser crystal.

The results that were presented in this study show that it is possible to perform intra-cavity selection of high-order modes with high purity and relatively higher energy extraction from the cavity compared to the fundamental Gaussian mode. For this higher energy extraction to translate to higher brightness lasers, it is important to perform extra-cavity improvement of its M^2 quality factor through a field mapping process for example, from a high-order LG mode to Gaussian beam. There are well known procedures that can be used to reshape any coherent field to another coherent field, for instance, from $p = 3$ order mode to $p = 0$ mode. Some of these procedures include complex amplitude modulation [61], geometrical transformations [63], interferometric beam combination [64], and refractive or diffractive beam shaping [65]. Employing a lossless improvement [65] [66] of the M^2 quality factor is usually achieved with two optical elements in two steps; the first step is to transform the phase and second to transform the intensity distribution. This approach has been used before experimentally [64] [68] to improve the beam quality factor and which in fact is evident from the reciprocity nature of light's propagation [25]. For example transforming a Gaussian to a flattop using beam shapers, in the reverse (flattop to Gaussian) would improve the beam quality factor of the beam.

The results of this research work therefore demonstrates a route to higher-brightness lasers using intra-cavity selection of high-order laser modes and subsequent extra-cavity improvement of the beam quality factor.

References

[1] Siegman, A. (1986) Lasers, California:University Science Books.

[2] Maiman, T. H. (1960) Stimulated optical radiation in Ruby, *Nature*, 187, pp. 493–494.

[3] Koechner, W. (2006) Solid-State Laser Engineering, New York:Springer.

[4] Fan, T.Y. and Byer, R.L. (1988) Diode Laser-Pumped Solid-state Lasers, *IEEE Journal of Selected Topics in Qauntum Electronics*, 24, pp. 895–912.

[5] Jankiewicz, Z. and Kopczyński, K. (2001) Diode-pumped solid-state lasers, *Opto-Elec. Rev.*, 9, pp. 19–33.

[6] Keyes, R. J. and Quist, T. M. (1974) Injection luminescent pumping of CaF2:U^{3+} with GaAs diode lasers, *Applied Physics Letters*, 4, pp. 50–52.

[7] Ross, M. (1968) YAG laser operation by semiconductor laser pumping, *Proc. IEEE.*, 56, pp. 196-197.

[8] Lu, J., Prabhu1, M., Song, J., Li, C., Xu, J., Ueda, K., Kaminskii, A.A., Yagi, H. and Yanagitani, T. (2000) Optical properties and highly efficient laser oscillation of Nd:YAG ceramics, *Applied Physics B Laser Optics*, 71, pp. 469-473.

[9] Naidoo, D. (2011) Transverse Modes in Solid-State Laser Resonators, *University of Kwazulu-Natal*, Pietermaritzburg.

[10] Yariv A. (1989) Quantum Electronics, *John Wiley and Sons.* New York.

[11] Saleh, B. E. A. and Teich, M. C. (1991) Fundamentals of Photonics, *John Wiley and Sons, Inc.*, New York, Chap. 14.

[12] Kogelnik, H. and Li, T. (1966) Laser Beams and Resonators. *Applied Optics.*, 5, pp. 1550–1566.

[13] Hodgson, N. and Weber, H. (2005) Laser Resonators and Beam Propagation 2nd edn, *Springer.*

[14] Allen, L., Beijersbergen, M. W., Spreeuw, R. J. C., and Woerdman, J. P. (1992) Orbital angular momentum of light and the transformation of Laguerre-Gaussian laser modes, *Physical Review A*, 45(11), pp. 8185–8189.

[15] Curtis, J. E., Koss, B. A., and Grier, D. G. (2002) Dynamic holographic optical tweezers, *Optics Communications*, 207, pp. 169–175.

[16] Kennedy, S. A., Szabo, M. J., Teslow, H., Porterfield, J. Z., and Abraham, E. R. I. (2002) Creation of Laguerre-Gaussian laser modes using diffractive optics, *Physical Review*, 66, pp. 0-043801.

[17] Beijersbergen, M. W., Coerwinkel, R. P. C., Kristensen, M., and Woerdman, J. P. (1994) Helical-wavefront laser beams produced with a spiral phaseplate, *Optics Communications*, 112, pp. 321.

[18] Thirugnanasambandam, M.P., Senatsky, Yu., and Ueda, K. (2010) Generation of very-high order Laguerre-Gaussian modes in Yb:YAG ceramic laser, *Laser Physics Letters*, 7, pp. 637-643.

[19] Senatsky, Y., Bisson, J. F., Li, J., Shirakawa, A., and Thirugnansambandam, M. (2012) Laguerre-Gaussian modes selection in diode-pumped solid-state lasers, *Optical Review*, 19, pp. 201–221.

[20] Heckenberg, N. R., McDuff, R., Smith, C. P., and White, A. G. (1992) Generation of optical phase singularities by computer-generated holograms, *Optical Letters*, 17, pp. 221–223.

[21] Kotlyar, V. V., Almazov, A. A., Khonina, S. N., Soifer, V. A., Elfstrom, H., and Turunen, J. (2005) Generation of phase singularity through diffracting a plane or Gaussian beam by a spiral phase plate, *Journal of the Optical Society of America A*, 22, pp. 849–861.

[22] Hasnaoui, A. and Aït-Ameur, K. (2010) Properties of a laser cavity containing an absorbing ring, *Applied Optics*, 49, pp. 4034–4043.

[23] Ngcobo, S., Aït-Ameur, K., Passilly, N., Hasnaoui, A., and Forbes, A. (2013) Exciting higher-order radial Laguerre–Gaussian modes in a diode-pumped solid-state laser resonator, *Applied Optics*, 52, pp. 093-2101.

[24] Ngcobo, S., Litvin, I., Burger, L. and Forbes, A. (2013) The digital laser, *Nature Communications*, 4, pp. 2289.

[25] Turnbull, G. A., Robertson, D. A., Smith, G. M., Allen, L., and Padgett, M. J. (1996) The generation of free-space Laguerre-Gaussian modes at millimeter-wave frequencies by use of a spiral phaseplate. *Optics Communications*, 127, pp. 183.

[26] Oron, R., Davidson, N., Hasman, E., and Friesem, A. (2001) Transverse Mode Shaping and Selection in Laser Resonators, In *Progress in Optics*, 6, pp. 325, ed. Wolf, E., Amsterdam:Elsevier.

[27] Koechner, W. (2006) Solid-State Laser Engineering, 6th ed, *Springer*, Berlin.

[28] Thirugnanasambandam, M., Senatsky, Yu., and Ueda, K. (2010) Generation of very-high order Laguerre-Gaussian modes in Yb:YAG ceramic laser, *Laser Physics Letters*, 7, pp. 637.

[29] Senatsky, Yu., Bisson, J.-F., Shelobolin, A., Shirakawa, A., and Ueda, K. (2009) Circular modes selection in Yb:YAG laser using an intracavity lens with spherical aberration, *Laser Physics*, 19, pp. 911.

[30] Thirugnanasambandam, M., Senatsky, Yu., Shirakawa, A., and Ueda, K. (2011) Multi-ring modes generation in YB:YAG ceramic laser, *Opt. Mater.*, 33, pp. 675.

[31] Thirugnanasambandam, M., Senatsky, Yu., and Ueda, K. (2011) Generation of rakially and azimuthally polarized beams in YB:YAG laser with intra-cavity lens and birefringent crystal, *Optical Express*, 19, pp. 1905.

[32] Thirugnanasambandam, M. (2011) High-order mode selection in Yb:YAG ceramic laser, *University of Electro-Communications*, Tokyo.

[33] He, G.Y., Guo, J., Jiao, Z. X. and Wang, B. (2012) Generation of high power and high stability azimuthally polarized beams in a Nd:YAG laser, *Laser Physics*, 22, pp. 1275.

[34] Meier, M., Romano, V. and Feurer, T. (2007) Material processing with pulsed radially and azimuthally poloarized laser radiation, *Applied Physics A*, 86, pp. 329.

[35] Okida, M., Omatsu, T., Itoh, M., and Yatagai,T. (2007) Direct genration of high power Laguerre-Gaussian output from a diode-pumped Nd:YVO_4 1.3μm bounce laser, *Optics Express*, 15, pp. 7616.

[36] Quabis, S., Dorn, R., Leuchs, G. (2005) Generation of a radially polarized doughnut mode of high quality, *Applied Physics B*, 81, pp. 597-600.

[37] Dorn, R., Quabis, S., Eberler, M., Glockl, O., Leuchs, G. (2000) Focussing light to a tighter spot, *Optics Communications*, 179, pp. 1.

[38] Alda, J. (2003) Laser and Gaussian Beam Propagation, *Encyclopedia of Optics Eng., Marcel Dekker*, New York, pp. 999–1012.

[39] Svelto, O. (1998) Principles of Lasers, *Springer*, New York.

[40] Born, M. and Wolf, E. (1980) Principles of Optics. *Pergamon*, New York.

[41] Paschotta, R. (2013) *Optical Intensity*, viewed 11 June, 2013, from `www.rp-photonics.com/optical_intensity.html`.

[42] Cousins, A. K. (1992) Temperature and Thermal Stress Scaling In Finite-Length End-Pumped Laser Rods, *IEEE Journal of Selected Topics in Qauntum Electronics*, 28, pp. 1057-1069.

[43] ISO Standard 11146 (2005) Lasers and laser-related equipment – Test methods for laser beam widths, divergence angles and beam propagation ratios *International Organization for Standardization.*

[44] Menzel, R. (2007) Photonics, *Springer-Verlag*, Berlin.

[45] Siegman, A. (2000) Laser Beams and Resonators: The 1960s, *IEEE Journal of Selected Topics in Qauntum Electronics*, 6, pp. 1380-1388.

[46] Belanger, P. A. and Pare, C. (1991) Optical resonators using graded-phase mirrors, *Optics Letters*, 16, pp. 1057.

[47] Pare, C. and Belanger, PA. (1992) Custom laser resonators using graded-phase mirrors, *IEEE J. Quantum Electron*, 20, pp. 355-362.

[48] Oron, R., Davidson, N., Hasman, E., and Friesem, A. (2001) Transverse Mode Shaping and Selection in Laser Resonators, In *Progress in Optics*, Chapter 6, vol. 42, pp. 329-352, ed. Wolf, E., Amsterdam:Elsevier.

[49] Leger, J. R., Chen, D. and Wang, Z. (1994). Diffractive Optical Element for Mode Shaping of a Nd: YAG Laser. *Optical Letters*, 19, pp. 108-110.

[50] Neste, R.van, Pare, C., Lachance, R.L. and Belanger, P.A. (1994) Graded-phase mirror resonator with a super-gaussian output in a CW-CO_2 laser, *IEEE Journ. of Quantum Electr.*, 30, pp. 2663-2669.

[51] Leger, J. R., Chen, D. and Dai, K. (1994) High modal discrimination in a Nd:YAG laser resonator with internal phase grating, *Optical Letters*, 19, 1976-1978.

[52] Kol'chenko, A. P., Nikitenko, A. G. and Troitskii, Y. K. (1980) Control of the structure of transverse laser modes by phase shifting masks, *Sov. J. Quantum Electron*, 10, pp. 1013–1016.

[53] Oron, R., Danziger, Y., Davidson, N., Fresem, A. A. and Hasman, E. (1999) Laser mode discrimination with intra-cavity spiral phase elements, *Optics Communications*, 69, pp. 115–121.

[54] Hamamatsu Photonics K.K. (2013) *Light phase control (LCOS-SLM): Application technology—Hamamatsu Photonics*, viewed 30 March, 2014, from `http://www.hamamatsu.com/jp/en/technology/innovation/lcos-slm/index.html`.

[55] Dudley A. (2012) Superpositions of light fields carrying orbital angular momentum. *University of Kwazulu-Natal*, Pietermaritzburg.

[56] Wong, D.W.K. and Chen, G. (2008) Redistribution of the zero order by the use of a phase checkerboard pattern in computer generated holograms, *Applied Optics* 47, pp. 602-610.

[57] Dainty, J. C., Koryabin, A. V. and Kudryashov, A. V. (1998) Low-order adaptive deformable mirror, *Applied Optics*, 37, pp. 4663-4668.

[58] Piehler, S., Weichelt, B., Voss, A., Ahmed, M. A. and Graf, T. (2011) Power scaling of fundamental-mode thin-disk lasers using intracavity deformable mirrors, *Optical Letters*, 37, pp. 5033-5035.

[59] Lubeigt, W., Valentine, G., Girkin, J., Bente, E. and Burns, D. (2002) Active transverse mode control and optimization of an all-solid-state laser using an intra-cavity adaptive-optic mirror, *Optical Express*, 10, pp. 550-555.

[60] Hasnaoui, A., Bencheikh, A., Fromager M., Cagniot E., Aït-Ameur, K. (2011) Creation of a sharper focus by using a rectified TEMp_0 beam, *Optics Communications*, 284, pp. 1331-1334.

[61] Hasnaoui, A., Godin, T., Cagniot, E., Fromager, M., Forbes, A. and Aït-Ameur, K. (2012) Selection of a LG$_{p0}$–shaped fundamental mode in a laser cavity: phase versus amplitude masks, *Optics Communications*, 285, pp. 5268–5275.

[62] Arrizon, V., Ruiz, U., Carrada, R. and Gonzalez, L. A. (2007) Pixelated phase computer holograms for the accurate encoding of scalar complex fields, *Journal of the Optical Society of America A*, 24, pp. 3500-3507.

[63] Bryngdahl, O. (1974) Geometrical transforms in optics, *Journal of the Optical Society of America*, 64, pp. 1092–1099.

[64] Ishaaya, A. A., Machavariani, G., Davidson, N. and Friesem, A. A. (2003) Conversion of a high-order mode beam into a nearly Gaussian beam by use of a single interferometric element, *Optical Letters*, 28, pp. 504–506.

[65] Dickey, F. M., Holswade, S. C. (2000) Laser Beam Shaping: Theory and Techniques, New York:*Marcel Dekker*.

[66] Dickey, F. M. and Holswade, S. C. (1996) Lossless laser beam shaping, *Journal of the Optical Society of America A*, 13, pp. 751–760.

[67] Friese, M. E. J., Nieminen, T. A., Heckenberg, N. R., and Rubinsztein, Dunlop, H. (1997) Optical torque controlled by elliptical polarization, *Optical Letters*, 23, pp. 1-3.

[68] Oron, R., Davidson, N., Friesem, A. A., and Hasman, E. (2000) Continuous-phase elements can improve laser beam quality, *Optical Letters*, 25, pp. 939–941.